Reducing payload motion during offshore operations

T. de Vlieger

TU Delft

JUMBO

Reducing payload motion during offshore operations

By

T. de Vlieger

Master Thesis

in partial fulfilment of the requirements for the degree of

Master of Science
in Mechanical Engineering

at the Department Maritime and Transport Technology of Faculty Mechanical, Maritime and Materials Engineering of Delft University of Technology

to be defended publicly on Tuesday, August 23, 2022 at 12:15 PM

Student number:	4570936	
MSc track:	Multi-Machine Engineering	
Report number:	2022.MME.8601	
Supervisor:	Dr. Ir. X. Jiang	
Thesis committee:	Prof. Dr. R.R. Negenborn,	TU Delft committee Chair, 3mE
	Dr. Ir. X. Jiang,	TU Delft committee member, 3mE
	Dr. Ir. J.O. Colomés Gené,	TU Delft committee member, CEG
	Ing. F.J. van der Werf,	Company Supervisor, Jumbo Maritime
	Ing. M. Teunis,	Company Supervisor, Jumbo Maritime
Date:	August 9, 2022	

Preface

Over the past nine months I received the opportunity to work on a very interesting and challenging subject. Throughout this period, things did not always go as expected, but in the end I am proud of the result, thankful to finish this adventure and eager to start a new one.

First and foremost I would like to thank Xiaoli Jiang. As my daily supervisor, you have guided me through tough times. I always enjoyed our meetings and drew motivation from these meetings, therefore I am glad that you were my daily supervisor. Also special thanks to Rudy Negenborn, as chair of my thesis committee, you have made me look critical at my own work and asked the right questions during our meetings.

Thanks to Jumbo Maritime for giving me the opportunity to set out my own project and work on a diverse topic in the offshore industry. Unexpectedly, after my literature project I needed to switch supervisors, luckily Jos van der Werf and Menko Teunis stepped up. I would like to thank you for always having time to support me and answer the endless stream of questions, I really enjoyed your supervision. Furthermore, the dynamic of having two company supervisors was ideal in my case because each of you helped me out with your expertise and knowledge, thank you for that.

Besides the supervisors, I would also like to thank Tiemen Hartmans, Krzysztof Jedruszek, Dimitar Stanchev, Ruben de Bruin and all other employees of Jumbo who answered my questions, helped me during my process or just had time for a nice conversation.

Lastly, I would like to thank my family and friends for their support over the past 9 months. In particular I would like to thank Yasmin, for being my biggest supporter and always being there for me.

Abstract

Offshore lifting operations must have reduced payload motion to increase safety and reduce operating time. When payload is retrieved from the splash zone to the deck, besides the crane block, no additional control can be applied on the underactuated system. Existing studies either assume more control over the payload or develop a control system based on a new crane. To reduce payload motion on current crane vessels, a conceptual model needs to be developed.

In this thesis, various state-of-the-art solutions are considered based on four criteria: Time reduction, motion reduction, initial investment required and power required. Eventually, the quantified criteria and an analytic hierarchy process established that the most promising concept is based on an automated side loader of a garbage truck.

The selected concept is developed based on a design process that focuses on optimized material usage. The geometry is determined according to requirements and forms the starting point of the circular design process. A dynamic analysis is conducted to obtain the dynamic response of the payload and eventually the reduced payload motion. The design cycle is complete after a finite element analysis has been conducted to verify the structural integrity of the model. After more than 20 cycles of the design process, the conceptual model is optimized and over 85% of motion is reduced in the X direction. The payload motion in Y- and Z-direction is 20% and 29% respectively.

The simulation results in this study show that the conceptual model is able to reduce the payload motion during offshore lifting operations whilst staying within the limits set by offshore standards. The motion reduction of the payload creates a safer and more efficient environment to execute offshore lifting operations.

Glossary

List of Acronyms

DPS	Dynamic Positioning System
ROV	Remotely Operated Vehicle
DOF	Degrees Of Freedom
RQ	Research Question
PHC	Passive Heave Compensation
AHC	Active Heave Compensation
PID	Proportional–Integral–Derivative
SHS	Special Handling System
AHP	Analytic Hierarchy Process
CR	Consistency Ratio
RAO	Response Amplitude Operator
FEA	Finite Element Analysis
CT	Constant Tension
BM	Benchmark
GR	Gripper
MPM	Most Probable Maximum
DNV	Det Norske Veritas

List of Symbols

Abbreviations

γ	peak enhancement factor [-]

γ_1	wave length [m]
ω	angular wave frequency [rad/s]
f_m	peak frequency [Hz]
H_b	Maximum wave height [m]
H_s	Significant wave height [m]
$H_{1/3}$	Significant wave height [m]
k_a	Axial stiffness gripper [N]
k_t	Torsional stiffness $[Nm^2]$
k_x	Bending stiffness in X direction $[Nm^2]$
k_y	Bending stiffness in Y direction $[Nm^2]$
L_1	Length of telescopic arm in load case 1 [m]
L_2	Length of telescopic arm in load case 2 [m]
L_3	Length of telescopic arm in load case 3 [m]
M_{bw}	Mass of balance weight [ton]
M_{cb}	Mass of crane block [ton]
M_p	Mass of payload [ton]
rho_s	Density steel $[kg/m^3]$
rho_w	Density water $[kg/m^3]$
S_ζ	Spectral Density $[m^2 s/rad]$
$S_{response}$	Spectral vessel response $[m^2 s/rad]$
T_p	Peak wave period [s]
V_p	Volume payload $[m^3]$
y_p	Y-coordinate payload [m]
y_{bw}	Y-coordinate balance weight [m]
A	Cross section surface of gripper $[m^2]$
d	Water depth [m]
E	Young's Modulus [Pa]
f	wave frequency [Hz]
G	Modulus of rigidity $[N/m^2]$
I	Moment of Inertia $[m^4]$
J	Polar moment of inertia $[m^4]$
k	Stiffness of the gripper [kN/m]
l	Length of payload
S	Spectral Density $[m^2/Hz]$
w	Width of payload

Table of Contents

List of Figures

List of Tables

Chapter 1

Introduction

1-1 Background

Global economic expansion has resulted in an increase in the demand for energy to meet the needs of people and industry. The depletion of easily accessible oil and natural gas fields has driven the industry offshore, where large floating platforms are used to extract, store, and process the retrieved goods. The wind energy industry is also moving offshore due to a lack of land. Both gray and green energy industries require heavy lift cranes to install their equipment. To reduce the cost of these installations, the limits at which offshore lifting operations are possible are pushed every day. Fast installation time and being able to lift during harsh circumstances are the two most important criteria to be competitive in the offshore installation industry.

Offshore cranes encounter more difficulties than land cranes with regard to the execution of lifting operations. Some of the difficulties the offshore cranes encounter at sea are high waves, sea currents and strong winds. These disturbances influence the Degrees Of Freedom (DOF) of the vessel that houses the offshore crane. Thus, offshore cranes experience more translations and rotations than land cranes due to the operational environment.

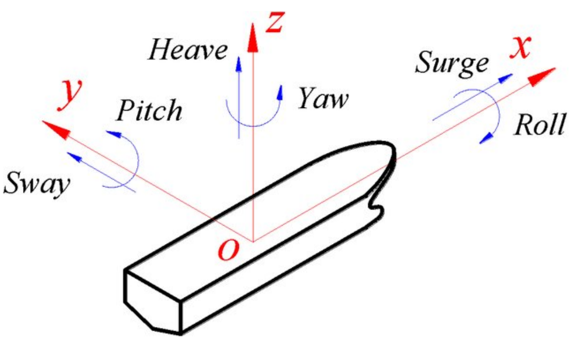

Figure 1-1: Degrees of freedom of a ship

Figure 1-2: Mast crane on offshore vessel

The environment-induced motions of the vessel cause uncontrolled motion of the payload that is lifted by the offshore crane in all DOF (See Figure 1-1). A swinging payload reduces the overall safety and efficiency of the offshore operation. Therefore, to maintain a safe working environment and complete operations efficiently, adequate reduction of motion is required to control the payload.

Jumbo Maritime uses mast cranes to execute offshore operations. This is the type of offshore crane shown in Figure 1-2. Typically, a mast crane is a system that is underactuated because there are more DOF than independent control inputs [Li et al., 2020]. Therefore, the swinging motion that occurs is hard to be controlled. Payload must be in control at all times to ensure

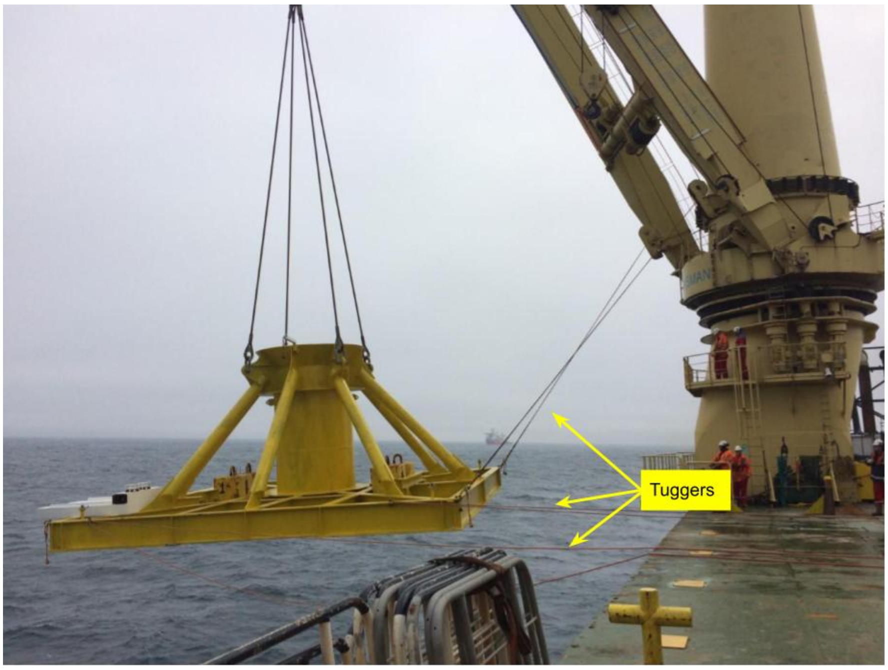

Figure 1-3: Example of payload that is retrieved using tuggers

safety during operations. When a payload is put overboard, one or multiple tuggers are used to control the payload. Tuggers are cables that are controlled by winches and are used to stabilize the motion of the payload (See Figure 1-3). In Lageveen [2014], van Wel [2021] and Wang et al. [2020], control systems with such tuggers are investigated. However, these studies only take into account the situation when the tuggers are attached. During the retrieval of a payload from the splash zone (i.e. the water surface) to the deck, no tuggers are attached yet. Therefore, an uncontrolled situation occurs when retrieving payload on board.

There are three solutions currently applied to deal with the occurring motion during the retrieval of the payload. First, the payload is lowered back into the water as soon as a swinging motion occurs. Second, a swinging motion occurs and the payload swings against the hull of the ship to damp and stabilize the motion there. And third, tugger cables are connected with an Remotely Operated Vehicle (ROV) before the payload leaves the splash zone. The third method is used as a benchmark for this study to compare the conceptual model developed with. Each of these methods leaves room for improvement, either with respect to safety or efficiency of the operation. Therefore, a safe and efficient solution that ensures reduced motion is required.

1-2 Research Questions

In order to approach this research structured, Klopper and Lubbe [2011] is used as a guideline. The first step consists of understanding the general problem that needs to be investigated. Next, sub-problems and sub-questions can be used to go further into detail. Each sub-problem corresponds to a specific set of sub-questions. Answering these questions will deliver the solution to their associated sub-problem. The combined solution for all solved sub-problems, should result in the solution for the general problem.

By applying the method mentioned above to this master thesis, the general problem of this research can be defined as follows:

> Mast cranes are commonly used to execute offshore lifting operations. Due to environment-induced motions, the payload of the crane can start moving undesirably. During the retrieval of the payload, reducing this undesired motion is vital for a safe and efficient lifting operation.

The main research question that accurately resembles this general problem is:

> How can a feasible conceptual model be developed to reduce payload motion during offshore lifting operations?

The following sub-problems are derived from the general problem:

1. Payload motion can be described in numerous ways and various factors can influence this motion.
2. Multiple industries need to deal with payload motion as a reoccurring problem in their everyday operations.
3. Nowadays, there is no effective solution to implement on existing mast cranes right away.
4. A great number of factors influence the concept development of a motion reduction concept.
5. Different approaches can be taken to optimize the most promising concept.
6. To optimize the conceptual model with various types of analyses, some significant assumptions are required.
7. Each type of analysis requires a different type of verification and validation.

After characterization of the sub-problems, the same number of research questions can be defined, while keeping them aligned with the sub-problems:

1. What theory and which factors are relevant for understanding payload motion in order to understand how to reduce it?
2. What are state-of-the-art solutions for motion reduction or motion compensation that are operational in industry or present in the literature?
3. Which of the state-of-the-art solutions can be translated to be applied on to mast cranes?
4. What selection criteria are important to conduct a concept selection for deriving the most promising concept?
5. What design process is required to optimize the conceptual model?
6. What assumptions are required for which analysis in order to optimize the conceptual model?
7. What research is required to verify and validate the various analyses that are done in this study?

1-3 Research Approach

A research approach is required to be able to answer each Research Question (RQ) stated in section 1-2. A graphical representation of the research approach is presented in fig. 1-4. It is observed that this study can be split up into two main parts. The first part (i.e. RQs 1 to 4) of the research consists of selecting the most promising concept. The second part consists of the development of the concept into a conceptual model (i.e. RQs 5 to 7). The results of the various analyses conducted in this study will be compared to the results of a current lifting operation. After this comparison has been made, it will be concluded if the developed conceptual model is indeed a feasible method to reduce payload motions during offshore lifting operations.

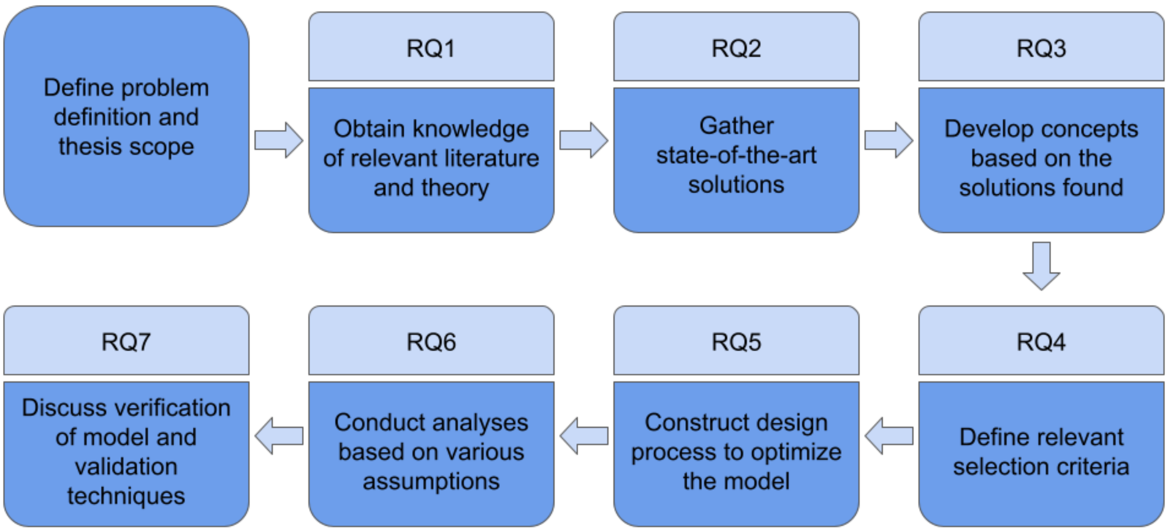

Figure 1-4: Graphical representation of research approach

1-4 Research Scope

The focus of this research is on reducing the payload motion of a single mast crane that executes a lift offshore. The vessel on which this thesis will focus will be the Jumbo Fairplayer (See Figure 1-2). The operational data that Jumbo maritime gathered throughout their projects is used as benchmark for this study. Since this data is validated, it is deemed to be accurate [Jumbo Maritime, 2022]. As this data is gathered from projects located in an ocean, the lifting operation that is analyzed also occurs on an ocean.

The lifting operation that is executed is determined to be lifted by the aft crane. Since this crane lies further from the center of mass of the vessel, its undesired motions will be larger compared to the front crane. The developed conceptual model is expected to endure loads from the front crane as well if the model is able to endure the loads from the aft crane.

The payload that is considered to be lifted is a pre-piling template (See Figure 1-3). This is considered one of the largest payload that are repeatably retrieved from the waterline [Jumbo Maritime, 2021]. Since this payload is heavy and its surface is large, the payload motion and its corresponding loads are considered to be the most extreme the system could experience. Thus, by selecting a pre-piling template, the model is determined to hold all other types of payload that have a smaller surface and/or weigh less.

1-5 Report Outline

The outline of this master thesis report corresponds to the research approach shown in Figure 1-4. First, the relevant theory related to reducing payload motion during offshore lifting operations from literature is discussed in Chapter 2. This includes a brief explanation of how the relevant factors for this study are described, such as environmental conditions and the definition of the payload. Furthermore, the state-of-the-art solutions, relevant selection criteria and the concept selection are discussed in this section as well. Subsequently, in Chapter 3 the methodology regarding the conducted analyses is proposed that are used to develop the conceptual model. This includes a dynamic analysis and a structural analysis with the proposed concept. The results obtained from these analyzes are presented and discussed in Chapter 4. To conclude, in Chapter 5, the final conclusions related to the results will be presented and the recommendations for further research will be suggested.

Chapter 2

Theory related to reducing payload motion during offshore lifting operations

In order to develop a conceptual model which is able to reduce payload motion during offshore lifting operations, sufficient knowledge about various topics related to this subject is required. First, the environmental conditions are touched upon, whereafter the vessel and crane motions are defined. Next, the payload is defined and the state-of-the-art solutions regarding motion reduction are presented. To finalize this chapter, various concept solutions are elaborated, and a selection procedure is provided to select the most promising concept.

2-1 Environmental conditions

During offshore operations, environmental loads influence the lifting operations. The environmental conditions influence the dynamics of the vessel, the crane and the payload. Below, the three main environmental loads are described.

2-1-1 Wave loads

Ocean waves can be generated by different sources such as tides and wind. There is no single mathematical solution able to represent all various wave types perfectly. However, there are various wave spectra that accurately represent a so-called sea state. A wave spectrum describes the distribution of wave energy with respect to the wave period. One of the most used spectra is the Pierson-Moskowitz spectrum (See Equation (2-1)).

$$S(f) = \frac{5}{16} H_{\mathrm{s}}^2 f_{\mathrm{m}}^4 f^{-5} \exp\left[-\frac{5}{4}\left(\frac{f}{f_{\mathrm{m}}}\right)^{-4}\right] \tag{2-1}$$

With the use of $f_m = \frac{1}{T_p}$ and $f = \frac{\omega}{2\pi}$ this equation is translated to Equation (2-2) which describes the wave energy spectrum in terms of wave height and wave period. H_s denotes the average of the highest 1/3 of the waves in a sea state, the notation $H_{1/3}$ is often used as well. T_p denotes the wave period with the highest energy and is derived as the inverted of the wave frequency.

$$S_\zeta(\omega) = 3060 * \frac{H_s^2}{T_p^4} * \omega^{-5} * \exp\left[-\frac{1948}{T_p^4} * \omega^{-4}\right] \tag{2-2}$$

This equation describes a fully developed sea. A sea is fully developed when the wind blows steadily over an area of hundreds of kilometers for several days. At this point, waves can travel hundreds of kilometers and they propagate independently from the wind. An ocean is an accurate example of a fully developed sea and therefore the Pierson-Moskowitz spectrum describes an oceanic sea state accurately.

Wave-induced motions can cause disturbances in all six degrees of freedom of the vessel. However, for this study, a vessel with a Dynamic Positioning System (DPS) is considered. This system enables station keeping of the vessel during offshore operations such as lifting and acts in the yaw, sway and surge directions [Jumbo Maritime, 2021]. Therefore, for this study, the vessel is only experiencing wave-induced motions in roll, pitch and heave motion.

For this study, the goal is to reduce the motion of the payload. This motion is influenced by the severity of a sea state. Some frequently occurring sea states are selected because they represent heavy sea states during offshore operations [Journee and Massie, 2001]. These sea states are stated by Jumbo Maritime as their operational limits based on data of recently executed projects [Jumbo Maritime, 2021]:

- $H_s = 2m$ & $T_p = 8s$
- $H_s = 2.5m$ & $T_p = 10s$
- $H_s = 3m$ & $T_p = 8s$

Figure 2-1 shows the wave spectra of the selected sea states. From left to right the plots are shown for ($H_s = 2m$ & $T_p = 8s$), ($H_s = 2.5m$ & $T_p = 10s$) and ($H_s = 3m$ & $T_p = 8s$). It can be seen there that with increasing H_s, there is more energy present in the waves. Moreover, the peak energy is gathered at $\frac{1}{T_p}$, thus the highest energy is gathered at that frequency.

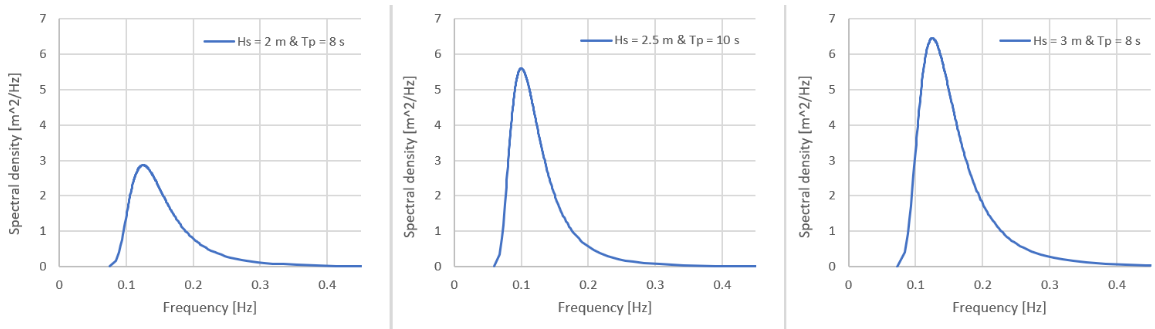

Figure 2-1: Wave spectra for selected sea states

2-1-2 Current loads

Currents affect all objects below the water surface. For offshore lifting operations, the loads mainly apply on the hull of the ship. Current loads are less fluctuating then wave loads and influence the station-keeping of the vessel. Since current loads can be controlled by the DPS of the vessel, their effect on the payload motion during lifting operations is determined to be negligible. Therefore, this study does not incorporate the effect of current loads on the designed system.

2-1-3 Wind loads

Above water, all objects are subjected to wind loads. The hull of the vessel, the crane and the payload all are subjected to these loads. Wind loads depend on the area normal to the wind flow direction and wind is usually characterized by large fluctuations in velocity and direction [Journee and Massie, 2001]. Wind loads tend to be small and thus, for simple design, the hydrodynamic loads are over-estimated and wind loads can be neglected [Journee and Massie, 2001]. Since this study focuses on the simple design of a conceptual model, wind loads are neglected.

2-2 Definition of vessel- and crane motion

The vessel is subjected to all the loads described in the previous section. The degrees of freedom of the vessel consist of three translations and three rotations. The three translations are:

- Surge is the longitudinal x-direction, positive forwards.
- Sway is the lateral y-direction, positive to port side.
- Heave is the vertical z-direction, positive upwards.

The three rotations are:

- Roll about the x-axis, positive right turning
- Pitch about the y-axis, positive right turning
- Yaw about the z-axis, positive right turning

In Figure 2-2, these DOF are shown. Here, the possible motions of the crane are shown as well. The slewing motion is used rotate the mast crane around the z-axis and allows the crane to locate the load from the sea towards the deck and vice versa. Luffing is used to alternate the angle of the crane boom. With increasing luffing angle, the moment of the load increases as well. Lastly, hoisting is used to change the vertical position of the payload.

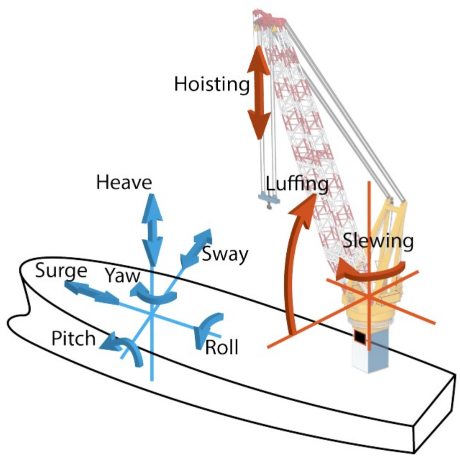

Figure 2-2: Definition of the degrees of freedom of the vessel and the crane motions [Buijs, 2017]

The response of the vessel depends on the energy density of the wave loads and the Response Amplitude Operator (RAO) of the vessel. The energy density is discussed in Section 2-1-1 but the RAOs of a vessel are not yet defined. An RAO is used to express the motions of a vessel in a certain sea state. This can be expressed for one particular DOF with one particular wave direction and wave period. The RAOs for the Fairplayer are already determined and validated by Jumbo Maritime and for each degree of freedom the RAOs are shown in Appendix C [Jumbo Maritime, 2022]. The response of the vessel can be calculated for each degree of freedom by combining Equation (2-2) with the RAO for that degree of freedom (See Equation (2-3))

$$S_{response}(\omega) = |RAO|^2 * S_{\zeta}(\omega) \tag{2-3}$$

The wave direction of the vessel is set at 165 degrees (See Figure 2-3). Ideally, the vessel wants to lie with its bow in the waves as the vessel absorbs wave motion best in its longitudinal direction. This is equal to a wave direction of 180 degrees. As waves are not always coming directly into a straight line at the vessel, any dynamic analysis should take into account ± 15 degrees in the distribution of the wave direction [Journee and Massie, 2001]. Therefore, 165 degrees is considered to be the wave direction throughout this study. Thus, the RAOs shown in Appendix C are determined for a wave direction of 165 degrees.

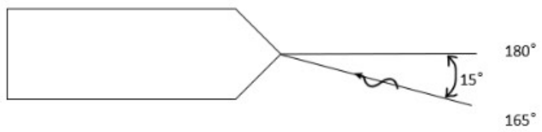

Figure 2-3: Wave direction

2-3 Definition of the payload

The payload that is lifted by the crane can be considered as a double pendulum as the payload and crane block both experience influence of the motion of the vessel. The scope of this study, as stated in Section 1-4, is to consider a pre-piling template to be the payload (See Figure 1-3), since the payload that is considered in this study must be valid for all types of payload. The forces that waves apply on the payload are dependent on the size of the payload. To maximize these forces and take into account a realistic but worst-case scenario, this pre-piling template is simplified to be modeled as a plate of 10 by 10 meter with a height of 1 meter [Jumbo Maritime, 2021]. In Figure 2-4, an example of such a lifted payload is shown. The clearances and crane wire lengths used are according to Det Norske Veritas (DNV) standards.

For this study, the lifted weight that is considered is lower than 1% of the displacement of the crane vessel, for the Fairplayer this is equal to 200 ton. This limit may not be exceeded because this is considered to be the limit for light lifts [Det Norske Veritas, 2011]. Remaining below this limit will ensure unaffected motion characteristics of the vessel at the crane tip due to the lift. The payload that must be lifted is hanging in a crane block and both the payload and the crane block are influenced by the occurring vessel motion. Since the crane block weighs 15 ton, the mass of the payload must be smaller than or equal to 185 tons [Jumbo Maritime, 2021].

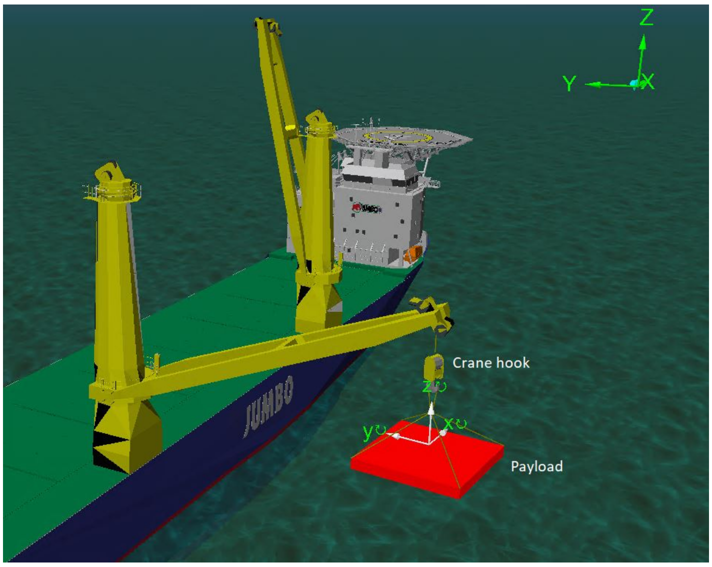

Figure 2-4: Double pendulum offshore crane

2-4 State of the art for motion reduction or motion compensation

Reduction or compensation of motion in lifting operations is considered in a number of researches over the years. Some studies describe systems that completely cancel out any motion, others only cancel out a single DOF. For each type of motion reduction or motion compensation there exists a certain state-of-the-art technique, these are introduced below.

Heave compensation
Heave compensation is used to decouple the load motion from the heave motion of the vessel, regardless of the type of heave compensation [Woodacre et al., 2015]. In general, there are two types of heave compensation: Passive Heave Compensation (PHC) and Active Heave Compensation (AHC).
PHC does not require energy as input in order to function and is designed to maintain a constant line tension. In principle, air or another gas acts as a low-rate spring as it is compressed by a piston. The restricted flow of this gas through the orifices acts as a damper thus, the PHC acts as a spring-damper system. In general PHC has a lower percentage of the heave compensation than AHC does but they come at a lower price. Active heave compensation, contrary to passive heave compensation, requires energy input to compensate the heave motion of the vessel. Closed-loop control ensures that when a vessel heaves upward, the load moves downward the same amount. AHC can be powered either hydraulically or electrically and often requires the use of an inertial measurement unit. These devices can be expensive due to gyroscopes and three-axis accelerometers, but cheaper alternatives are being developed using low-cost GPS receivers [Blake et al., 2008]. In order to decide whether an application requires AHC or PHC, a trade-off between costs and performance must be made.

Anti sway control

During crane control by the operator, an anti sway controller can use fractions of the input velocities of the operator to cancel out oscillations. This can be achieved by moving the crane in the direction of the load sway to dissipate energy from the system [Van Albada et al., 2013]. Depending on the sea state, the fraction at which the controller intervenes can be adjusted. There are already active applications for anti-sway control in the industry. Some examples are Siemens [2016], CMCO [2016] & KoneCranes [2016]. These companies mainly focus on gantry cranes or overhead cranes. As the geometry of gantry and overhead cranes allows for better kinematic description. Therefore, the number of publications related to these cranes is relatively high compared to those of the mast cranes [Ramli et al., 2017]. However, Liebherr [2014] already developed a land-based crane, that has a similar geometry to the mast crane, which is able to move a load without swing. All these anti-sway control applications focus on single pendulum motion, but several studies already take into account double pendulum motion as well such as [Li et al., 2020] and [Sun et al., 2018].

3D motion compensated cranes

In the industry, a considerable amount of 3D motion compensated cranes are already being used. It is noteworthy that most cranes use different techniques to achieve motion compensation.

Figure 2-5: Ampelmann E5000 [Ampelmann, 2019]

The E5000 of Ampelmann (see Figure 2-5) uses six actuators to make sure the base of the crane is not affected by the motion of the vessel [Ampelmann, 2019]. The down side of this system is that its maximum lifting capacity is 5 tons, making it not qualified for lifting offshore equipment and more suitable for offshore cargo handling.

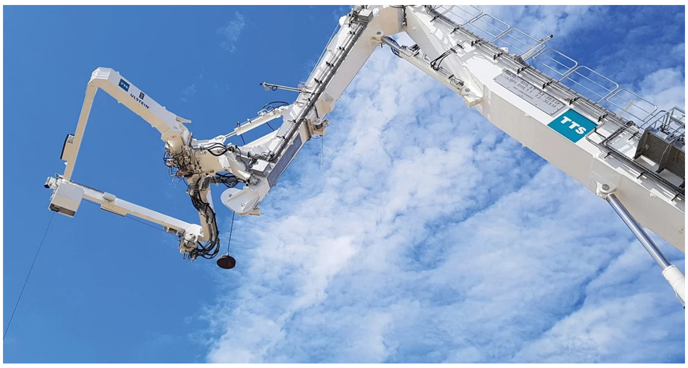

Figure 2-6: MacGregor Colibri [MacGregor et al., 2018]

Figure 2-7: Large Vessel Interface Lift On/Lift Off [Oceaneering, 2013]

A different approach is taken by multiple companies, both Red Rock [2020] and MacGregor et al. [2018] have a similar working principle to provide 3D motion compensation (See Figure 2-6). Opposed to Ampelmann, these cranes reduce the compensated mass to a minimum by only compensating the tip of the crane. The maximum lifting capacity is, with 10 tons equal to, twice the capacity of the crane of Ampelmann while cranes require less power to compensate for the motion. Oceaneering [2013] has an application that combines the concepts of Ampelmann and MacGregor. Six actuators at the crane tip are used to compensate for the motion of the vessel (see Figure 2-7). This solution can carry up to 18 tons, but at the moment it is only suitable for containerized cargo.

Lastly, there exists a method to compensate 3D motions with an offshore crane using a telescopic arm. Both MacGregor [2014] and SMST [2016] developed a crane based on this working principle. Figure 2-8 shows the 3D motion compensated crane of SMST. The maximum lift capacity of this crane is 20 tons.

The above-mentioned cranes are state of the art when it comes to motion compensation, however these cranes can not hold a solution for mast cranes. First, the lifting capacity of these cranes is roughly one-tenth of the required capacity for offshore lifting operations. Second, the geometry of these solutions does not allow implementation on an existing mast crane. Thus, different 3D motion compensated cranes can lift small cargo safely but are not suitable for the offshore lifting operations that are considered in this study.

Figure 2-8: SMST 3D motion compensated crane [SMST, 2016]

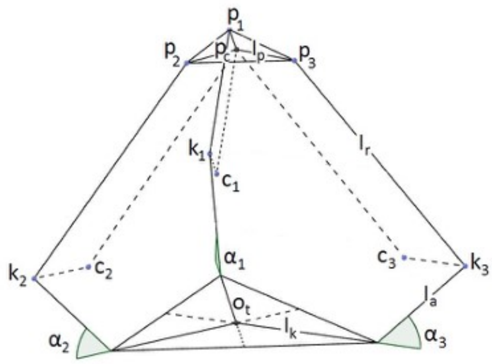

Figure 2-9: Delta parallel robot [Henriksen et al., 2016]

Delta parallel robot

In addition to new crane configurations, there is also a study that aims to adjust the crane head to compensate for the motion of the vessel. This, so-called delta parallel robot, compensates the motions of the ship in three axis [Henriksen et al., 2016]. In order to do so, the robot uses Proportional–Integral–Derivative (PID) controllers to control the crane head. The rigid structure is highly nonlinear, requiring advanced control algorithms, therefore the kinematics for the delta parallel robot are analysed and modeled (See Figure 2-9). The disturbances on the system are used in the compensation procedure with the help of translating and rotating the crane head frame of reference. Although this study shows promising simulations, suspended load is not taken into account. In the study, the researchers identified a tool center point and the workspace requirements are to keep this point still. However, the suspended load is not yet included; thus, in order to move the payload safely, the workspace requirements need to be altered accordingly, perhaps resulting in different results. Although this design seems promising, implementation on an existing mast crane is not possible, since the geometry of the crane does not allow this.

Special Handling System (SHS)

Axtech [2015] has built a system that is able to launch and recover equipment up to 420 tons (See Figure 2-10). It uses a hydraulic winch and vertical rails to guide the equipment through the splash zone while minimizing the accelerations, velocities and amplitudes acting on the lifted equipment [Dahle et al., 2016]. The downside to this system is that is only able to reach 400 meter water depth. However, both the lifting capacity and the geometry of the system are promising. The rails with its heave compensated basket could be integrated with the geometry of the mast crane in order to achieve a motion compensated system on the Fairplayer.

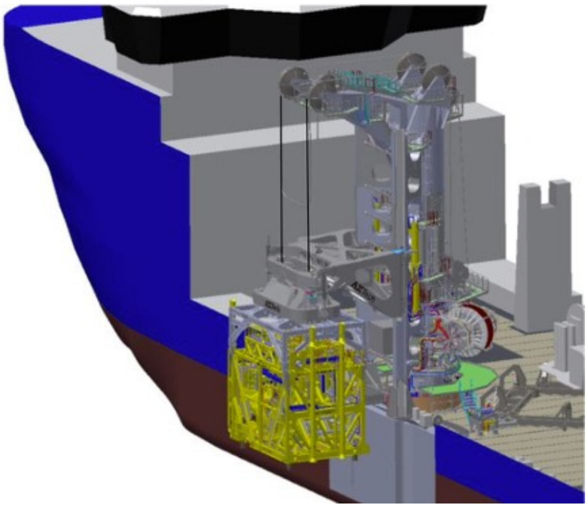

Figure 2-10: SHS Axtech in action [Dahle et al., 2016]

Gyroscopic stabilization

Gyroscopic stabilizers are used to stabilize the rolling motion of a ship. This is currently applied on luxurious yachts. These ships have a gyroscopic flywheel on board from companies such as Seakeeper. The flywheel is placed in a vacuum sphere and rotates to counteract the rolling motion of the ship. The angular moment of the flywheel and the angular velocity vector around the precession axis create a stabilizing torque. This torque is applied on the ship to keep the oscillatory amplitude of the ship to a minimum [Pongduang et al., 2021]. This process is shown schematically in Figure 2-11. Additionally, the flywheel requires a small amount of power because it is located in a vacuum.

Besides stabilizing vessels in roll motion, gyroscopes are also used to stabilize lifting operations. Verton Technologies developed a lifting beam that uses gyroscopic technology to stabilize a lifted object. In Figure 2-12, one of the lifting solutions of verton is shown. Within the lifting beam, several gyroscopes are placed to counteract the rotational motion during a lifting motion. Such products make tuggers or other lines redundant while still ensuring safe lifting.

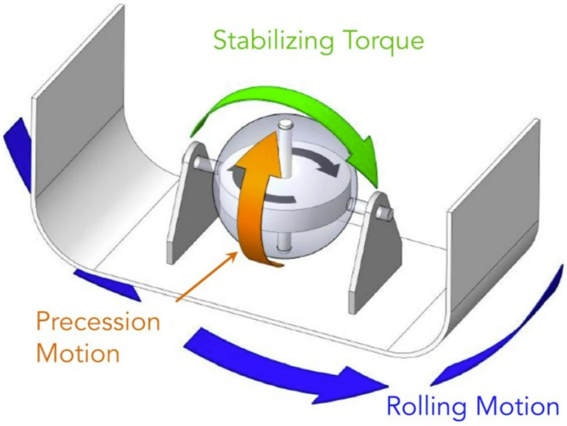

Figure 2-11: Gyroscopic stabilizer principle [Giallanza and Elms, 2020]

Figure 2-12: Everest 6 [Verton Technologies, 2019]

Automated side loader

Lifting objects does not always include the usage of a crane. For example, the waste management industry has some innovative solutions for efficiently emptying garbage bins. Nowadays, garbage truck drivers do not need to exit their vehicle to empty a garbage bin. They use an automated side loader that does the work for them. In Figure 2-13, an automated side loader is shown.

Figure 2-13: Automated side loader HEIL[Raymax Equipment, 2020]

Automated side loaders have various configurations and multiple studies are related to the optimization of these side loaders. In Altare et al. [2016], intelligent flow control is used to optimize the side loader arm. Optimization is done regarding control of the arm, efficiency and productivity (i.e. cycle times). Other studies focus to optimize the accuracy of the trajectory of the arm and the smoothness of its motions [Yi and Liu, 2017]. Minimizing the deviation of the trajectory of the key point and the standard deviation of the angular velocity of the garbage bin are optimization targets. Parameters such as arm length are used as design variables in order to optimize the model. This solution is promising since this is a robust design that can be applied on an offshore vessel.

Concepts with potential

Several operative solutions and promising studies related to motion reduction or motion compensation are discussed in this section. Some of these systems could be developed into a promising and suitable concept for existing mast cranes of the Fairplayer. However, due to the focus of this study, not all state-of-the-art solutions can be translated to fit on a mast crane. The concepts with potential and the execution of the selection process are explained in Section 2-5.

2-5 Concept selection

The concepts considered in this study are discussed in Section 2-5-1. To be able to select the most promising concept, certain selection criteria are required. The relevant selection criteria are elaborated in Section 2-5-2. Based on the selection criteria, the concepts are graded with the help of a selection procedure, Section 2-5-3 explains this procedure and its results.

2-5-1 Concepts

The goal of this study is to design a conceptual model that is able to reduce the motion of the payload that hangs from the crane wire. This goal can be reached by concepts from several categories.

The first category is damping the motion. Second, modifying the lifting path could hold the best concept solution. The third and last possible category to reduce the motion is to attach a tool. Besides different categories, the concepts also come in different forms. Hardware, software and hybrid are the three forms that are possible for the concepts. Below four concepts with potential are explained and their form and category are mentioned as well:

- **Control system:** This concept belongs in the category 'damping the motion' and the solution would come in a software form. The idea is based on the already existing sway control systems that are applied on the land crane control solutions. As soon as the payload starts to swing, the control system should adapt and damp the motion by strategically positioning the crane tip with respect to the payload.
- **Gyroscopic stabilizer:** The gyroscopic stabilizer is based on a combination of the products of Seakeeper and Verton Technologies. This hybrid concept also damps the motion in order to reduce it. The working princple of this technology is based on a gyroscope that is installed between the crane and the payload on the crane wire. This solution also requires a software part, since the gyroscope requires control to rotate at a certain speed in a specific direction depending on the occurring motion.
- **Rails with support basket:** The general principle of this concept is based on the SHS that AXTech developed (See Figure 2-10). The rails would be installed on the side of the hull of the ship. An active heave compensated basket would be guiding the crane block and a payload through the splash zone and back. The concept would modify the lifting path since the payload can only be lowered through the guided basket. It would be a hybrid solution since the basket needs to have active heave compensation that requires a certain control mechanism as well.
- **Automated side loader:** For this concept, innovative applications from a different industry are used. As explained, the waste management industry uses automated side loaders that grab garbage bins and empties the bins in the garbage truck (See Figure 2-13). For this concept, the crane wire would still carry the payload, however the automated side loader would prevent any uncontrolled motion of the payload. This concept would attach a tool to reduce the motion and can be classified as a hybrid solution. The arm is the hardware but a software control system is needed to have communication between the lifting path of the crane and the guidance of the arm.

2-5-2 Selection criteria

In order to select the concept with the most potential, some selection criteria are required. These criteria need to be quantified for each concept and they consist of important factors that are required to achieve the goal of this study. With the help of a selection procedure (see Section 2-5-3), these criteria are weighed against each other and then the most promising concept is selected. Below, the four selection criteria are discussed:

Time: Time plays a vital role when it comes to executing lifting operations efficiently. Every minute an offshore operation lasts longer, costs 85 euros. This price is based on the daily rate of the Fairplayer including crew and equipment. The benchmark for the concept is based on the duration of the connecting of the tugger lines. An ROV requires 30 minutes to connect the tugger lines, so at most 30 minutes per lifted object can be reduced [Jumbo Maritime, 2021]. The actual lifting is not considered for these 30 minutes since this needs to happen either way, therefore the focus is solely on making the connection.

Motion: The root cause of this study is the motion of the payload. In order to execute a lifting operation safely, the uncontrolled motion needs to be reduced. This is expressed in percentages since motion occurs in several directions. The percentage at which this motion might be reduced when one of the concepts is applied is an important criterion. For each concept, when the amount of motion reduced is equal to 100%, the payload is not moving.

Initial investment: Where time could be considered part of operational costs, capital cost is also an important selection criterion. The initial investment that is required is determined in euros. The costs that are taken into account are required to manufacture the concept. The costs required to develop the concept are not taken into account.

Power: Every concept requires a certain amount of power to reduce the motion. The required power can be seen as another part of operational costs, but the required power will be expressed in kilowatts. The source of this power is not taken into account when determining the initial investment. Moreover, the operational costs for the power requirements are not calculated either since the ratio of power of each concept satisfies as a clear selection criterion itself.

Quantifying the criteria

The criteria that are selected, need to be quantified for each concept of Section 2-5-1. In Table 2-1 the quantified criteria are shown for each concept. Reasoning regarding the values is provided below.

Table 2-1: Criteria quantified per concept

	Time reduced [min]	Motion reduced [%]	Initial investment [€]	Power required [kW]
Control system	30	95	2.000.000	270
Gyro stabilizer	30	50	400.000	6
Rails with support basket	30	95	2.000.000	825
Automated side loader	20	95	100.000	40

The time that can be reduced per lifting operation is determined to be 30 minutes for three of the four concepts. The automated side loader is estimated to reduce only 20 minutes since the automated side loader must be attached to the payload. Contrary to the other concepts that are permanently ready to act.

Regarding motion reduction, three of the four concepts are determined to reduce motion by 95%. There are concepts based on the same working principles already operating in the field thus this is determined to be true for a conceptual model as well. There is a 5% buffer taken into account for stiffness of the hardware solutions and responsiveness of the software solutions. The gyro stabilizer is estimated to reduce motion by only 50%. In operational solutions, gyroscopes currently only prevent rotational motions. Although Verton Technologies is working on a concept that could reduce translations as well, no studies are currently available regarding this subject. Therefore, due to the uncertainty of translation reduction, only the three rotations are presumed to be canceled out and thus only 50% reduction of the motion is determined.

When determining the initial investment, some estimations are done based on similar solutions that are already operational. The control system would require a new electric drive and according to an expert from Huisman this is roughly 2 million euros [Huisman, 2022]. When changing the electric drive, it is noteworthy that larger motors might not be geometrical feasible. If that is the case, a new crane is required, which will cost 8 million according to an expert at Jumbo Maritime. The gyro stabilizer of Seakeeper, which has a capacity of 100 tons, has a retail price of 300.000 euro. Together with additional costs for installation this concept has an estimated value of 400.000 euro. Regarding the rails with support basket, the SHS of AXTech is used as a comparison. The entire system was valued at 17 million euros. However, implementation of this concept does require only the rails with the heave compensated basket. It is estimated that this roughly equals one-eight of the total cost resulting in roughly 2 million euros. Lastly, the costs for the automated side loader are estimated. An entire garbage truck can be bought for approximately 100.000 euros. It is estimated that the automated side loader consist of one-tenth of that price. Furthermore, the side loader should be scaled by a factor of 10 for this application. Thus, the overall investment for the automated side loader is roughly 100.000 euros.

The power required is calculated for all concepts on the basis of known values from similar solutions that are already used in the industry. For applying the control system, an expert from Huisman provided the power requirements that such a system would require [Huisman, 2022]. In total, this adds up to roughly 270 kW. The gyro stabilizer has, due to the vacuum sphere, a very low power requirement. Based on the product of Seakeeper with similar capacity, only 6 kW is considered to be sufficient. The SHS of AXTech requires up to 3300 kW at full capacity, however, only a third of the capacity is needed for this application [AXTech, 2015]. Thus, roughly 825 kW is required for the rails with the support basket. Lastly, the automated side loader uses hydraulics to operate. The power is calculated based on the required fuel flow, the pressure within the system and the scaling factor to scale the side loader to the required size. This results in a power requirement of approximately 40 kW.

2-5-3 Selection procedure

The selection procedure that is used for selecting the concept with the most potential is the Analytic Hierarchy Process (AHP) from Saaty [1987]. This process is a multi-criteria decision-making method that uses pairwise comparison between concepts and criteria. First, the hierarchy of the decision should be clear (See Figure 2-14). This process descends from the goal, down to the selection criteria and finally to the alternatives that represent the concepts.

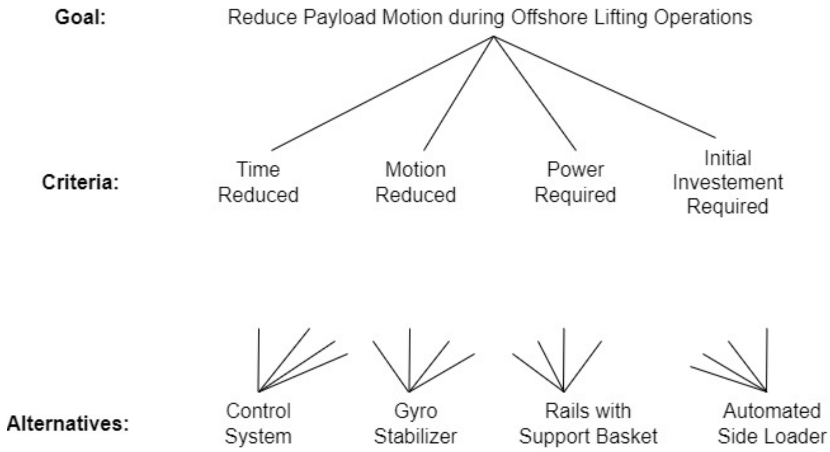

Figure 2-14: AHP Diagram

The pairwise comparison is conducted five times. Once to compare the criteria versus each other and four times for comparing each alternative regarding a criterion. In Table 2-2 the scale at which the comparison is conducted is shown. If two concepts are compared to each other an both are of equal importance, then both receive a one. Similarly, if concept A is of extreme importance over concept B then A is assigned a 9 and B the reciprocal value (i.e. 1/9).

Table 2-2: The fundamental scale of AHP [Saaty, 1987]

Intensity of importance on an absolute scale	Definition
1	Equal importance
3	Moderate importance of one over the other
5	Essential or strong importance
7	Very strong importance
9	Extreme importance
2, 4, 6, 8	Intermediate values between two adjacedent judgements
Reciprocals	In the matrices pairs occur twice, the reciprocal value of the number assigned to one half of the pair needs to be placed at the other half

The pairwise comparison for the selection criteria is shown in Table 2-3. It can be seen that the motion reduced is of extreme importance when compared to the power required. Time reduced is of essential importance over power required and so on. The assigned values are based on the prerequisite that Jumbo Maritime deemed to be more important.

Table 2-3: Selection criteria pairwise comparison

	Time reduced	Motion reduced	Initial investment	Power required	**Criteria weights**
Time reduced	1	1/3	2	5	**0,237**
Motion reduced	3	1	4	9	**0,563**
Initial investment	1/2	1/4	1	4	**0,151**
Power required	1/5	1/9	1/4	1	**0,049**

CR = 0,02291

The matrix is solved for the principal eigenvector and the result is normalized. Thereafter, the relative weights are obtained from the matrix and these are displayed in the last column of Table 2-3. The most important selection criterion is the motion reduced with 56,3%. The time reduced (23.7%) and the initial investment required (15,1%) are second and third respectively. Lastly, the power required only represents 4,9%, making it the least important selection criterion.

When comparing criteria or alternatives with the AHP, it is important to look at the consistency at which the process is conducted. According to Saaty [1987], it is acceptable to have an Consistency Ratio (CR) of 10% or lower. The rate is determined according to the standards that are set by Saaty. The essence of the CR is that every comparison in the matrix has a relationship with the other comparisons. The question is whether the comparison is conducted consistently throughout the entire process. The selection process becomes less subjective if the consistency ratio adheres to the limit of 10%. Below Table 2-3 the CR is shown and is equal to 2,29%, which is sufficient.

The alternatives (i.e. the concepts) are compared separately for every selection criterion. These comparisons are displayed in Appendix B. The grades are assigned based on the quantified selection criteria of Table 2-1 and in accordance with the AHP standards. The last column of each table represents values that are scored and normalized for each alternative related to that criterion. In Table 2-4, all these columns are merged into one matrix. These values are multiplied with the criteria weights to reach a weighted sum value. This value represents the final score and thus which alternative complies best with all criteria in order to reach the goal.

Table 2-4: Overall weighted matrix

	Time reduced	Motion reduced	Initial investment	Power required	**weighted sum value**
Control system	0,300	0,308	0,064	0,083	**0,258**
Gyro stabilizer	0,300	0,077	0,221	0,587	**0,176**
Rails with support basket	0,300	0,308	0,064	0,049	**0,256**
Automated side loader	0,100	0,308	0,652	0,282	**0,309**

Out of the weighted matrix, it can be seen that both the control system and the rails with support basket lose out because of their high initial investment. The gyro stabilizer loses out because of its lack of motion reduction. Furthermore, it can be seen that the most preferred method to reduce payload motion during offshore lifting operations is the automated side loader with a score of 0,309. Therefore this concept is considered to be the most optimal concept to reduce payload motion during offshore lifting operations. The next chapter will discuss the required methodology for developing this concept into an accurate conceptual model.

Chapter 3

Methodology

In the previous chapter, the theory related to reducing payload motion during offshore lifting operations is discussed. First, the environmental conditions consisting of wave-, current-, and wind loads are discussed. Next, the vessel- and crane motion is defined, as is the payload. Then the state-of-the-art solutions that are available for reducing payload motion were shown. In addition, concepts are selected out of the available solutions. To conclude, an AHP is used to select the most promising concept to reduce payload motion.

The automated side loader, that was selected in the previous chapter to be the most promising concept, needs to be developed into a conceptual model. A methodology is required to accurately model this concept.

The design process required for concept development is discussed in Section 3-1. The requirements from Jumbo Maritime and offshore standards are discussed in Section 3-2. The geometry that is based on the requirements is discussed in Section 3-3. Section 3-4 elaborates on the dynamic analysis that has been conducted. Lastly, the structural analysis is discussed in Section 3-5.

3-1 Design process

The first step in developing a conceptual model for the automated side loader is constructing the appropriate design process. This process is needed to develop a feasible model. Furthermore, this process is used to optimize the gripper and to define when it is optimal and with respect to what. In Figure 3-1 the flowchart of the design process is shown. The process is circular because with each rotation, the conceptual model will be closer to its optimized end result.

First, the requirements are established based on offshore guidelines and design requirements of Jumbo Maritime. These requirements do not change per rotation in the design process but they need to be met either way. They are defined in Section 3-2 and based on these requirements a first geometry is configured.

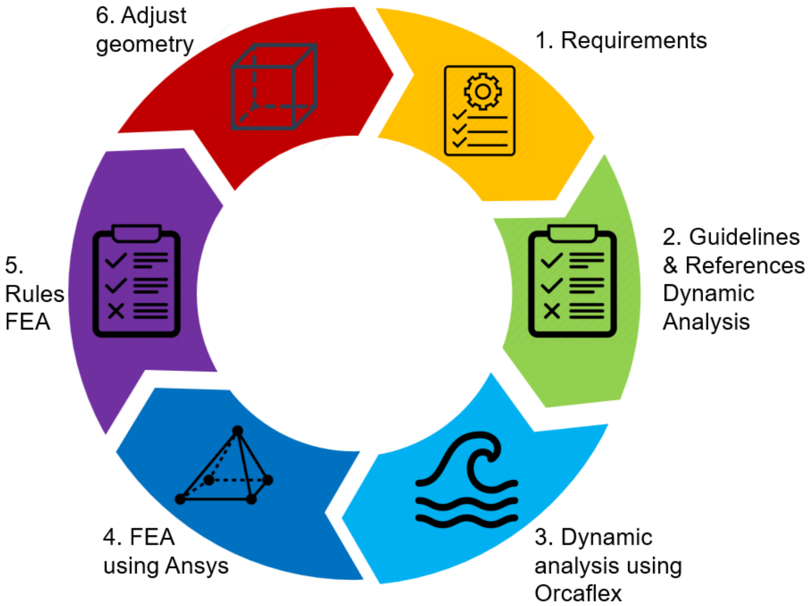

Figure 3-1: Flowchart design process

The next step, guidelines and references for the dynamic analysis, is also independent of the number of rotations in the design process. Based on the guidelines of DNV and references of relevant literature the benchmark for the dynamic analysis is set. Yet, for each rotation, the concept needs to comply with these guidelines and references.

In the third step, the dynamic analysis is conducted, this is done with the help of Orcaflex. This analysis needs to be adjusted per cycle in the process as the model has an updated geometry each cycle. This influences the dynamic analysis as well, thus change is required. The dynamic analysis is used to retrieve loads that will act on the automated side loader, these loads are used as input for the next step.

With the help of a Finite Element Analysis (FEA), the loads are applied on the automated side loader in the adjacent stage. Ansys is used to conduct this FEA. Similar to the dynamic analysis, this stage changes per cycle, since the geometry is updated.

Next, the rules regarding FEA are compared to the results of the FEA and this step is the measuring point to determine whether the model is feasible and optimized (See Figure 3-2) . If the results, (i.e. deformations and stresses) within the model are higher than the allowable results according to the rules, the model is not feasible and the design process continues. On the other hand, if the results comply with the rules, it does not necessarily mean that the model is optimal. In order to optimize the model, the material usage should be minimized whilst remaining within the limits stated by the rules. The model is considered optimal if it complies between 80 and 100% of the allowable results. For example, the thickness of the geometry can be adjusted to reduce the material usage such that the model has results that are at least 80% of the limiting rules for these results. Note that the rules are superior over the material reduction, first the FEA must meet the allowable deformations and stresses. Then, the material reduction is taken into account. This means that it might be possible that the stress is between 80 and 100 % of the allowable stress but the deformation is at 50 % of the allowable deformation criterion and vice versa. The limit of 80% is set in accordance with Jumbo Maritime as there exists no clear rules for when something is considered optimized. Setting an 80% limit is deemed to be high enough to yield an optimized solution and low enough to yield a feasible solution.

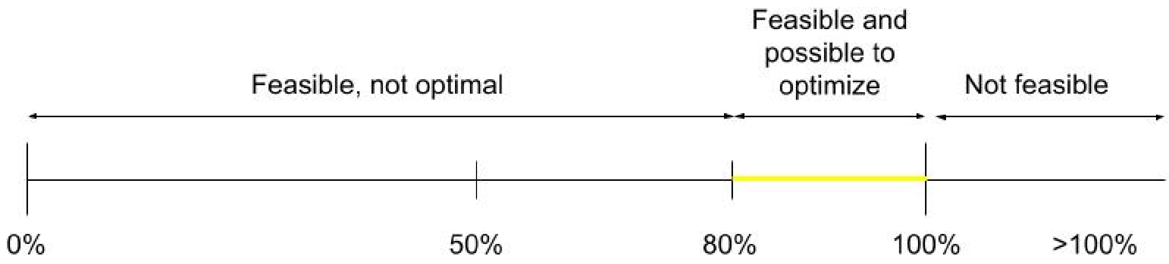

Figure 3-2: Scale for design process based on percentages of allowable limits

Finally, if the FEA results do not comply with the FEA rules or if none of the results are within 80% of the rule limits, the geometry of the model is adjusted. This completes the cycle and means that another repetition is necessary. The process only stops if the model complies with the rules of the FEA and is within 80% of the allowable deformations and/or stresses for example. The model is optimized regarding the material usage as a lighter model means a lower initial investment and lower power requirements. Both these criteria are considered important as stated in Section 2-5.

3-2 Requirements

The concept that is selected in Section 2-5 needs to adhere to certain requirements. These requirements are based on offshore guidelines and design requirements stated by Jumbo Maritime. Together with the selected concept of Section 2-5, they form the starting point for a conceptual model. Below the requirements are listed:

- As mentioned in Section 2-3, the weight capacity of the payload and the crane block is 200 tons. This is the maximum value for which the concept needs to be able to reduce the payload motion during offshore lifting operations.
- The minimum horizontal clearance that is required between the lifted payload and the hull of the ship is 5 meters. This is based on the DNV standard for lifting operations that ensures safe lifting operations [Det Norske Veritas, 2014]. This area is indicated by the red lines in Figure 3-3.
- The reach of the model should match the reach of the crane. In Figure 3-3, the minimum required reach of the model is indicated with the yellow lines. Horizontally, the concept should be able to have a reach between 10 and 35 meters measured from the center of the crane. Vertically, the model should be able to reach at least 2 meter below the waterline and reach the deck of the vessel.

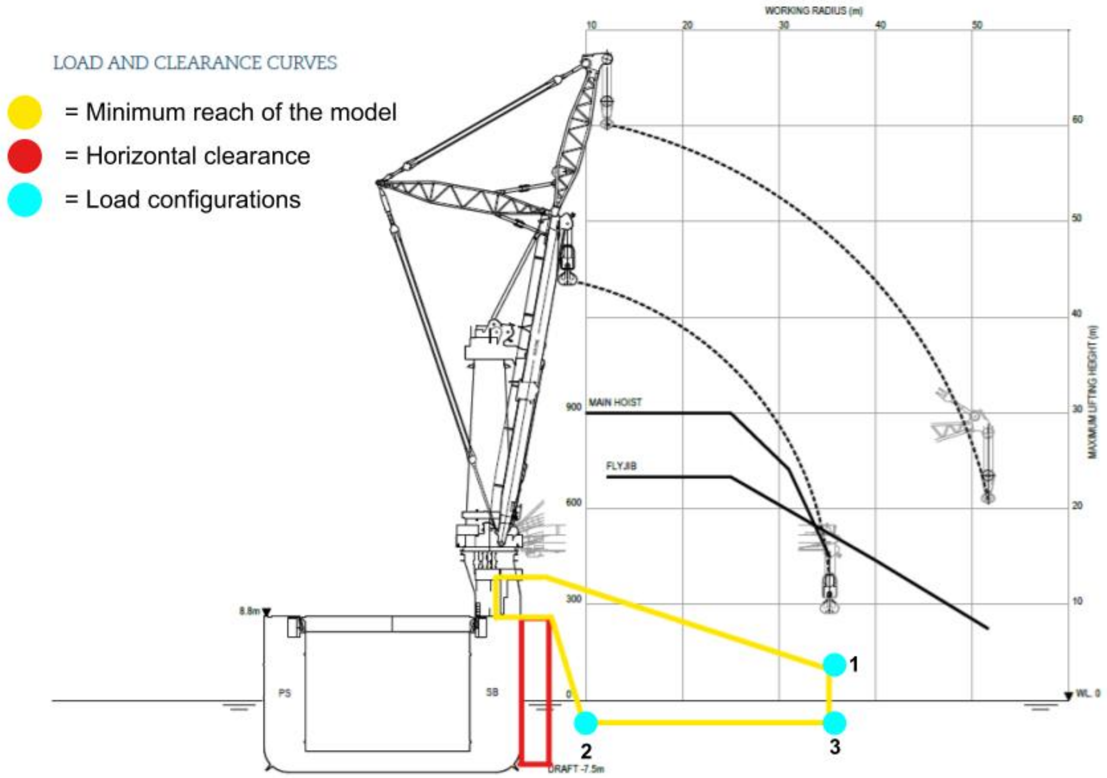

Figure 3-3: Required reach of the model

Load configurations:
The required reach of the model is considered as the limits at which the model will operate, therefore this reach is analysed by selecting three load configurations (See Figure 3-3). These load configurations are selected because they are located at the boundary of the required reach. Therefore, it is determined that these load configurations represent the limiting states of the automated side loader and they endure different load cases at different configurations. To complete an accurate analysis, these three load cases need to be analysed.

1. The first load configuration has the biggest arm while not enduring any forces from the waves. Only gravity and the swinging payload act on this load configuration. This configuration contains the swinging payload motion that needs to be reduced.
2. The second load configuration has to endure the gravity and forces from the payload at a steep angle close to the vessel. But contrary to load configuration 1, this configuration has to deal with the waves acting upon the payload as well.
3. The third load configuration has a fully extended arm. This load case will be considering the same loads as the second load configuration (i.e. gravity, forces from the payload and wave loads). However, due to its longer moment arm, this load configuration needs to endure more extreme conditions than the second state.

3-3 Geometry

Based on the requirements of Section 3-2, a geometry can be configured. This geometry is configured based on the selected concept of Section 2-5 and these requirements. The geometry is modelled in Solidworks and the most important parts of this model and the made design choices are discussed below.

Telescopic arm:
In Figure 3-3 the minimum required reach of the model is shown. The automated side loader needs to be able to reach all the boundaries of the required reach. The required length to reach all the boundaries of the required reach is determined with Pythagoras as shown in Equation (3-1).

$$\text{Length of arm} = \sqrt{\text{horizontal reach}^2 + \text{vertical reach}^2} = \sqrt{35^2 + 15^2} = 38 \text{ meter} \tag{3-1}$$

However, it would be inconvenient to have an automated side loader with an arm that is permanently 38 meter long. In Altare et al. [2016], an automated side loader is shown with a telescopic arm, this is a solution to overcome the design problem. This telescopic arm is hydraulically actuated and is scaled up compared to the arm of the garbage truck. The 3D model of the telescopic arm is shown in Figure 3-4.

Figure 3-4: First 3D model telescopic arm

The telescopic arm consists of one non-extendable part and multiple extendable parts. The length of the non-extendable part is set to 9 meters. This is selected because it guarantees the clearance between the gripper mounting and the payload.

The extendable part needs to cover the other 29 meter of required arm length. For the conceptual model this part is divided into three pieces as this divides each section in an equal length. Furthermore, this will enable every section to be pulled into the non-extendable section. The thickness of each smaller section fits perfectly in the previous section as each section has the same plate thickness.

For the finite element analysis the model will be split up into two sections, the extendable and the non-extendable section. This simplifies the model and enables for analytical verification (See Section 3-5-1).

Besides the length of the sections, cross sections are defined as well. For the first dimensions of the cross section an educated guess is used. Circulating the design process described in Section 3-1 results in appropriate dimensions for the cross section. The final dimensions of the cross sections are shown in Section 4-1.

Mounting to deck:
The automated side loader of Altare et al. [2016] is attached to a garbage truck and this attachment is the backbone of the system. This automated side loader concept also requires such a central connection point, this is the mounting to deck. This mounting is attached to the slewing support, the telescopic arm and the hydraulic actuator. The height of the mounting is 6 meters to ensure that a payload does not hit the ship hull when retrieving the payload. The connection to the hydraulic actuator is set at the bottom of the mounting to reduce the moment that acts on the mounting. In Figure 3-6, the mounting is indicated by side b.

Hydraulic actuator:
Similar to the design of Altare et al. [2016], a hydraulic actuator is used to alter the angle of the telescopic arm (See Figure 3-5). The telescopic arm, the mounting to the deck, and the hydraulic actuator form a triangle (See Figure 3-6). Side a represents the non-extendable part of the telescopic arm, side b represents the mounting to deck and side c represents the hydraulic cylinder. Based on the required reach of the model, the minimum and maximum value for γ are determined. The values for a, b, γ_{min} and γ_{max} are shown in Table 3-1. Since there is no 90 degree angle in this triangle, the cosine rule is required instead of Pythagoras (See Equation (3-2)). The maximum value of c cannot be greater than 80% of the minimum value, as it is limited by the stroke of the actuator [Enerpac, 2020].

Figure 3-5: 3D model hydraulic actuator

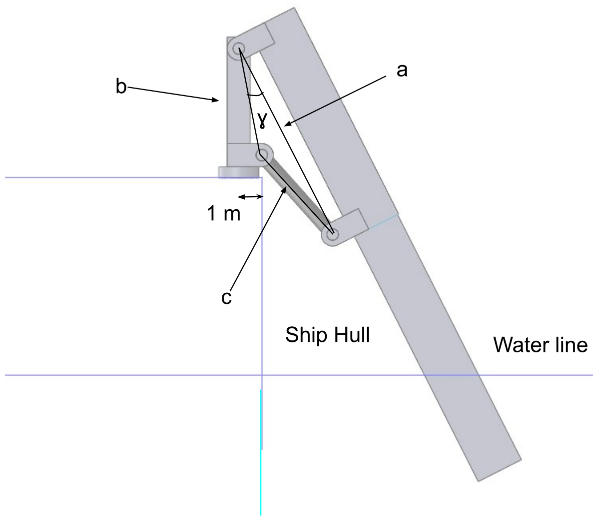

Figure 3-6: Dimensions 3D model

$$c = \sqrt{(a^2 + b^2 - 2abcos(\gamma)} \tag{3-2}$$

In Table 3-1, the calculated minimum and maximum values of the hydraulic cylinder are shown. These values represent the minimum and maximum required reach of the hydraulic actuator. The maximum value is exactly 1.8 times as big as the minimum value, thus the stroke of the actuator remains possible.

Table 3-1: Cosine rule values

Geometry	Value
a	9 m
b	4.6 m
γ_{min}	12°
γ_{max}	72°
c_{min}	4.6 m
c_{max}	8.28 m

Hydraulic gripper:
Once the automated side loader is lowered towards the payload, a hydraulic gripper is needed to grab the payload (See Figure 3-7). The geometry of the gripper is based on that of a garbage truck gripper. The actual attachment to the payload requires a attachment tool on the payload. Since this study focuses on the conceptual development of the general geometry this is not taken into account. Thus, a detailed attachment to the payload is considered out of scope for this study.

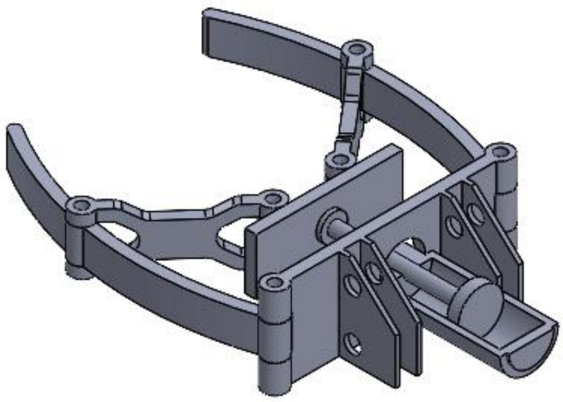

Figure 3-7: 3D model hydraulic gripper

Slewing support:
The side loader is connected to the deck in a similar manner as the mast cranes. The side loader needs to be able to rotate around its axis and thus a slewing support is required. This is simplified for this model since this study focuses on the conceptual development in stead of detailed designing. The slewing support enables the side loader to rotate 360 degrees around its axis such that the payload can be guided from the water to the deck.

A top view of the Fairplayer is shown in Figure 3-8. The slewing reach of the mast cranes on the Fairplayer is shown with a radius of 35 meter. In yellow, the possible installation areas for the automated side loader are shown. This area is 4.2 meters wide, thus the connection to the deck should fit within that dimension. Since the side loader can be placed at different points along the ship, the reach of the side load covers the reach of both mast cranes on the entire vessel.

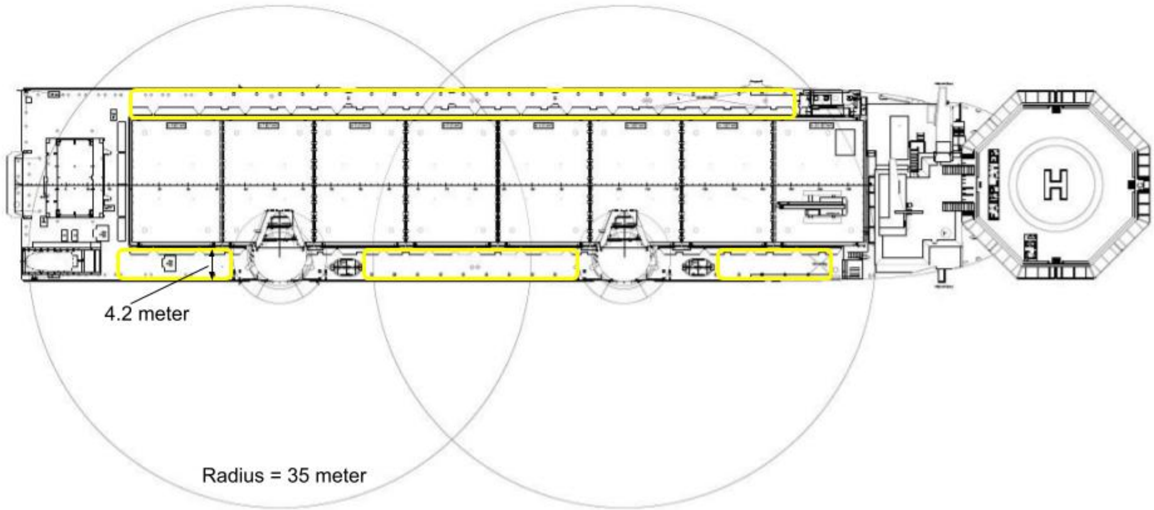

Figure 3-8: Slewing reach Fairplayer

Padeyes:
In the designed geometry in Solidworks, multiple padeyes are used for the pin connections. According to DNV standards, the radius of the outside of the padeye main plate, shall be no less than the diameter of the pin hole [DNV, 2018]. This standard is used as a minimum for designing all the padeyes in the geometry.

3-4 Dynamic Analysis using Orcaflex

After establishing the geometry that is required for developing a conceptual model, the load configurations that were described in Section 3-3 need to be analysed. For this a dynamic analysis is done and Orcaflex is used to model the dynamics. Orcaflex is a dynamic analysis software that is used to analyse offshore marine systems. Jumbo Maritime already uses this software and therefore a model of the Fairplayer is already present. This model is used, however, other assumptions and parameters are required in order to determine a correct model for this study.

First, the basic theory behind Orcaflex is explained in Section 3-4-1. Then, the environmental parameters of the Orcaflex model are discussed in Section 3-4-2. Next, Section 3-4-3 and Section 3-4-4 elaborate on the properties of the payload and the balance weight in the model respectively. The method that is used to model the gripper and how its parameters are derived are discussed in Section 3-4-5. Lastly, the model and its different load configurations are shown together with the parameters that are used for the dynamic analysis in Section 3-4-6.

3-4-1 Basic theory behind Orcaflex

As explained in Section 2-2, the motion of the vessel is influence by the waves. Orcaflex is tool that can simulate sea states for a specified amount of time in order to show the response of the vessel to a certain sea state. The response of the vessel is dependent on the energy density of the wave spectrum and the RAOs of the vessel.

The energy density of a wave is dictated by the wave height and the wave period. The selected sea states are already discussed and the correct method to implement these sea states into Orcaflex is discussed in Section 3-4-2.

Since Jumbo Maritime already uses Orcaflex to analyse their vessel dynamics during operations, an extensive set of RAOs is already present. The relevant RAOs are shown in Appendix C and these are implemented in Orcaflex. The software combines the inserted sea state with the specified RAOs to show the dynamic response of the vessel. Dynamic modelling with Orcaflex is common in the maritime industry as this software provides accurate dynamic analyses and is certified by multiple international classification bureaus such as DNV.

Not only the vessel but cranes, payload and other equipment can be modelled in Orcaflex to analyse their dynamic behaviour towards one another. Since this study is focused on dynamic relations between payload and the developed concept, Orcaflex is suited to conduct the dynamic analysis.

3-4-2 Environment

In order to have a correct model, the environment should be simulating a similar environment as the real world operational environment. For this study, this means setting the parameters for the seabed and the waves, since both the current and the wind where determined to be negligible for this study in Section 2-1.

Seabed:
Since this model should analyse a offshore lifting operation at the ocean, it is necessary that no shallow water effects occur. According to DNV standards regarding modelling and analysis of marine operations, the breaking wave limit at deep water corresponds to a maximum steepness of 1/7 [Det Norske Veritas, 2011]. Equation (3-3) is used to describe this phenomenon with the maximum wave height H_b, wave length γ_1 and water depth d.

$$\frac{H_b}{\gamma_1} = 0.142 tanh(\frac{2\pi d}{\gamma_1}) \tag{3-3}$$

To retrieve a minimum water depth from this formula, it is necessary to see where it converges to 1. This is done by plotting the formula with an unknown variable d (See Figure 3-9). The formula converges to 1 for a water depth of roughly 200 meters. Therefore, in the software model, the seabed depth is set at 200 meters as well.

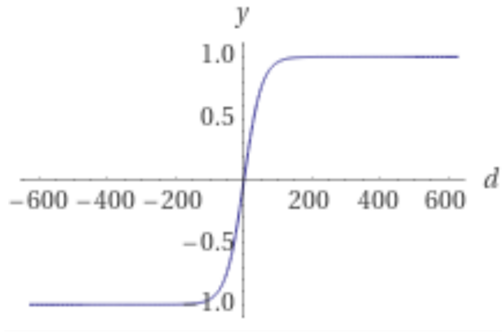

Figure 3-9: Plot for seabed depth

Waves:
The sea states that are selected to be analyzed were discussed in Section 2-1-1. There, it was also explained that a Pierson-Moskowitz wave spectrum will be used to model the sea state similar to that of an Ocean.

The parameters for modeling the wave spectrum correctly into Orcaflex are highlighted in Figure 3-10. The direction of the waves is set to 165 degrees as was explained in Section 2-1-1, this parameter will remain constant for all different sea states. The wave height H_s and the wave period T_p will vary according to which sea state is analysed. The three sea states that were selected are:

- $H_s = 2$ and m $T_p = 8$ s
- $H_s = 2.5$ m and $T_p = 10$ s
- $H_s = 3$ m and $T_p = 8$ s

As said, the Pierson-Moskowitz wave spectrum was selected but in order to model this correctly in Orcaflex, a JONSWAP wave spectrum is selected with a peak enhancement factor γ of 1. The JONSWAP wave spectrum is formulated based on the Pierson-Moskowitz wave spectrum and is used to describe smaller seas such as the North Sea. However, if a JONSWAP spectrum has its additional peak enhancement factor γ set equal to 1, this spectrum is identical to the Pierson-Moskowitz spectrum.

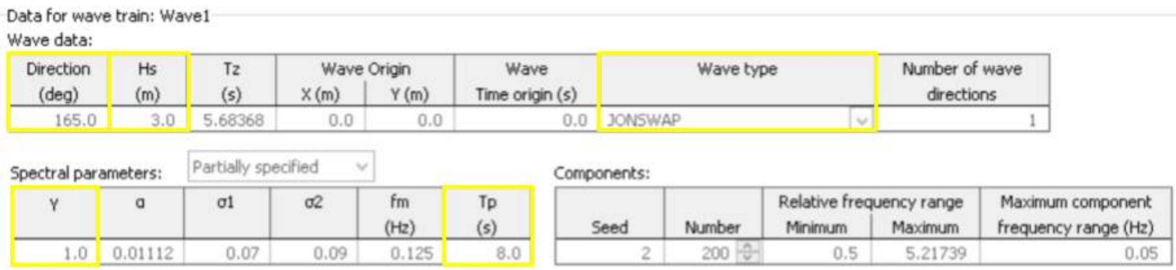

Figure 3-10: Wave parameters

With both the seabed and the wave parameters set to accurately model the real world problem, the environmental parameters of the Orcaflex model are set.

3-4-3 Payload

As explained in Section 2-3, the payload itself is a 185-ton plate that is 10x10x1 meter. The payload is influenced by more then a swinging vessel alone since this is an object that is submerged in the water in some load configurations as well. Several factors influence the payload when calculating the hydrodynamics. These are discussed below:

Buoyancy:
Buoyancy is an upward driven force that pushes against an object that is partially or fully submerged. The magnitude of the load is as big as the weight of the fluid that has been displaced by the volume of the submerged object. Buoyancy acts on all objects in the water, the vessel and the payload both experience their own buoyancy force. The volume of the payload and the level at which it is submerged are important for determining the buoyancy.

To determine the volume of the payload, first the wet weight of the payload needs to be considered. This is determined by dividing the dry weight by the density of steel and multiplying this with the density of steel minus the density of water (i.e. (185000/7850)*(7850-1000)). Equation (3-4) shows the formula for determining the volume of the payload V_p based on its wet weight, with the steel density ρ_s and water density ρ_w. The wet weight of the payload is calculated and with the known mass, the volume is calculated to be 23.6 m^3

$$V_p = \frac{M_p}{\rho_s - \rho_w} = \frac{161433}{7850 - 1000} = 23.6m^3 \tag{3-4}$$

The height is the vertical extent of the payload, and this is homogeneous distributed about the center of volume of the payload. The height is equal to 1 as the plate is 1 meter thick and is taken to be independent of buoy rotation.

Mass moment of inertia:
Each object that has a mass, has a mass moment of inertia. It depends on the mass distribution over the body and how its principal axis of rotation are chosen. The mass moment of inertia determines how much force is needed to reach a desired acceleration in a specified direction.

Large bodies with large moments of inertia require more torque to rotate around their axes. Since the payload is a solid square plate, the weight distribution is homogeneous and the principal axis is selected to be normal to the three main directions.

The formulas used to determine the mass of inertia for the three axes are determined by Equation (3-5). Parameter w & l are equal to 10 meters and the mass M is 185 tons.

$$\begin{aligned} I_x &= (M/12) * w^2 = 1542 ton * m^2 \\ I_y &= (M/12) * l^2 = 1542 ton * m^2 \\ I_z &= (M/12) * (w^2 + l^2) = 3083 ton * m^2 \end{aligned} \tag{3-5}$$

Drag:
Once an object is moving in a fluid, drag influences its dynamics. Drag is also known as fluid resistance and is expressed as a force that is acting in opposite direction of the relative motion of the moving object regarding its surrounding fluid. Drag is influenced by the velocity at which the object moves, the density of the fluid, the cross-sectional area normal to the motion and a dimensionless drag coefficient. The drag coefficient is associated with the geometry of the object and bureaus like DNV have established standardized values for these coefficients (See Figure 3-11) [Det Norske Veritas, 2011]. Fluid resistance influences the dynamics both in translational and rotational motion.

Since the drag area of the payload is represented by the effective size off the payload as it is facing the fluid flow around it. For the drag area in the X direction, the dimensions of Y and Z are simply multiplied to derive the drag area ($10*1 = 10\ m^2$). A similar multiplication is execute for the other two areas, the values are shown in Figure 3-13. Note that the aerodynamic drag is not include since wind loads are not considered in this study.

The values for Cd are based on the DNV Guidelines on modeling and analysis of marine operations [Det Norske Veritas, 2011]. Figure 3-11 shows the drag coefficients for the plate and the selected coefficients are highlighted. The Cd values for the X- and Y-directions are equal, as the plate is symmetrical in these directions. Moreover, a condition for these Cd values is that the Reynolds number should be larger than 10^3. Considering that water flow has a kinematic viscosity of $10^{-6}\frac{m^2}{s}$, the water velocity should be less than 0.001 $\frac{m}{s}$ to not meet the condition. Since the considered sea states have water velocity that are a lot higher than 0.001 $\frac{m}{s}$, the condition is met.

Geometry	*Dimensions*	*C_{DS}*
Rectangular plate normal to flow direction 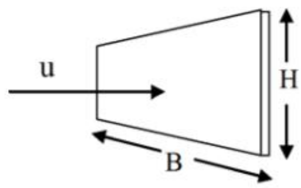	B/H 1 5 10 ∞	 1.16 1.20 1.50 1.90 $R_e > 10^3$

Figure 3-11: Drag coefficients plate [Det Norske Veritas, 2011]

The drag moment of area is the third moment of the drag area about the axis of rotation. It represents an element of drag area at an absolute distance from the axis of rotation. The area moment has the dimensions m^5. For a rectangular plate such as the payload with length l and width w, the third moment of area about the line in the plane of the rectangle and through its centre in the length direction is $\frac{lw^4}{32}$. The third moment of area about the line in the plane of the rectangle and through its centre in the width direction is $\frac{wl^4}{32}$. For the Z-direction, the same formula is used and the values are shown in Figure 3-13. The drag coefficients for the drag moment are similar to the drag coefficients for regular drag in their principle axis.

Fluid inertia:
When an object moves in a fluid, besides the mass of the object, the fluid itself also has a moment of inertia. As the object translates or rotates in the fluid, it must move a certain volume of this fluid. This volume, together with the density of the fluid, creates a so-called added mass or hydrodynamic mass. The added mass depends on added mass coefficient that is determined by the geometry of the object. For objects that are relatively light weight added mass can be significant but for heavier weights, the effect of added mass is small. Therefore the rotational added mass is considered negligible in this study, as the rotational displacement of the object will be small compared to the translational displacement and a heavy weight is considered.

The translational fluid inertia is defined by the hydrodynamic mass, the added mass coefficient Ca and the fluid acceleration force coefficient Cm. The hydrodynamic mass is calculated by multiplying the volume V_R of Figure 3-12 and the density of water. This results in the values shown in Figure 3-13. This hydrodynamic mass represents the submerged volume that displaces a certain amount of water.

Ca represents the added mass coefficient and the values are obtained from the DNV guideline regarding modeling and analysis of marine operations [Det Norske Veritas, 2011]. In Figure 3-12, the selected coefficients are highlighted. The fluid acceleration force coefficient is represented by Cm and its value is equal to Ca + 1.

	Body shape	*Direction of motion*	C_A				V_R
Flat plates			*b/a*	C_A	*b/a*	C_A	
	Rectangular plates 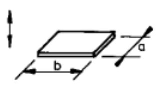	Vertical	1.00	0.579	3.17	0.840	$\frac{\pi}{4} a^2 b$
			1.25	0.642	4.00	0.872	
			1.50	0.690	5.00	0.897	
			1.59	0.704	6.25	0.917	
			2.00	0.757	8.00	0.934	
			2.50	0.801	10.00	0.947	
			3.00	0.830	∞	1.000	

Figure 3-12: Added mass coefficients [Det Norske Veritas, 2011]

Slam force:
Every time an object enters or exits the water surface with a significant velocity, slam loads occur. The area normal to the water surface during the entry or exit of the water surface plays a big role. Upon touching the water surface, the vertical forces consist on the buoyancy and drag forces but the slam forces are high when the initial contact is made.

The slam area is equal to the area that is parallel to the water surface, in this case 100 m^2. According to DNV, the slam force data for both entry and exit can be set equal to 2π [Det Norske Veritas, 2011].

Modelling payload in Orcaflex:
All the factors that are discussed above, need to be modelled into Orcaflex to conduct an accurate dynamic analysis. In Figure 3-13, the properties of the plate as it is modeled in Orcaflex are shown.

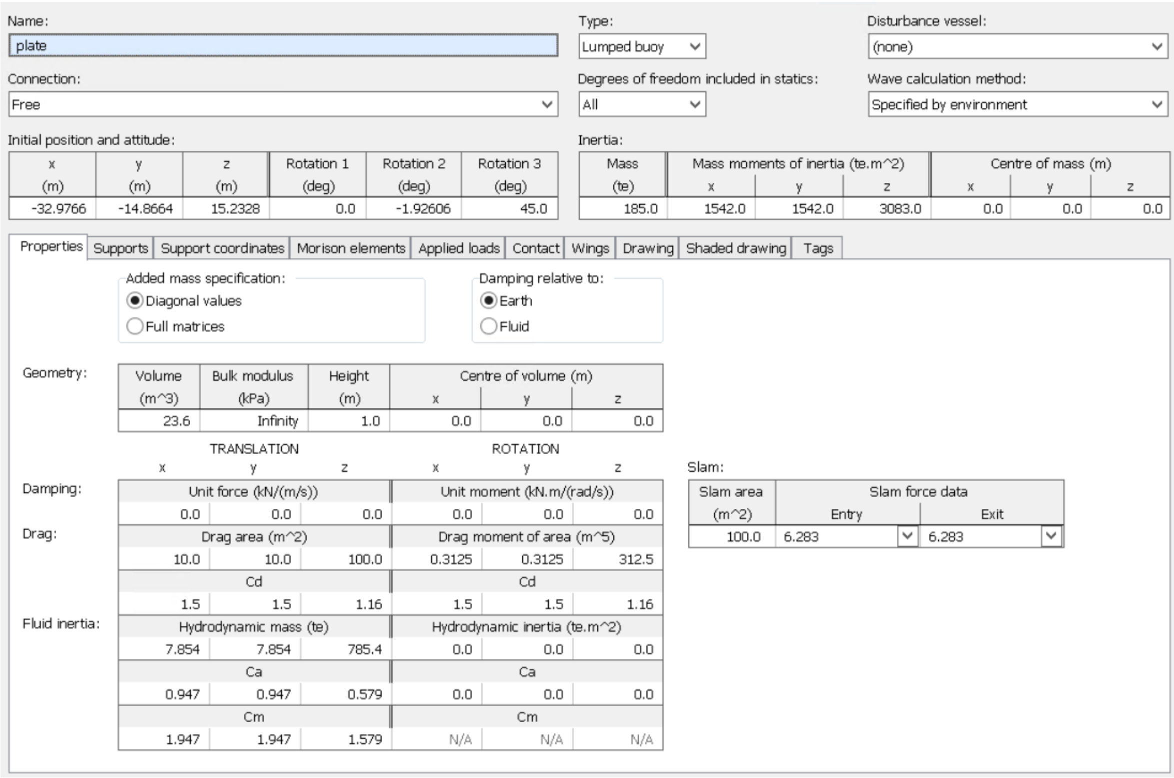

Figure 3-13: Properties of plate in Orcaflex

3-4-4 Balance weight

During actual lifting operations, pumps are continuously making sure that the required balance weight is present in the ballast tanks of the vessel to provide balance. In Figure 3-14, the necessity of the balance weight is shown. As both weights create a moment that needs to balance the other momentum around the center of gravity of the vessel.

Equation (3-6) is used to determine the weight that is required to balance the vessel. With the mass of the balance weight M_{bw}, the mass of the payload and crane block $M_p + M_{cb}$, the Y-coordinate of the payload y_p and the Y-coordinate of the balance weight y_{bw}. Note that the payload weighs less in states 2 and 3 compared to state 1 because wet weight is considered there. In Table 3-2, the values are shown per load case.

$$M_{bw} = (M_p * y_p)/y_{bw} \tag{3-6}$$

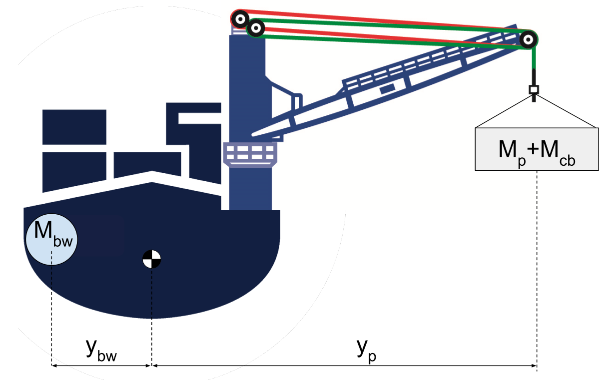

Figure 3-14: Balance weight

Table 3-2: Balance weight determination for different load cases

Load case	y_p [m]	y_{bw} [m]	$M_p + M_{cb}$ [ton]	M_{bw} [ton]
1	45	11	200	818
2	24	11	176	385
3	45	11	176	7

For modeling it in Orcaflex, the balance weight is simplified in the form of a 3D buoy with a specific mass. Only the mass and the coordinates at which the balance weight is attached to the ship are relevant for the model. The coordinate at which the balance weight will be attached is similar for all three different loading configurations as the ballast tanks are also stationary. The weight is placed below deck, and the (X ; Y) coordinates are (33,5 ; 11) meters. This X-coordinate is selected because the weight is at the same longitudinal coordinate as the aft crane and the lifted payload. The Y coordinate is at the limit of the port side of the ship, maximizing the moment and thus minimizing the required balance weight.

3-4-5 Gripper

The automated side loader can be simplified as a spring damping system that attaches the payload to the vessel. A spring damper system requires both a stiffness and a damping profile.

The arm of the automated side loader has four types of stiffnesses that are relevant; axial stiffness k_a, torsional stiffness k_t and bending stiffness in X and Y direction k_x and k_y respectively. In the following, the four formulas used are shown in Equation (3-7).

$$\begin{aligned} k_a &= E * A \\ k_t &= G * J \\ k_x &= E * I_x \\ k_y &= E * I_y \end{aligned} \tag{3-7}$$

The stiffnesses depend on the cross section area A, the polar moment of inertia G and the moments of inertia I_x & I_y. These variables are based on the educated guess that was first selected for the geometry. As the design process is going through some iterations, the values for these variables will be adjusted accordingly.

The Young's modulus E (210 GPa) and the modulus of rigidity G (80 GPa) are based on the material properties of S355 steel and these will not be adjusted during the iteration process. Section 3-5-2 elaborates further on the material selection.

Lastly, the gripper requires a damping profile to fully mimic a spring-damper system. This also models the hydraulics of the telescopic arm more realistically. The damping profile that has been used is based on the damping profile of a PHC that was used by Jumbo in a recent project. This profile was chosen since the PHC acts similar to the hydraulic actuator in the telescopic arm.

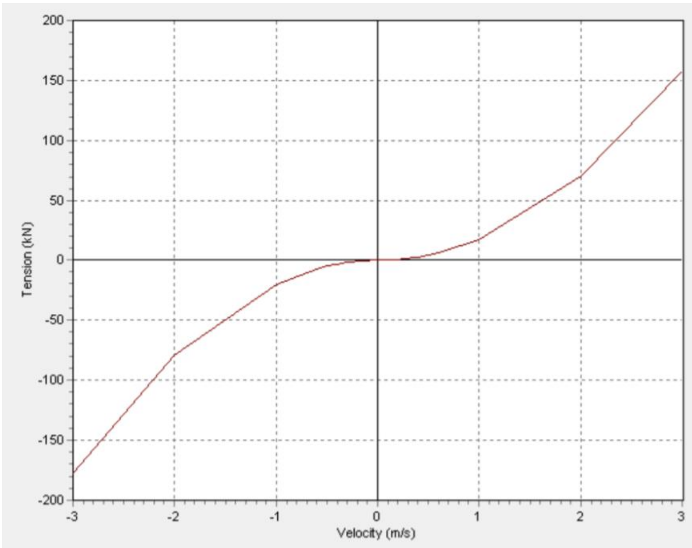

Figure 3-15: Gripper damping profile

3-4-6 Model

Before starting the dynamical analysis for the different load cases, one last property needs to be set. The duration of the simulation time needs to be set. The analysis that will be done consists of two parts, the build-up and first stage. The build-up will last 60 seconds and enables the model to build-up the sea state. Building up the sea state before starting the actual analysis results in more realistic results. If this phase is not included, the model will show extraordinary behavior and in order to prevent that, the build-up is included.

After the build-up, the first stage will start and the results of this stage will be used for this study. To determine the length of this stage, a consideration is required between computational time and accurate results. A dynamic analysis is considered to contain the Most Probable Maximum (MPM) for a simulation of three hours since the maximum wave has passed during this simulation time [Journee and Massie, 2001].

To reduce the computational time, the results of a short analysis (i.e. 10 minutes) are compared with the results of a three-hour analysis. To see whether 10 minutes is sufficient simulation time to describe the behaviour accurately, an extrapolation with a Rayleigh distribution is conducted. The MPM of the three-hour analysis is compared to the MPM of the 10-minute analysis. Both analyses take into account a wave period of 10 seconds, as this is the longest wave period considered in this study (See Section 2-1-1). If three hours are sufficient to yield the results accurately for waves with a 10 second wave period, then the results will be even more accurate for waves with a shorter wave period (i.e. 8 seconds) since more waves have passed in the same simulation time.

Since this study is interested in the maxima of the system, an upper tail Rayleigh distribution is applied, as the lower tail distribution would yield the minima. The MPM can, under the Gaussian assumption, be described by Equation (3-8) with mean μ, standard deviation σ_1, storm duration T and mean up-crossing period T_z:

$$MPM = \mu + \sigma_1 \sqrt{2ln(\frac{T}{T_z})} \tag{3-8}$$

The analysis of 10 minutes yielded a MPM that was 5% higher than the MPM of the three-hour simulation. This was due to the difference in standard deviation, as the standard deviation for the short analysis was twice the value of the three-hour analysis. Since a higher MPM will result in a more robust conceptual model, an analysis of 10 minutes is determined to be accurate to conduct the dynamic analysis.

Another reason for only analysing 10 minutes instead of three hours is the type of operation. Lifting operations such as the ones considered in this study, will not last three hours and will be rather close to 10 minutes. Thus by taking the maximum values of a three hour simulation time, the hydrodynamic forces are over-estimated allowing the development of a more robust conceptual model.

With all the relevant properties set, the Orcaflex model is ready to run the dynamic analysis. The different load configurations as shown in Figure 3-3 are modeled in Orcaflex. Figure 3-16,Figure 3-17 & Figure 3-18 show the first, second and third state of the Orcaflex model respectively.

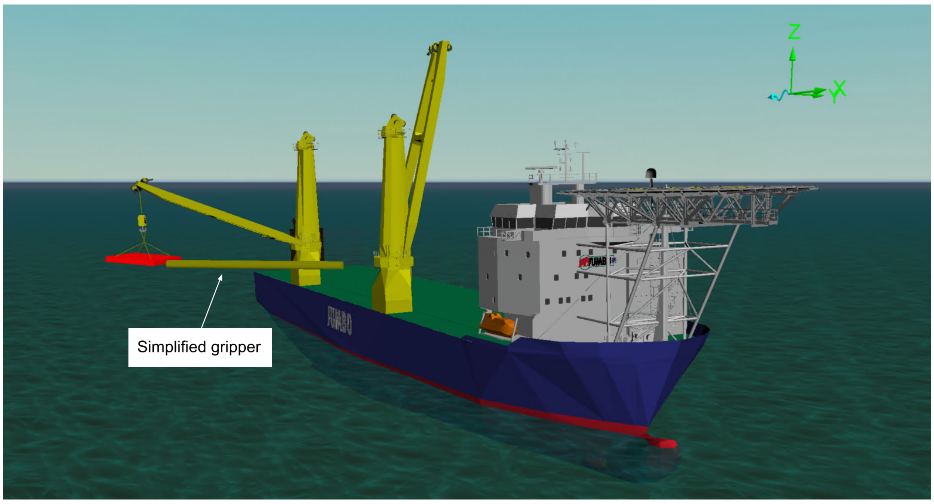

Figure 3-16: State 1 orcaflex model

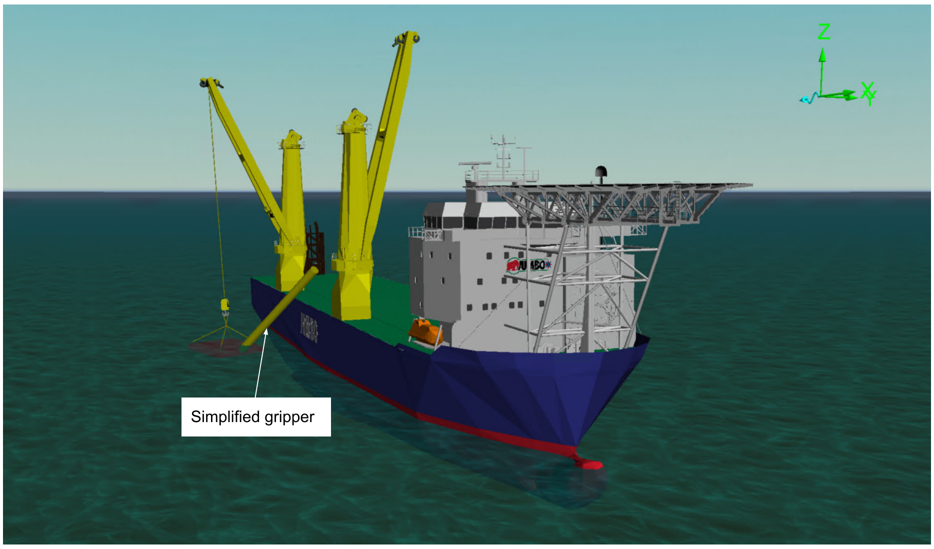

Figure 3-17: State 2 orcaflex model

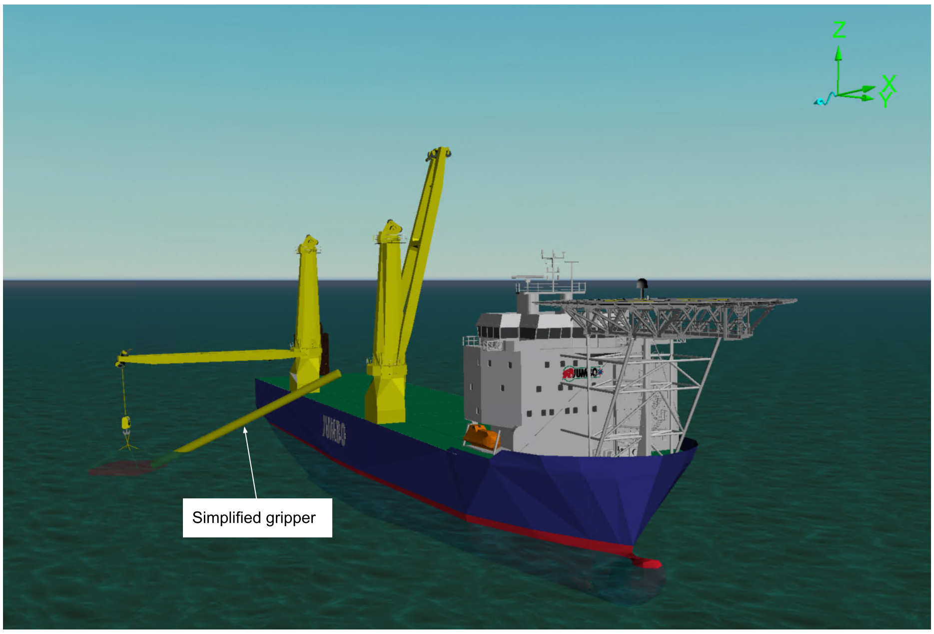

Figure 3-18: State 3 orcaflex model

3-5 Structural analysis

The telescopic arm that is designed according to the geometry (See Section 3-3) needs to be structurally analyzed. This analysis consists of two parts, an analytic method to calculate the deflection of the beam and a finite element analysis with Ansys. The analytic method is elaborated in Section 3-5-1, this is used as a verification for the FEA results. The basic theory behind FEA and how the FEA model is constructed is explained in Section 3-5-2.

3-5-1 Analytic method

In order to derive the deflection of the telescopic arm, an analytic method is conducted by hand. This method considers the load case as shown in Figure 3-19. The shear force in Y direction and the effective tension in axial direction, which are retrieved from Orcaflex, are applied. The telescopic arm is represented by a beam model that is shown in Figure 3-20. The non-extendable part is represented by the beam with I_1 and the extendable part is simplified to one beam with moment of inertia I_2.

Figure 3-19: Load case for analytic method

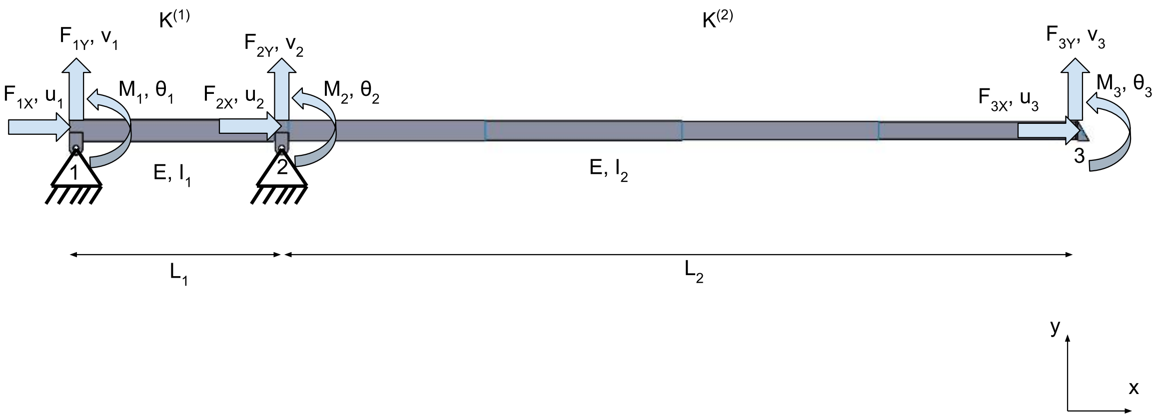

Figure 3-20: Beam model of telescopic arm

The telescopic arm is split up into two beam elements. The beam is a conservative system since the external work that is done is equal to the internal energy stored. Equation (3-9) and Equation (3-10) show the formulas that can be used to describe the deformations together with the stiffness matrices for beam element 1 and 2 respectively.

$$K^{(1)}\vec{u_1} = \vec{F_1} \tag{3-9}$$

$$K^{(2)}\vec{u_2} = \vec{F_2} \tag{3-10}$$

Written out, these formulas are shown in (3-11) and (3-12). Since the elements are connected, a global stiffness matrix can be configured accordingly, this is shown in (3-13).

$$\begin{bmatrix} \frac{A_1E}{L_1} & 0 & 0 & \frac{-A_1E}{L_1} & 0 & 0 \\ 0 & \frac{12EI_1}{L_1^3} & \frac{6EI_1}{L_1^2} & 0 & \frac{-12EI_1}{L_1^3} & \frac{6EI_1}{L_1^2} \\ 0 & \frac{6EI_1}{L_1^2} & \frac{4EI_1}{L_1} & 0 & \frac{-6EI_1}{L_1^2} & \frac{2EI_1}{L_1} \\ \frac{-A_1E}{L_1} & 0 & 0 & \frac{A_1E}{L_1} & 0 & 0 \\ 0 & \frac{-12EI_1}{L_1^3} & \frac{-6EI_1}{L_1^2} & 0 & \frac{12EI_1}{L_1^3} & \frac{-6EI_1}{L_1^2} \\ 0 & \frac{6EI_1}{L_1^2} & \frac{2EI_1}{L_1} & 0 & \frac{-6EI_1}{L_1^2} & \frac{4EI_1}{L_1} \end{bmatrix} \begin{Bmatrix} u_1 \\ v_1 \\ \theta_1 \\ u_2 \\ v_2 \\ \theta_2 \end{Bmatrix} = \begin{Bmatrix} F_{1X} \\ F_{1Y} \\ M_1 \\ F_{2X} \\ F_{2Y} \\ M_2 \end{Bmatrix} \tag{3-11}$$

$$\begin{bmatrix} \frac{A_2E}{L_2} & 0 & 0 & \frac{-A_2E}{L_2} & 0 & 0 \\ 0 & \frac{12EI_2}{L_2^3} & \frac{6EI_2}{L_2^2} & 0 & \frac{-12EI_2}{L_2^3} & \frac{6EI_2}{L_2^2} \\ 0 & \frac{6EI_2}{L_2^2} & \frac{4EI_2}{L_2} & 0 & \frac{-6EI_2}{L_2^2} & \frac{2EI_2}{L_2} \\ \frac{-A_2E}{L_2} & 0 & 0 & \frac{A_2E}{L_2} & 0 & 0 \\ 0 & \frac{-12EI_2}{L_2^3} & \frac{-6EI_2}{L_2^2} & 0 & \frac{12EI_2}{L_2^3} & \frac{-6EI_2}{L_2^2} \\ 0 & \frac{6EI_2}{L_2^2} & \frac{2EI_2}{L_2} & 0 & \frac{-6EI_2}{L_2^2} & \frac{4EI_2}{L_2} \end{bmatrix} \begin{Bmatrix} u_2 \\ v_2 \\ \theta_2 \\ u_3 \\ v_3 \\ \theta_3 \end{Bmatrix} = \begin{Bmatrix} F_{2X} \\ F_{2Y} \\ M_2 \\ F_{3X} \\ F_{3Y} \\ M_3 \end{Bmatrix} \tag{3-12}$$

$$\begin{bmatrix}
\frac{A_1E}{L_1} & 0 & 0 & \frac{-A_1E}{L_1} & 0 & 0 & 0 & 0 & 0 \\
0 & \frac{12EI_1}{L_1^3} & \frac{6EI_1}{L_1^2} & 0 & \frac{-12EI_1}{L_1^3} & \frac{6EI_1}{L_1^2} & 0 & 0 & 0 \\
0 & \frac{6EI_1}{L_1^2} & \frac{4EI_1}{L_1} & 0 & \frac{-6EI_1}{L_1^2} & \frac{2EI_1}{L_1} & 0 & 0 & 0 \\
\frac{-A_1E}{L_1} & 0 & 0 & \frac{A_1E}{L_1} + \frac{A_2E}{L_2} & 0 & 0 & \frac{-A_2E}{L_2} & 0 & 0 \\
0 & \frac{-12EI_1}{L_1^3} & \frac{-6EI_1}{L_1^2} & 0 & \frac{12EI_1}{L_1^3} + \frac{12EI_2}{L_2^3} & \frac{-6EI_1}{L_1^2} + \frac{6EI_2}{L_2^2} & 0 & \frac{-12EI_2}{L_2^3} & \frac{6EI_2}{L_2^2} \\
0 & \frac{6EI_1}{L_1^2} & \frac{2EI_1}{L_1} & 0 & \frac{-6EI_1}{L_1^2} + \frac{6EI_2}{L_2^2} & \frac{4EI_1}{L_1} + \frac{4EI_2}{L_2} & 0 & \frac{-6EI_2}{L_2^2} & \frac{2EI_2}{L_2} \\
0 & 0 & 0 & \frac{-A_2E}{L_2} & 0 & 0 & \frac{A_2E}{L_2} & 0 & 0 \\
0 & 0 & 0 & 0 & \frac{-12EI_2}{L_2^3} & \frac{-6EI_2}{L_2^2} & 0 & \frac{12EI_2}{L_2^3} & \frac{-6EI_2}{L_2^2} \\
0 & 0 & 0 & 0 & \frac{6EI_2}{L_2^2} & \frac{2EI_2}{L_2} & 0 & \frac{-6EI_2}{L_2^2} & \frac{4EI_2}{L_2}
\end{bmatrix}
\begin{Bmatrix} u_1 \\ v_1 \\ \theta_1 \\ u_2 \\ v_2 \\ \theta_2 \\ u_3 \\ v_3 \\ \theta_3 \end{Bmatrix}
=
\begin{Bmatrix} F_{1X} \\ F_{1Y} \\ M_1 \\ F_{2X} \\ F_{2Y} \\ M_2 \\ F_{3X} \\ F_{3Y} \\ M_3 \end{Bmatrix}
\tag{3-13}$$

In order to solve the equations that can be derived from the global stiffness matrix, boundary conditions are needed. The boundary conditions consist of loads, moments and constraints. These are based on the configuration shown in Figure 3-20:

$$\begin{aligned} F_{3X} &= -272kN, \\ F_{3Y} &= -250kN, \\ M_1 = M_2 = M_3 &= 0, \\ u_1 = u_2 &= 0, \\ v_1 = v_2 &= 0 \end{aligned} \tag{3-14}$$

Besides identifying boundary conditions, the variables in the global stiffness matrix need to be quantified to determine the unknown variables. The variables that need to be quantified are shown in Table 3-3. L_1 and L_2 add up to the length of the two sections of the telescopic arm combined. I_1 and I_2 are based on one of the first iterations for the telescopic arm. The Young's Modulus E of S355 steel is used as this material was selected according to Section 3-5-2. Furthermore, F_{3Y} and F_{3X} are retrieved from the dynamic analysis of Section 4-2 for the shear force in the Y direction and the effective tension in the X direction, as shown in Figure 3-19. These loads are retrieved from the dynamic analysis using the dimensions of the geometry of one of the first iterations.

Table 3-3: Quantification of variables for analytic method

Variable	Value	Unit
L_1	9.5	m
L_2	29.35	m
E	210	GPa
I_1	0.09422	m^4
I_2	0,07545	m^4
F_{3Y}	-250	kN
F_{3X}	-272	kN

Solving the matrix of (3-13) by implementing the boundary conditions of (3-14) and the quantified variables from Table 3-3 yields:

$$\begin{aligned}
F_{1X} &= 0 \\
F_{1Y} = F_{3Y}\frac{L_2}{L_1} &= -772.37kN \\
F_{2X} = -\frac{A_2E}{L_2}u_3 = -F_{3X} &= -272kN \\
F_{2Y} = -F_{3Y}(1+\frac{L_2}{L_1}) &= 1022.37kN \\
\theta_1 = \frac{-\theta_2}{2} &= 0.00058718rad \\
\theta_2 = \frac{-F_{3Y}L_2^2}{6EI_2} - \theta_3 + \frac{2v_3}{L_2} = \frac{v_3}{L_2} - \frac{F_{3Y}L_2^2}{3EI_2} &= -0.00117437rad \\
\theta_3 = \frac{F_{3Y}L_2^2}{6EI_2} + \frac{v_3}{L_2} &= -0.00797028rad \\
u_3 = \frac{F_{3X}L_2}{A_2E} &= -0.1584mm \\
v_3 = \frac{F_{3Y}L_2^3}{3EI_2} + \frac{F_{3Y}L_1L_2^2}{3EI_1} &= -167.44mm
\end{aligned} \tag{3-15}$$

To ensure that this analytic method is executed properly, the force equilibrium needs to add up to zero for both X and Y directions. All forces acting in Y direction add up to zero, the same goes for the forces acting in X direction. Therefore, this analytic method is deemed to be accurate for this study.

The analytical method yields a deflection of 167.44 mm at node 3, which is used to verify the model that is used for the finite element analysis. This model is first discussed below after which the comparison between the model and the analytical method is made.

3-5-2 Layout of Finite Element Analysis

Finite element analysis is conducted on the beam model of Figure 3-20 to conduct a structural analysis. First, the basic theory behind FEA is explained before the parameters of the model are discussed. In order to verify if the model is accurate, the deflection of v_3 that was derived by hand with the analytic method is used.

Basic theory behind FEA

Finite element analysis divides the body of a model, the telescopic arm in this study, into an equivalent system of many smaller bodies (finite elements). The smaller bodies are constructed by meshing the object, which creates a space discretization of the dimensions in space. Each body is connected with adjacent bodies at nodes and every body interacts with its neighbors. These interactions can be described by equations and together they form a system of algebraic equations. In order to solve this system of equations various parameters need to be set. Ansys is a software that conducts FEA if these parameters are entered. The parameters that are used for this study are explained in the remainder of this section.

Material

For this model, the most commonly used offshore steel is selected; S355. This is a high strength steel and its material properties are shown in Table 3-4.

Table 3-4: Properties of selected material

Property	S355	Unit
Density	7850	kg/m^3
Young's Modulus	210	GPa
Poisson's Ratio	0.3	-
Compressive Yield Strength	355	MPa
Compressive Ultimate Strength	470	MPa
Tensile Yield Strength	355	MPa
Tensile Ultimate Strength	470	MPa

Mesh

Meshing a general finite element model is mainly depended on the mesh size. Finer mesh will result in longer computational time and coarser mesh will result in less accurate result of the model. If the mesh size is too small, extreme high peak stresses will show in the results. The deformation converges for an increasing number of elements. An iterative process is conducted to determine the size of the mesh. This iteration resulted in a mesh size of 100 mm to be accurate. Decreasing the mesh size more will result in higher computational time and extreme high peak stresses.

Contacts

The model consists of multiple parts and in order to solve the system of equations with FEA, contacts between these parts need to be defined. As the elements of two overlapping parts touch each other, an interaction occurs. For the beam model of the telescopic arm, all parts are bonded together. This means that no sliding or separation between faces or edges is allowed. These regions are "glued" together and this allows for a linear solution as the contact area will not change during the load application.

Boundary conditions

Boundary conditions are required to constrain the beam model. Often these consist of specified values on the boundaries of the model. Figure 3-20 represents how the model is constraint, both nodes 1 and 2 cannot move in the X or Y direction. To mimic this constraint, the faces of the padeye holes are set to a fix support. The padeyes are attached to the beam by a bonded contact thus the whole system is limited by this boundary condition. The fixed support is attached in the hole of each padeye as this accurately represents the actual connection the beam will have with the rest of the model.

Loads

The model will not experience any deformation or stress if no loads are applied. The loads are applied by quantifying their magnitude and direction, in a similar manner as shown in Section 3-5-1 for both F_3X and F_3Y. However, in the model an in-plane force is also applied representing the shear load in X-direction as this is retrieved from the dynamic analysis as well. Lastly, gravitational acceleration is added on the entire structure as the model must endure gravity in the operational environment as well.

Verification of the model

The beam as depicted in Figure 3-20 is entered in Ansys. The parameters of the Ansys model are equal to those described above. In order to verify whether this model is accurate, the deflection of the model should be compared to the determined deflection of the analytic method. The deflection in Y direction of the FEA model is shown in Figure 3-21 and v_3 is equal to 167.23 mm. The deflection with the analytic method is equal to 167.44 mm. Thus the error margin is equal to 0.13%. Thus, the model for the finite element analysis is deemed to be accurate as it is verified by the analytic method.

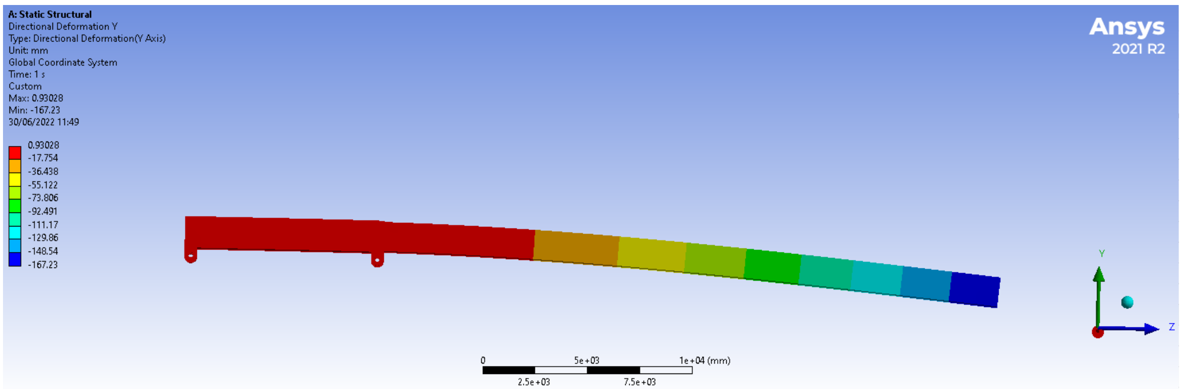

Figure 3-21: Verification of FEA model

Criteria

Since the FEA model is verified, it can be used to conduct a finite element analysis for the different load configurations described in this thesis. The results of the FEA are analysed on deformation and stress to conduct a general structural analysis. DNV guidelines for lifting appliances state the required limits for both deformation and stress [DNV, 2018];

The uniform deflection (i.e. the deformation) of the beam under tension must be below the rod length divided by 50. For this study, the deflection should not be larger than 760 mm since the rod length is defined as 38 meter (See Section 3-3).

The maximum allowable stress depends on the yield strength of the material and a safety factor. For regular operational loads and the dead weight of the model the safety factor γ_s is equal to 1.48 [DNV, 2018]. Equation (3-16) shows the formula for determining the allowable stress σ_{zul}.

$$\sigma_{zul} = \frac{f_{yr}}{\gamma_s} \tag{3-16}$$

f_{yr} is equal to 355 MPa for plate thicknesses up to 40 mm and 335 for plates that are thicker than 40 mm [Meadinfo, 2015]. Therefore the allowable stress σ_{zul} will be 240 MPa and 226 MPa respectively.

Based on the design process described in this study, the allowable deformation and allowable stresses need to be analyzed by the FEA in order to determine whether the conceptual model is feasible and optimized. The results of the analyses, that are described in this chapter, are discussed in the next chapter.

Chapter 4

Results & Discussion

This chapter will provide the results of this thesis. Along the design process that is used for the development of the conceptual model, various results arose. First, the optimized geometry is discussed in Section 4-1, then the loads that are retrieved from the dynamic analysis are shown in Section 4-2. Subsequently, these loads are applied in the FEA and this is discussed in Section 4-3. Lastly, the motion reduction of the payload is presented in Section 4-4 as this is also retrieved from the dynamic analysis. Along the entire chapter, results are discussed and called into question.

4-1 Geometry

The design process used in this study consists of iterations to determine an optimized geometry. The first geometry that enters the design process is selected based on an educated guess and from there the dimensions of the arm are optimized regarding material usage. The dimensions are optimized when the stress and/or deformation are at least 80% of the allowable limits but lower than the allowable limits (See Section 3-1). The iteration process of the different geometries is shown in Figure 4-1. The deformation and stresses are obtained from the FEA and based on the limits indicated in Figure 4-1, it is decided whether another iteration is possible and necessary.

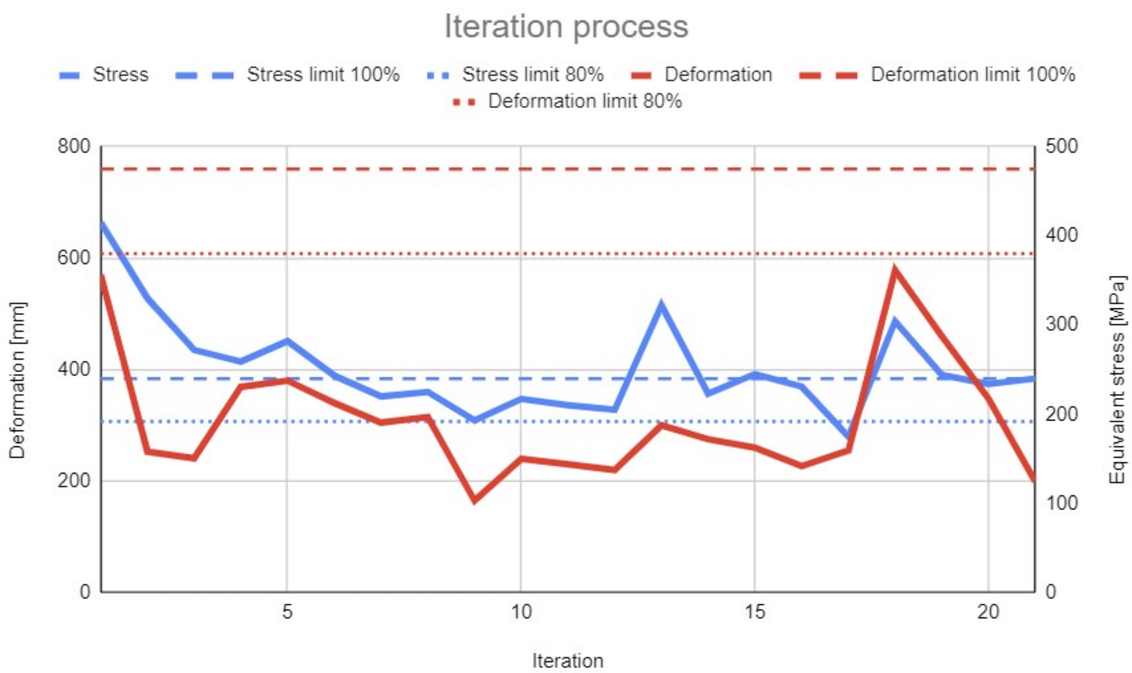

Figure 4-1: Iteration process

The variables of the cross section of the telescopic arm are shown in Figure 4-2. Equation (4-1) shows the formula to determine the moment of inertia for the sections of the telescopic arm. The moment of inertia can be determined for bending along the X- or Y-axis (i.e. horizontal and vertical respectively). The different moments of inertia can be determined by switching the variables B & H with the variables b & h respectively.

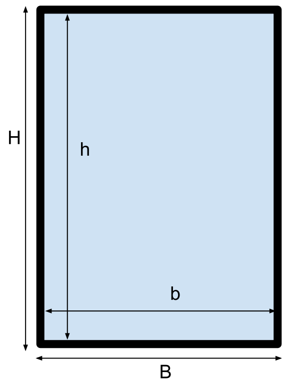

Figure 4-2: Cross section telescopic arm

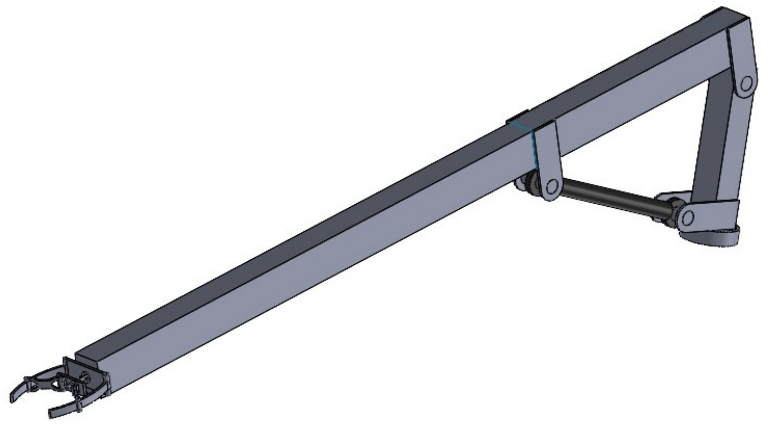

Figure 4-3: Conceptual 3D model

The first dimensions (i.e. the first iteration of the design process) are shown in the second and third column of Table 4-1. After more than 20 iterations, the optimized geometry is determined. These values are shown in the fourth and fifth column of Table 4-1. The stress and deformation of the first dimensions and the optimized geometry that is obtained from the FEA are shown in Section 4-3. Optimization of the geometry with respect to material usage resulted in approximately 90 tons of steel saved. This number is based on the density of S355 steel and the volume of the first iteration minus the volume of the optimized geometry.

$$I = \frac{BH^3}{12} - \frac{bh^3}{12} \tag{4-1}$$

Table 4-1: Dimensions cross section telescopic arm

	First dimensions non-extendable part	First dimensions extendable part	Optimized non-extendable part	Optimized extendable part
B [m]	2.1	2	1.18	1.1
H [m]	3	3	1.48	1.4
b [m]	2	1.9	1.1	1.02
h [m]	3	2.9	1.4	1.32
I_x $[m^4]$	0.22500	0.63841	0.06724	0.05604
I_y $[m^4]$	0.31525	0.34241	0.04736	0.03855
A $[m^2]$	0.5	0.49	0.2064	0.1936

An overview of the conceptual 3D model is presented in Figure 4-3. This model is capable of reaching every corner of the required reach. The first, second and third load configuration are shown in Figure 4-4, Figure 4-5 and Figure 4-6 respectively.

The geometry of the model, is used as input for the dynamic analysis and the finite element analysis. After each iteration, other dimensions are used as input as each iteration, the design process gets closer to the optimized geometry.

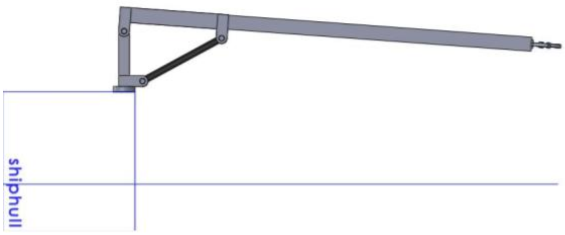

Figure 4-4: Geometry state 1

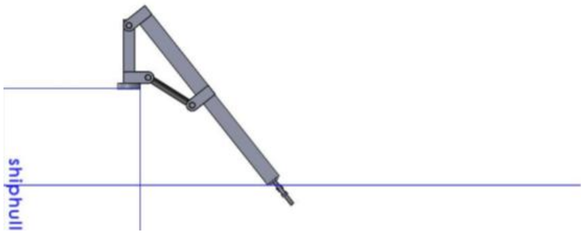

Figure 4-5: Geometry state 2

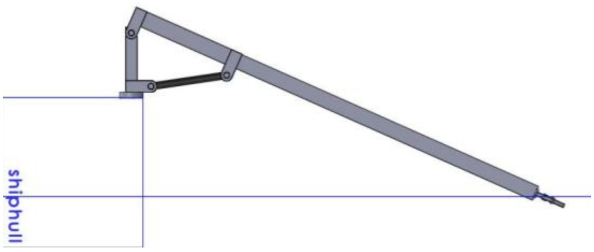

Figure 4-6: Geometry state 3

4-2 Loads dynamic analysis

The dynamic analysis described in Section 3-4 yields the loads on the automated side loader, which are applied as input for the finite element analysis. The loads that are retrieved from the dynamic analysis act on the gripper at the attachment point to the payload. The orientation of the loads is shown in Figure 4-7, with the Z-axis pointing in the axial direction of the modeled telescopic arm. The orientation of the payload is also shown in Figure 4-7. The X-axis of the payload orientation is aligned with the Z-axis of the gripper. Due to the method that is used for modeling, the Z-axis of the gripper is not pointing in the same direction as the Z-axis of the payload. This does not influence the results although caution is required when analyzing these results in the correct orientation. The loads that are retrieved from the analysis are shown in Table 4-2, where the effective tension acts in the axial direction of the gripper.

Table 4-2: Loads dynamic analysis

	Effective tension (kN)	**Shear X (kN)**	**Shear Y (kN)**
State 1 Tp 8 Hs 2	280	150	57
State 1 Tp 10 Hs 2.5	318	**151**	49
State 1 Tp 8 Hs 3	**350**	141	**80**
State 2 Tp 8 Hs 2	109	36	46
State 2 Tp 10 Hs 2.5	114	33	47
State 2 Tp 8 Hs 3	**224**	**57**	**76**
State 3 Tp 8 Hs 2	443	35	103
State 3 Tp 10 Hs 2.5	438	42	97
State 3 Tp 8 Hs 3	**503**	**54**	**141**

The largest loads for both the second and third load configuration are from the sea state

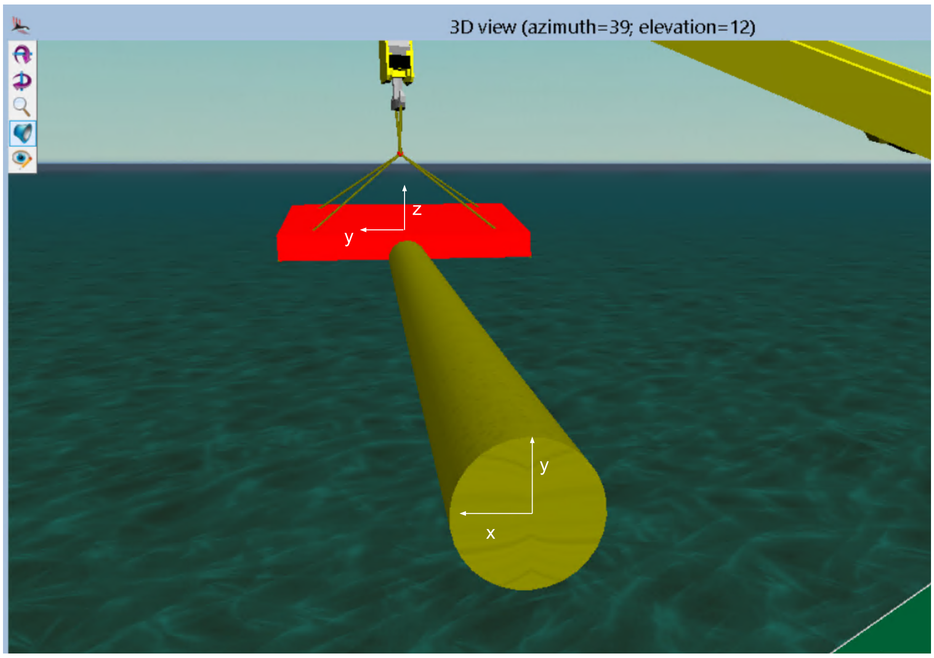

Figure 4-7: Orientation loads

with a significant wave height of 3 meter and a wave period of 8 seconds. The waves in this sea state contain the most energy and since the payload is still in the water, the payload is affected by these wave loads. The loads on the payload and subsequently the attached gripper are logically larger for the sea state with the highest energy.

In contrast to the second and third states, the shear in the Y direction for the first state has its highest result in a different sea state. The payload is not affected by the wave loads directly as the crane lifts the payload out of the water in this load configuration. However, the payload motion is affected by the response of the vessel to the sea state. Appendix C shows the RAOs of the vessel and the amplitude response of the vessel for a wave period of 10 seconds is larger in all six DOFs. Thus, the wave period of 10 seconds excites the response of the vessel more than a wave period of 8 seconds. Since the vessel motions are more severe in this sea state, the payload motions are more extreme as well. In addition to that, no drag resistance is acting on this payload, thus it is expected that these loads will be slightly lower in the actual environment due to wind loads.

The magnitude of all the loads is divided in a similar manner for all sea states in the second and third load configuration. The effective tension is the largest load, then the shear in Y-direction and lastly the shear in X direction. The reason why the effective tension is the largest is because the axial stiffness of the gripper absorbs all the payload motion that normally would occur in line with the gripper. The positioning of the gripper with respect to the payload and its axial stiffness result in decreased motion but an increased effective tension. This result can be explained as the motion that is reduced results in higher loads in the object that reduces the motion, in this case the gripper. With similar reasoning, the lower load in shear X-direction can be explained. Since less motion is reduced in the shear X direction (Y direction of the payload), the load the gripper endures in this direction is also lower.

Again, the first load configuration differs from the second and third states as the motion comes solely from the vessel motion. The shear load in the Y direction is lower since no wave loads excite the payload in this configuration. Contrary to the other states where the payload is not only influenced by the vessel motion but by the wave loads as well. Since the payload does not experience any drag, the roll motion of the vessel affects the payload motion and thus the shear load in the X-direction, more extremely in the first configuration. This results in the higher shear load in X-direction compared to the other load configurations.

In general, it can be concluded that loads are larger if more motion is reduced as the energy is absorbed by the gripper. Furthermore, if the payload is submerged, the loads are higher in axial direction and shear Y direction on the gripper due to both vessel dynamics and wave loads acting on the payload. However, the largest shear load in X-direction occurs if the payload is retrieved from the water. Acting as a double pendulum, there is no other resistance acting on the payload other than the gripper. The structural integrity of the gripper is analysed for each loading configuration in the next section.

4-3 Finite element analysis

The loads that are shown in Section 4-2 need to be implemented in Ansys to check the structural integrity of the model. The verified model described in Section 3-5 is used for this finite element analysis in Ansys together with the described parameters. The loads that yielded from the dynamic analysis were implemented in the structural model.

Three different load combinations are applied on the structure for each of the corresponding load configurations. The load cases are the result of the maximum possible loads per direction for each configuration. Table 4-3 shows the applied loads per load configuration.

Table 4-3: Applied loads per load configuration

	Effective tension (kN)	**Shear X (kN)**	**Shear Y (kN)**
State 1	350	151	80
State 2	224	57	76
State 3	503	54	141

Besides the applied loads, gravitational acceleration is added since the self weight applies loads on the model as well. The deformation of the model is analyzed in the X-, Y- and Z-direction by δ_x, δ_y and δ_z respectively. Furthermore the equivalent stress σ is retrieved from the model. As stated in Section 3-5-2, the deformation should be below 760 mm and the maximum allowable stress is 240 MPa (for plate thickness up to 40 mm).

The FEA results of the first iteration of the design process are shown in Table 4-4. Since the plate thickness is 50 mm for this iteration, allowable stress is limited to 226 MPa [Meadinfo, 2015]. Load configuration 1 has 84% of the allowable stress (190/226). However, all other results are well below the preferred limit of 80%. Therefore, there is room left to optimize this model further.

Table 4-4: FEA Results first iteration

	δ_x [mm]	δ_y [mm]	δ_z [mm]	σ [MPa]
Load configuration 1	35	5	38	190
Load configuration 2	9	3	37	140
Load configuration 3	9	4	41	147

The design process eventually yielded an optimized geometry that is shown in Section 4-1. The FEA results of the optimized geometry are shown in Table 4-5. Load configuration 1 is still the configuration that is closest to the allowable limits. The entire finite element analyse model of the optimized geometry is shown in Appendix D.

Table 4-5: FEA results

	δ_x [mm]	δ_y [mm]	δ_z [mm]	σ [MPa]
Load configuration 1	141	10	161	240
Load configuration 2	53	8	158	192
Load configuration 3	51	9	199	226

The first load configuration has the highest δ_x as the shear load in X-direction is also the largest for this state. The relatively large load in this direction causes the stress in this configuration to be the highest as well because the model is not designed to take up large loads in shear X-direction. The third load configuration has a higher δ_z but a lower equivalent stress, which also proves this point.

The aim of the finite element analysis is to verify the structural integrity of the conceptual model. If the model was designed too small, the allowable limits of 760 mm deformation and 240 MPa stress would be exceeded. To optimize the material usage of the model, it was stated in the design process (See Section 3-1) that the stress and/or deformation (if possible) should be between 80 and 100 % of the allowable limits. However, the design process also indicated that the allowable limits are superior over the minimum border of 80%. The FEA results yielded that for the first load configuration, the stress limit is met at 100%. Meaning, there is no room left to optimize further by decreasing the size of the gripper arm.

4-4 Motion reduced

The geometry of the telescopic arm that is optimized, is implemented in Orcaflex to retrieve the motion of the payload for these parameters. Besides the loads on the gripper, the dynamic analysis also yields the motion of the payload. The payload motion in X, Y and Z direction can be plotted for both the Benchmark (BM) model (i.e. no gripper attached) and the dynamic model with a Gripper (GR) attached to the payload. This comparison is conducted for the first load configuration as the payload does not experience any wave loads directly. Furthermore, the motion that occurred in this load configuration was the root cause of this study.

The payload motions differ per sea state and are shown in Figure 4-8, Figure 4-9 and Figure 4-10. These 3D images of the payload motion can be hard to interpret and therefore other angles of these plots are shown in Appendix E.

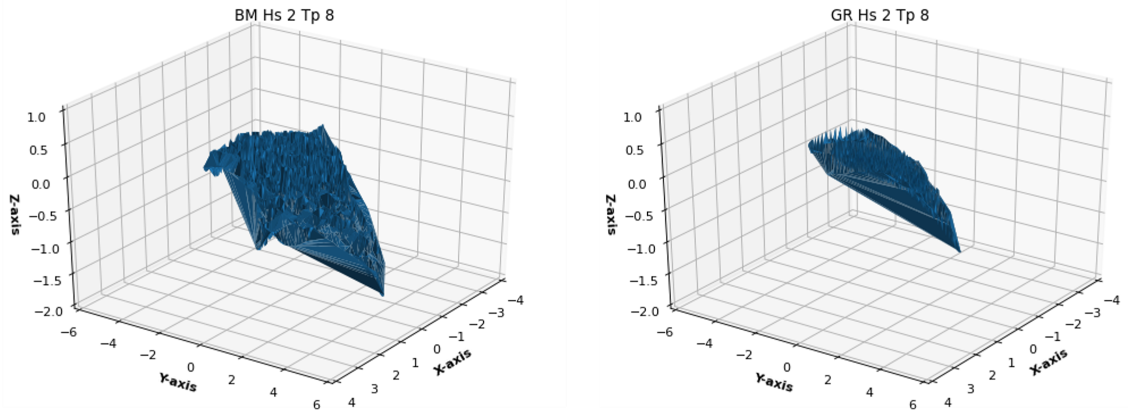

Figure 4-8: Payload motion at H_s 2 m & $T_p = 8$ s

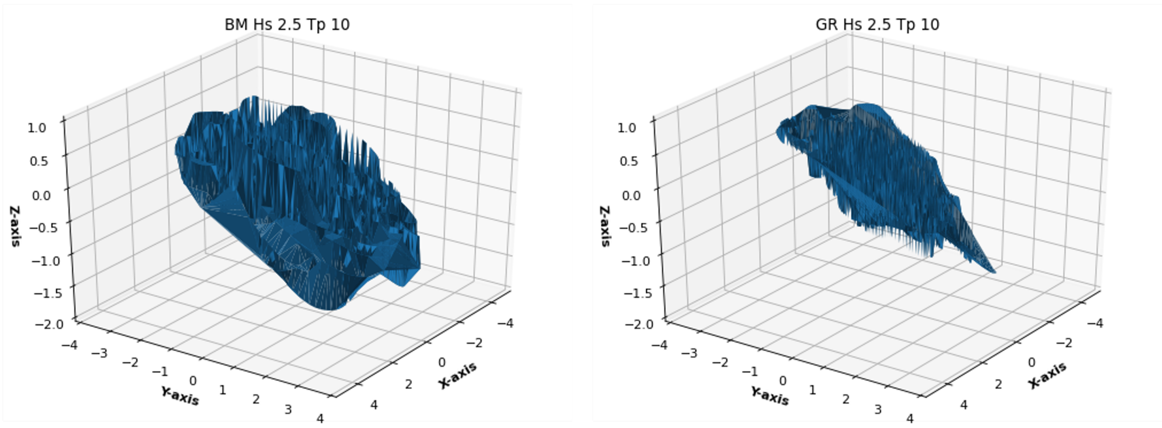

Figure 4-9: Payload motion at H_s 2.5 m & $T_p = 10$ s

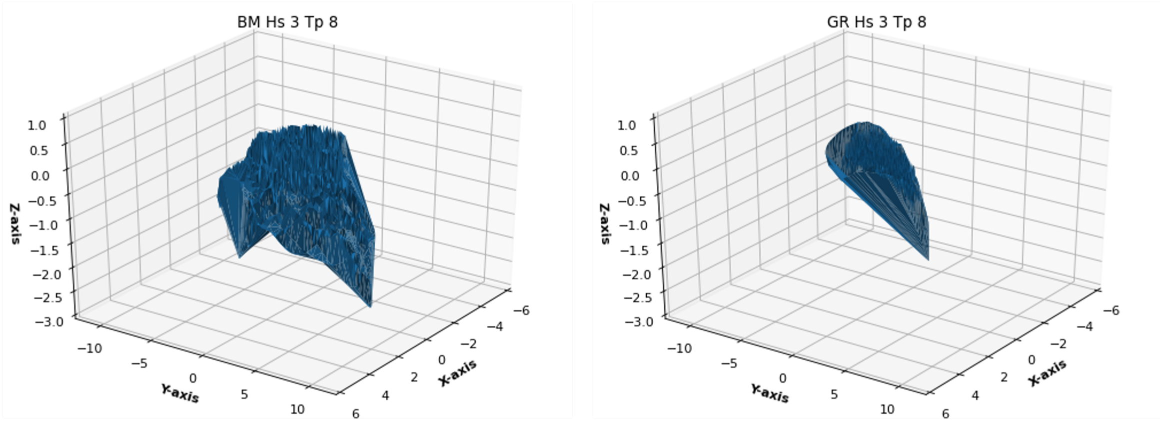

Figure 4-10: Payload motion at H_s 3 m & $T_p = 8$ s

The payload motion for the benchmark model is visibly larger in all sea states, thus the gripper reduces the payload motion. In order to determine the amount of motion reduced more accurately, the results are translated to percentages. Equation (4-2) shows the equation that is used to express the reduced motion in percentages.

$$\text{Motion reduced [\%]} = \frac{\text{Maximum BM [m] - Maximum GR [m]}}{\text{Maximum BM [m]}} * 100 \tag{4-2}$$

The maxima are determined by the dynamic analysis and the formula described above is applied for each sea state. Table 4-6 shows the payload motion reduced in percentages.

Table 4-6: Reduced payload motion in percentages

	Dynamic X [%]	Dynamic Y [%]	Dynamic Z [%]
$H_s = 2$ m & $T_p = 8$ s	87.16	26.42	32.88
$H_s = 2.5$ m & $T_p = 10$ s	83.68	4.15	16.41
$H_s = 3$ m & $T_p = 8$ s	82.94	28.38	37.04

The payload motion is reduced drastically in X-direction but it has a less drastic effect on the Y and Z motions. Since the gripper is stiff in axial direction and the payload motion in X-direction is in line with the gripper, the logical consequence is a big effect on the occurring motion.

The lower results in Y-direction can occur due to inaccuracy in the dynamic model. The gripper is not modeled with its slew bearing in Orcaflex and therefore motion occurs in Y-direction. If this bearing is accurately modeled, the movement of the payload is also constrained in Y-direction. This would result in a higher reduced motion but would also yield higher loads on the gripper.

To check whether the dynamic response is as expected, certain patterns can be noticed. For example, Figure 4-8 and Figure 4-10 show quite similar results except for the magnitude of the plot. However, this result is logically as both sea states have a similar wave period and only the magnitude of the wave height differs.

Moreover the dynamic response shown in Figure 4-9 is large compared to the other sea states. This can be explained due to the fact that the RAOs of the vessel are larger for each DOF for a wave period of 10 seconds compared to 8 seconds.

The motion reduction in the sea state with $H_s = 2.5$ meter & $T_p = 10$ seconds is significantly lower than the motion reduction of the other two sea states. The reason for this difference originates in the difference in the wave period. Since both sea states of 8 seconds experience more motion reduction compared to the sea state of 10 seconds while a higher and a lower significant wave height are analyzed. Thus, the wave period influences the results of the model and this could be caused by the natural frequency of the model. Since the natural frequency of the telescopic arm, can cause resonance due to the excitation from the waves. In order to verify whether that is indeed the cause of the motion in this sea state, a modal analysis is required.

If this modal analysis yields that the natural frequency is indeed close to the wave period of 10 seconds then a possible solution can be to reduce the range of motion of the gripper. Reducing the range of motion of the gripper means decreasing the length of the telescopic arm for the concerned sea state. If the length is decreased, the natural frequency increases and thus the occurring motion will decrease. In order to accurately verify the motion reduction, a modal analysis should be executed first.

Chapter 5

Conclusion & Recommendations

5-1 Conclusion

The general problem described in this thesis is that during offshore lifting operations, in particular during the retrieval of payload, undesired motion occurs. The goal of this study is to reduce this motion in order to guarantee a safe and efficient lifting operation. In order to reach this goal, the following research question was configured:

How can a feasible conceptual model be developed to reduce payload motion during offshore lifting operations?

To answer this question first, the theory and factors that are relevant for understanding payload motion are described. For this study, a Pierson-Moskowitz wave spectrum is used and the operational sea state limits of an offshore company at the ocean are analyzed:

1. $H_s = 2$ meter & $T_p = 8$ seconds
2. $H_s = 2.5$ meter & $T_p = 10$ seconds
3. $H_s = 3$ meter & $T_p = 8$ seconds

These operational limits influence the vessel motion through its RAOs and this study only considers wave loads, neglecting current and wind loads. Furthermore, the considered payload is a 185 ton pre-piling template as this payload maximizes the loads on the entire system. Thus it can be concluded that any payload with lower mass and/or surface will fall within the scope of this study.

Then, the state-of-the-art solutions that compensate or reduce motion are analyzed. There is a variety of solutions both in literature and in industry such as heave compensation, a delta parallel robot and 3D motion compensated cranes. However, these solutions cannot be transformed to be applied on to mast cranes, do not provide enough motion reduction or cannot fulfill the weight capacity requirements. In this study only four solutions are selected that hold promising potential for reducing the payload motion.

These solutions are; a gyroscopic stabilizer, software motion control, rails with a support basket and an automated side loader. For each concept solution, besides motion reduction, required time, money and power are considered to be important selection criteria. Based on the quantified selection criteria and with the help of an analytic hierarchy process, the automated side loader of a garbage truck is considered the most promising concept.

This concept is developed into a conceptual model with a design process that optimizes the material usage whilst monitoring if the model complies with all the relevant offshore standards. First the geometry is built up based on the requirements, then, according to offshore standards, a dynamic analysis is executed. The loads retrieved from that analysis are used as input for the finite element analysis. The structural integrity of the geometry is verified and based on that geometry the reduced payload motion is retrieved from the dynamic analysis.

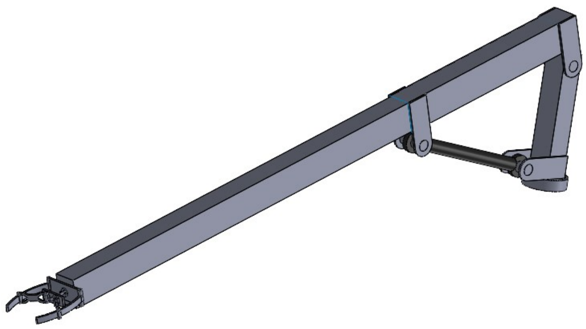

Figure 5-1: Conceptual 3D model

The geometry of the conceptual model (See Figure 5-1) is able to match the reach of the mast cranes on a heavy-lift crane vessel. The design is based on the assumptions such as actuator stroke, safety clearances from offshore standards and simplified attachment to the payload. Furthermore, the gripper is modelled as spring-damper system in the dynamic analysis and a simplified beam model is used to conduct the FEA.

The iterative design focused on optimization of material usage. Compared to the first iteration, over 90 tons of steel is saved due to this optimization process.

The dynamic analysis yielded that, in general, the largest loads occur in the direction where the motion is reduced most. This is the axial direction (i.e. X direction), where on average 85% of the initial payload is reduced. For payload motion in Y and Z direction the reduction is less drastic with an average reduction of 20 % and 29 % respectively.

With the findings in this study combined, it can be concluded that a feasible conceptual model can be developed to reduce payload motion during offshore lifting operations. This model would consist of an automated side loader that is optimized to reduce payload motions. With this concept, the industry could evolve further toward a safer and more efficient operational environment offshore.

5-2 Recommendations

The assumptions made in this thesis form the limitations of this study and open up opportunities for further research. Below, the possibilities for further research are discussed:

Improve conceptual model
The dynamic analysis yielded large forces in shear X direction for some of the load configurations. However, the model cannot absorb these loads effectively, resulting in high stress for these configurations. To decrease this stress and enable further optimization of the model, an improvement can be made. To increase the stiffness in the X direction, two Constant Tension (CT) winches could be attached to the end of the gripper (See Figure 5-2). These winches increase the load capacity the model can absorb in the X-direction. Therefore, less material could be required for the telescopic arm, further optimizing the material usage of the model. Developing such an improvement would require further research, as this requires new dynamic analysis, FEA and a control system for the CT winches.

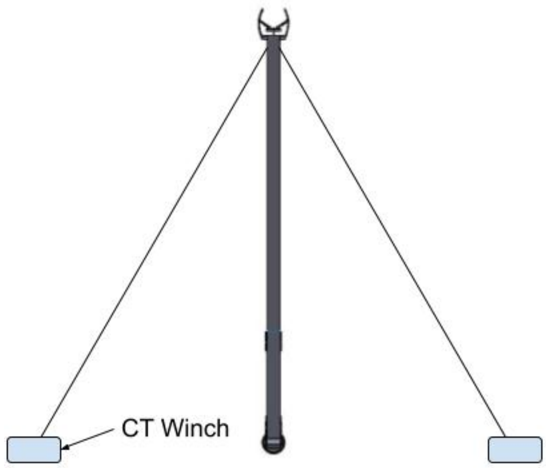

Figure 5-2: Possible improvement model

Detailed finite element analysis
In order to develop the conceptual model into a detailed model, a detailed FEA should be conducted. The current analysis only takes into account the deformation and equivalent stress. Detailed analysis could include analysis on the welds, buckling analysis and fatigue analysis to verify the lifetime of the concept. In addition to static analyses, modal analysis could be conducted as well to determine the natural frequency of the model. This study provides a starting point for the development of a detailed concept, but these analyses should be executed to complete a detailed design.

Extend dynamic analysis
The dynamic analysis described in this study satisfies developing a conceptual model, however, it should be extended to develop a detailed concept design. The slew bearing of the gripper will constrain movement in shear X-direction, if that could be modeled correctly, a more accurate dynamic response of the payload can be retrieved from the analysis. In addition to the modeling of the concept, the scope of the analysis can be broadened as well. A large sequence of sea states could be included in the scope as well as a large diversity in wave directions. Including these factors in the dynamic analysis will show the operational boundaries of the model and expose its weaknesses.
It would also be interesting to observe the behaviour of the model during the entire lifting cycle. Currently, only three load configurations are analyzed, but by simulating the lifting cycle, a more accurate description of the behaviour of the model can be constructed. Extensive dynamic analysis could largely improve the current model and verify whether the model is effective throughout its entire lifting cycle.

Attachment between gripper and payload
The current study assumes that the gripper attaches to the payload if the arm reaches the payload. However, this is not realistic and since a variety of payloads should be retrieved with this model, a study could be conducted to analyze the possibilities of an attachment tool. This tool could be attached to the payload (i.e. welded or bolted) and simplifies the attachment of the gripper to the payload. The validation of attachment should be taken into the scope of this research as well. Since the attachment occurs in the splash zone, visual conformation might be hard. Therefore, a validation technique on whether the connection is made should be configured in this study as well.

Control of conceptual model
With this new conceptual model, a new problem arises, namely the control of the model. As the model has a hydraulic actuator and hydraulic-actuated telescope arm, a control structure could be constructed. Such a control system should take into account vessel and wave dynamics to accurately control the payload. If an active control system is designed, it should also interact with the crane control system, as both systems would influence each other. Accurate control could improve the damping of the motion making the lifting operation safer and more efficient.

Kinematic analysis of gyroscopic stabilizer
Apart from the developed automated side loader, other concepts where taken into consideration in this study as well. The gyroscopic stabilizer is a concept that has a lot of potential, as it would require a low initial investment and is easy to integrate in the current crane configuration. However, an analysis regarding the kinematics of a gyroscope should prove whether this concept is able to reduce the payload motion. Verton Technologies is trying to develop a solution, but currently no such solution exists.

Bibliography

G. Altare, G. Franzoni, J. Harsia, and T. Hickey. Latest Technology Advancements in Hydraulic Systems for Refuse Vehicle Applications: The Case of an Automated Side Loader. In *10th International Fluid Power Conference*, 2016.

Ampelmann. E5000, 11 2019. URL https://www.ampelmann.nl/systems/e5000.

AXTech. Solutions for heavy lifting for offshore and maritime industry, 2015. URL https://www.axtech.no/.

Axtech. 420T Special Handling System, 12 2015. URL https://www.axtech.no/news/420t-special-handling-system.

Stephen Blake, Chris Hill, Terry Moore, Chris Hide, and David Park. A Heave Compensation Algorithm Based on Low Cost GPS Receivers. *Journal of Navigation*, 61(2), 2008. ISSN 03734633. doi: 10.1017/S0373463307004651.

J.R. Buijs. *3D Motion Compensation for an Offshore crane*. PhD thesis, Delft University of Technology, Delft, 11 2017.

CMCO. Sway Control System (SCS®) Series 2, 2016. URL https://www.columbusmckinnon.com/en-us/products/power-and-motion-technology/ac-motor-control-systems/drive-support-tools/sway-control-system-scs-series-2/.

Mikal Dahle, Loic Meignan, and Rafael Rossi. Large module installation and intervention system at aasgard. In *Proceedings of the Annual Offshore Technology Conference*, volume 3, 2016. doi: 10.4043/27078-ms.

Det Norske Veritas. Modelling and Analysis of Marine Operations. *Practice*, DNV-RP-H103 (April), 2011.

Det Norske Veritas. OFFSHORE STANDARD DET NORSKE VERITAS AS Lifting Operations (VMO Standard-Part 2-5). Technical report, DNV, 2014. URL www.dnvgl.com.

DNV. DNVGL-ST-0377 Shipboard lifting appliances. Technical report, DNV, 2018. URL http://www.dnvgl.com,.

Enerpac. How to choose the right hydraulic cylineder, 10 2020. URL https://blog.enerpac.com/how-to-choose-the-right-hydraulic-cylinder/#:~:text=Stroke%20is%20defined%20as%20the,cylinders%20including%20low%2Dheight%20versions.

Antonio Giallanza and Tony Elms. Interactive roll stabilization comparative analysis for large yacht: gyroscope versus active fins. *International Journal on Interactive Design and Manufacturing*, 14(1), 2020. ISSN 19552505. doi: 10.1007/s12008-019-00618-y.

Vegard Wie Henriksen, Audun Gerhardsen Røine, Espen Skjong, and Tor Arne Johansen. Three-axis Motion Compensated Crane Head Control. *IFAC-PapersOnLine*, 49(23):159–166, 2016. ISSN 24058963. doi: 10.1016/j.ifacol.2016.10.337.

Huisman. Personal communication (mail), 4 2022.

J.M.J Journee and W.W. Massie. *Offshore Hydrodynamics, First Edition*. Delft University of Technology, Delft, 2001.

Jumbo Maritime. Internal data, 2021.

Jumbo Maritime. JM-MEMO-701 J-Type Validation in Orcaflex, 2022.

Rembrandt Klopper and Sam Lubbe. Using matrix analysis to achieve traction , coherence , progression and closure in Problem-Solution Oriented Research. *Alternation Special Edition*, 4(2011), 2011. ISSN 1023-1757.

KoneCranes. Sway Control, 2016. URL https://www.konecranes.com/en-us/equipment/overhead-cranes/safe-features-for-overhead-cranes/sway-control.

H Lageveen. Modelling and Steering of Tuggerwinch. Technical report, University of Technology Delft, Delft, 4 2014. URL http://resolver.tudelft.nl/uuid:52f82120-3728-48f7-abd1-be5f891d2bb3.

Zhi Li, Xin Ma, and Yibin Li. Anti-swing control for a double-pendulum offshore boom crane with ship roll and heave movements. In *IEEE International Conference on Control and Automation, ICCA*, volume 2020-October, 2020. doi: 10.1109/ICCA51439.2020.9264524.

Liebherr. Anti-sway system Cycoptronic, 2014. URL https://www.liebherr.com/en/sgp/products/maritime-cranes/maritime-technology/cycoptronic/cycoptronic.html#!/advantages=more-productivity+increased-safety.

MacGregor. 3-axis motion compensation cranes, 2014. URL https://www.macgregor.com/Products/products/offshore-and-subsea-load-handling/3-axis-motion-compensation-cranes/.

MacGregor, Ulstein, and TTS. Offshore cranes - Colibri 3D motion compensated, 2018. URL https://www.macgregor.com/Products/products/tts-products/Offshore-cranes---Colibri-3D-motion-compansated/.

Meadinfo. Material Properties of S355 Steel - An Overview, 8 2015. URL https://www.meadinfo.org/2015/08/s355-steel-properties.html.

Oceaneering. Large Vessel Interface Lift On/Lift Off, 2013. URL https://www.oceaneering.com/otech/seabasing/.

Sathit Pongduang, Chatchapol C., and Phansak Iamraksa. Non-linearity Analysis of Ship Roll Gyro-stabilizer Control System. *Sustainable Marine Structures*, 3(1), 5 2021. doi: 10.36956/sms.v3i1.316.

Liyana Ramli, Z. Mohamed, Auwalu M. Abdullahi, H. I. Jaafar, and Izzuddin M. Lazim. Control strategies for crane systems: A comprehensive review, 2017. ISSN 10961216.

Raymax Equipment. HEIL Automated Side Loader, 3 2020. URL https://www.raymaxequipment.com/product/heil-automated-side-loader-1.

Red Rock. 3D Motion Compensated Crane (RMCK), 2020. URL https://www.redrock.no/portfolio/3d-motion-compensated-crane-rmck/.

R. W. Saaty. The analytic hierarchy process-what it is and how it is used. *Mathematical Modelling*, 9(3-5), 1987. ISSN 02700255. doi: 10.1016/0270-0255(87)90473-8.

Siemens. SIMOCRANE Sway Control, 2016. URL https://mall.industry.siemens.com/mall/en/WW/Catalog/Products/10165521#Application.

SMST. 3D Motion Compensated Cranes, 2016. URL https://www.smstequipment.com/offshore-cranes/3d-motion-compensated-cranes/.

Ning Sun, Yiming Wu, Yongchun Fang, and He Chen. Nonlinear Antiswing Control for Crane Systems with Double-Pendulum Swing Effects and Uncertain Parameters: Design and Experiments. *IEEE Transactions on Automation Science and Engineering*, 15(3), 2018. ISSN 15455955. doi: 10.1109/TASE.2017.2723539.

Siebe B. Van Albada, G. Dick Van Albada, Hans Petter Hildre, and Houxiang Zhang. A novel approach to anti-sway control for marine shipboard cranes. In *Proceedings - 27th European Conference on Modelling and Simulation, ECMS 2013*, 2013. doi: 10.7148/2013-0249.

Daan van Wel. The next step for load control with tugger winches. Technical report, Rotterdam Mainport Institute, Rotterdam, 12 2021.

Verton Technologies. EVEREST 6, 2019. URL https://www.verton.com.au/everest-6.

Sheng Hai Wang, Zhao Peng Ren, Jia Lu Du, Hai Quan Chen, and Yu Qing Sun. Payload swing suppression for offshore cranes using a novel triple-tagline system: Theory and experiment. *Proceedings of the Institution of Mechanical Engineers Part M: Journal of Engineering for the Maritime Environment*, 234(2), 2020. ISSN 20413084. doi: 10.1177/1475090219874546.

J. K. Woodacre, R. J. Bauer, and R. A. Irani. A review of vertical motion heave compensation systems, 2015. ISSN 00298018.

Binlin Yi and Jiangnan Liu. Multi-objective optimization design of automated side loader of arm actuator. In *Lecture Notes in Electrical Engineering*, volume 408, 2017. doi: 10.1007/978-981-10-2875-5{_}109.

Appendix A

Research Paper

Developing a feasible conceptual model that reduces payload motion during offshore lifting operations

T. de Vlieger, Dr. Ir. X. Jiang, Ing. F.J. van der Werf, Ing. M. Teunis, Prof. Dr. R.R. Negenborn

***Abstract*— Offshore lifting operations need to have reduced payload motion to increase safety and reduce operating time. When payload is retrieved from the splash zone to the deck, besides the crane block, no additional control can be applied on the under-actuated system. Existing studies either assume more control over the payload or develop a control system based on a new crane. To reduce the payload motion on current crane vessels, a conceptual model is developed based on an automated side loader of a garbage truck. In this paper, a dynamic analysis is conducted to obtain the dynamic response of the payload. Moreover, a finite element analysis is used to verify the structural integrity of the geometric model. Simulation results show that the model is able to reduce the payload motion during offshore lifting operations whilst staying within the limits set by offshore standards.**

Keywords—*Conceptual model development, offshore lift operation, motion reduction, dynamic analysis, finite element analysis*

I. Introduction

Global economic expansion has resulted in an increase in the demand for energy to keep up with the needs for people and industry. The depletion of easily accessible oil and natural gas fields has driven the industry offshore, where large floating platforms are used to extract, store and process the retrieved goods. The wind energy industry is also moving offshore due to shortage of land. Both gray and green energy industries require heavy lift cranes to install their equipment. In order to reduce the cost of these installations, the limits at which offshore lifting operations are possible are pushed everyday. Fast installation time and being able to lift during harsh circumstances are the two most important criteria to be competitive in the offshore installation industry.

A heavy lift vessel, has a crane installed on its deck and its relatively high lifting capacity exceeds more than provisions and other resupplies (See Fig. 1). Since the crane is installed on the vessel, the vessel dynamics influence the crane dynamics. Because there are only three control inputs and six DOFs, the heavy lift crane vessel is an under-actuated system which makes it hard to be controlled [Li et al., 2020].

Environment-induced motions such as waves cause uncontrolled movement of the crane tip. Payload that is lifted with a crane block which is suspended from the crane tip is subjected to this uncontrolled motion, as this whole system acts as a double pendulum.

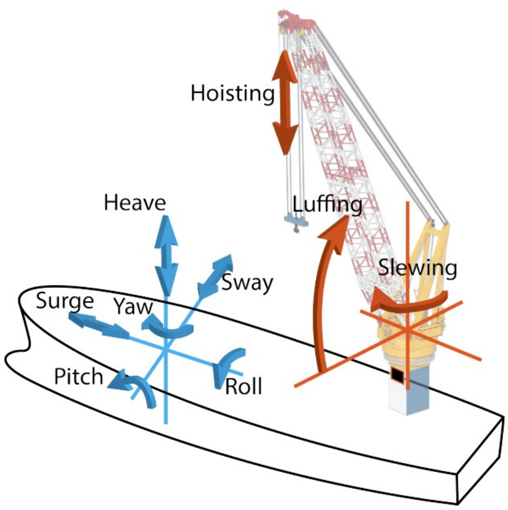

Fig. 1. Heavy lift crane vessel, where the degrees of freedom (DOF) of the vessel are shown in blue and the control inputs for the crane are shown in red. [Buijs, 2017]

The weight capacity of the payload that is considered in this paper is equal to 200 ton. This ensures unaffected motion characteristics of the vessel at the crane tip due to the lift [Det Norske Veritas, 2011]. Moreover, the developed concept needs to match the reach of the cranes that are present on a heavy lift vessel. This range varies between 10 and 35 meter horizontally extended, measured from the centre line of the cranes. Vertically, the model should be able to reach both the deck and the water line including safety margins.

There is a distinct between different offshore lifting operations; a payload is set overboard or a payload that is retrieved from the sea surface. Multiple research has been completed regarding the first stage such as [Lageveen, 2014], [Wang et al., 2020] and [van Wel, 2021]. During this stage, so-called tugger lines are attached to the payload to gain control over the under-actuated motions of the payload. Tugger lines are controlled by winches and provide an additional control input for the under-actuated system. However, when retrieving the payload, these tugger lines are not attached to the payload and gaining control by attaching the tugger lines whilst the payload is in the sea takes up precious installation time.

If no tuggers lines are attached during the retrieval of a payload, installation time is reduced but this causes the payload to swing uncontrolled transforming the payload into a wrecking ball. To prevent a dangerous situation while reducing the installation time, a concept needs to be developed to reduce payload motion during these offshore lifting operations.

Over the last few years, multiple research has been conducted regarding this problem. This resulted in multiple different concepts of motion compensated cranes. However, these concepts all have a maximum lifting capacity of 20 ton or lower. This is not suitable for executing lift operations offshore that are part of an installation procedure as payloads can weigh up to 200 ton.

The solutions that come forth out of the research that has been done, require a new crane that is motion compensated or new motors need to be installed which is almost equally expensive as rebuilding the entire crane [Huisman, 2022]. New conceptual development could innovate the industry by looking at solutions from other industries.

The waste management industry has been using automated side loaders for years (See Fig. 2). Automated side loaders consist of a hydraulic arm that grabs garbage bins and controls them from their starting point to the garbage truck and back. Such a gripper could, if scaled up and designed correctly, provide the solution that the offshore installation industry is looking for.

Fig. 2. Automated side loader HEIL[Raymax Equipment, 2020]

The goal and main contribution of this work is to develop a conceptual model, based on the principle of an automated side loader, that will reduce both installation time and, more importantly, payload motion during offshore lifting operations. Relevant design criteria will define the scope of this paper which will create a benchmark for the development of the conceptual model. To verify that the conceptual model will hold against extreme environmental conditions, a dynamic analysis is executed that mimics the conditions during offshore operations on the Atlantic Ocean. The loads that are retrieved from the dynamic analysis are used to conduct a finite element analysis, this will verify the structural integrity of the conceptual model. To conclude whether the developed concept improves the lifting operation, the motion reduction is assessed. The optimization of this conceptual model is considered to be based on the reduction of material required to ensure structural integrity whilst reducing payload motion.

The rest of the paper is constructed as follows; Section II presents the design process that is required to develop the conceptual model. Section III and Section IV elaborate on the dynamic analysis and finite element analysis respectively. Subsequently, Section V discuss the simulation results for the conceptual model followed by the conclusion in Section VI.

II. Design Process

To develop an automated side loader into an optimized conceptual model, a design process is required (See Fig. 3).

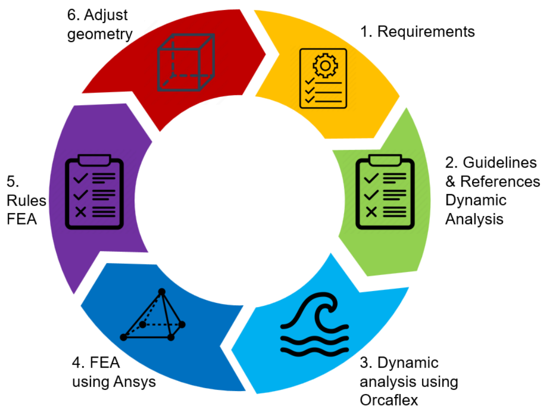

Fig. 3. Flowchart design process

1) The first step consist of the requirements that are established by the offshore industry. These requirements form the boundaries of the design scope and a first geometry is configured based on the requirements.
2) Secondly, guidelines and references are compiled to create a benchmark for the dynamic analysis.
3) The dynamic analysis is conducted by using software called Orcaflex. An heavy lift vessel with payload and the automated side loader are modelled in this software. Various extreme sea states are send towards the vessel to analyse the response of the vessel and the lifted payload in particular. The loads acting on the side loader, that are retrieved from the dynamic analysis, are used as input for the next step.
4) The finite element analysis is conducted by using software called Ansys. The retrieved loads of the dynamic analysis are applied on the geometry of the model. Structural integrity is checked based on deflection and stress.
5) The deflection and stress of the FEA model must comply with rules that are set by the offshore industry standards. If the model complies with the rules and is within 80% of the allowable deflection and/or stress,

the model is considered optimized. The design process ends at this step, however if this is not the case, the process continues.

6) If the allowable stress and/or deformation limits are exceeded, the geometry needs to be adjusted accordingly. The model is also not considered optimal if, both the stress and deformation are less than 80% of the allowable limits. The adjusted geometry, needs to circulate the entire design process again to make sure that the model complies with all rules and guidelines. Moreover, a different geometry yields different outputs for both the dynamic analysis and the FEA.

The requirements of the reach of the crane and its required capacity are combined with the design of an automated side loader [Altare et al., 2016]. This combination yielded a conceptual 3D model (See Fig. 4). The dimensions of this 3D model are used as input for both the dynamic analysis and the finite element analysis.

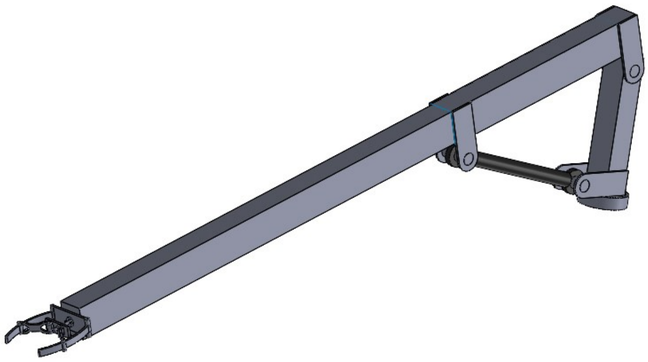

Fig. 4. Conceptual 3D model

III. Dynamic analysis

In this section the dynamics of a heavy lift vessel and its payload are modelled in two steps. First a model to model the waves accurately is proposed and then the dynamic response of the vessel and its payload are modelled based on validated values of a maritime company.

A. Modelling environmental loads

For this study, only wave loads are assumed to be influencing the vessel's motion. Waves have the largest impact on the motion of the vessel and this assumption simplifies the model by leaving wind and current loads out of the equation.

Waves can be described by a wave spectrum, this describes the distribution of wave energy with respect to the wave period. The Pierson-Moskowitz wave spectrum (See Eq. 1) is assumed for this paper because this is the most accurate description to represents a fully-developed sea such as the Atlantic Ocean [Journee and Massie, 2001]. The wave spectral density S_ζ depends on the significant wave height H_s and the wave period with the highest energy T_p.

$$S_\zeta(\omega) = 3060 * \frac{H_s^2}{T_p^4} * \omega^{-5} * \exp\left[-\frac{1948}{T_p^4} * \omega^{-4}\right] \quad (1)$$

A sea state is describe in terms of H_s and T_p. The current limiting sea states at which the offshore industry is able to operate are:

1) $H_s = 2m$ & $T_p = 8s$
2) $H_s = 2.5m$ & $T_p = 10s$
3) $H_s = 3m$ & $T_p = 8s$

These sea states are analysed as the current limiting sea states yield the greatest payload motion due to more extreme environmental loads.

B. Modelling the dynamic response of the vessel

Any object that is floating at sea is subjected to the wave spectrum that is described in the previous section. The response of each object depends on its so-called response amplitude operator (RAO). The RAOs of a vessel are defined transfer functions for each DOF that consist of parameters for that DOF. Based on the data of a maritime company, the RAOs used in this study are shown in Appendix I [Jumbo Maritime, 2022]. The direction at which the waves approach the vessel influence the RAOs. During offshore lifting operations a vessel wants to face the waves head on which is equal to a wave direction of 180 degrees. As waves, never go in one straight direction, a 15 degree error margin is taken into account [Journee and Massie, 2001]. Thus the wave direction for the RAOs of Appendix I is equal to 165 degrees.

By combining the wave spectrum with the RAOs of the vessel, the dynamic response spectra of the vessel can be calculated in all six DOFs (See Eq. 2).

$$S_{response}(\omega) = |RAO|^2 * S_\zeta(\omega) \quad (2)$$

The vessel dynamics can be translated directly onto the crane tip as the simplification is used that the crane consists of a rigid body. Therefore, the motion of the crane tip is only subjected to the vessel dynamics. During offshore lifting operations, a payload is subjected to these crane tip motions and that causes undesirable swinging, pendulum-like motions of the payload. To control this motion, the automated side loader or gripper grabs the payload below the waterline. The swinging motion only occurs above the waterline as the water damps most of the motions if the payload is still in the water.

The gripper is modelled as a spring damper system in Orcaflex, which is marine software for dynamic analyses. The stiffness depends on the dimensions of the cross section of the telescopic arm. The damping mimics the damping of a passive heave compensator, which resembles the hydraulic actuator accurately [Jumbo Maritime, 2021]. This spring damper system is constraint between the vessel and the payload to construct the actual attachment of the gripper.

The payload is a 10 by 10 meter pre-piling template that is subjected to multiple factors in order to model the payload accurately; *Buoyancy:* This upward driven force

has a magnitude that is equal to the weight of the displaced fluid. This factor depends on the wet weight of the payload and the volume. For this study a payload of 161 tons wet weight and a volume of 23.6 m^3 is considered.
Mass moment of inertia: The amount of force required to reach a desired acceleration in a specified direction is specified by the mass moment of inertia. This depends on the mass distribution over the body and how its principle axis of rotation are defined. For the payload in this study the mass moments of inertia, with homogeneous mass distribution and axis of rotation normal to its outer planes, are 1542 $ton * m^2$ for the X- and Y-axis and 3083 $ton * m^2$ for the Z-axis.

Drag: Fluid resistance or drag is expressed as a force that is acting in opposite direction of the relative motion of a moving object regarding its surrounding fluid. Drag depends on the velocity at which the object moves, the density of the fluid, the cross sectional area normal to the motion and a dimensionless drag coefficient. For this study all variables are implemented according to the offshore standards of DNV [Det Norske Veritas, 2011].
Fluid inertia: When an object moves in fluid, not only the object but the fluid it moves has a moment of inertia. This moment of inertia is often called added mass or hydrodynamic mass. Rotational fluid inertia is considered negligible as it is marginal compared to the inertia of the payload itself.
*Slam forces:*If the payload enters or exists the water, slam forces apply load on the payload. These forces apply on the area normal to the water surface during the initial contact which is considered to be 100 m^2 for this study.

All these factors are assigned a value based on calculations and offshore standards. Together, they describe the behaviour of the payload that will yield a dynamic response by using Orcaflex. One of the selected sea states is send towards the vessel for 10 minutes to simulate the behaviour of the system. After the simulation, a Rayleigh distribution is used to extrapolated the data to its extreme value statistics of three hours. Within three hours, the highest maximum wave of a sea state has passed thus the limiting states for the system are modelled [Journee and Massie, 2001]. The gathered data contains loads on the modelled side loader and this is used as an input for the finite element analysis.

IV. Finite element analysis

The gathered loads of the dynamic analysis are applied on the telescopic arm from the geometry of the conceptual model. This FEA consists of a general structural analysis regarding the deformation and equivalent stress of the model. Detailed FEA such as buckling, fatigue or analysis of welds is not considered in this study. The structural integrity of the 3D model is verified along the allowable limits for deformation and equivalent stress according to DNV offshore standards. The allowable deformation for lifting appliances is 760 mm and the allowable stress is equal to 240 MPa for S355 Offshore steel.

The telescopic arm is converted into a beam model which allows for a verification by hand calculation and easier implementation in the FEA model (See Fig. 5).

The hand calculation consists of two stiffness matrices, one for each beam element in the model. By combining these stiffness matrices, a global stiffness matrix can be constructed. Solving the global stiffness matrix by implementing the boundary conditions yields formulas to describe each unknown variable. The deflection at node 3 (i.e. v_3) is used to verify the accuracy of the FEA model (See Eq. 3).

$$v_3 = \frac{F_{3Y} L_2^3}{3EI_2} + \frac{F_{3Y} L_1 L_2^2}{3EI_1} \tag{3}$$

When the variables within Equation 3 are inserted, v_3 is determined to be 167.44 mm. This value is used to determine the FEA model. When the exact same variables are implemented in the constructed model, it yields a deformation at the third node of 167.23 mm. Since this is an error margin of 0.13 %, the model is presumed to be accurate enough to analyse the structural integrity of the telescopic arm.

V. Results

Since the design process of Figure 3 is used to optimize the conceptual model regarding the required material, there are four types of results. The dimensions of the telescopic arm, the loads retrieved from the the dynamic analysis, the FEA results and lastly, the payload motion reduced.

A. Dimensions of telescopic arm

The dimensions of the telescopic arm are optimized for both the non-extendable part of the arm ($K^{(1)}$ in Fig 5) and the extendable part of the arm ($K^{(2)}$ in Fig 5). The optimization focused on required material and these dimensions are used for the dynamic analysis and the FEA as well (See Tab. I).

TABLE I
Cross section telescopic arm dimensions

Property	Non-extendable part	Extendable part
Outer width	1.18 m	1.1 m
Outer height	1.48 m	1.4 m
Inner width	1.1 m	1.02 m
Inner height	1.4 m	1.32 m

B. Loads retrieved from dynamic analysis

The selected sea states are analysed for different load configurations in the dynamic analysis. In the first load configuration, the payload is lifted out of the water thus only vessel motions cause the payload to swing similar to a pendulum. In the second configuration, the payload is submerged into the water, 10 meter horizontally away from the centre axis of the gripper and the crane. Both the vessel motion and the wave loads influence the payload in this configuration. The third state is 35 meter horizontally away

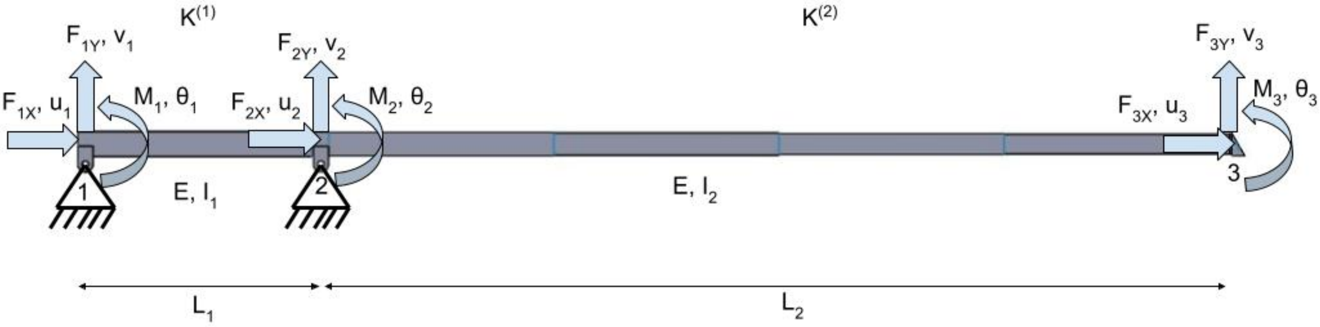

Fig. 5. Beam model of gripper

from the centre axis of the crane but other than that it is similar to the second load configuration.

The loads in axial direction of the gripper arm are largest in the third load configuration as both wave loads and vessel motion influence the payload (See Tab. II). Moreover, the arm is fully extended in this load configuration compared to the second load case. The first load case has the largest shear load in X-direction as the payload is a pendulum that is not damped in any direction. Contrary to the other load cases, where the water is damping the motion of the payload, in this load case the gripper absorbs all loads in that direction.

TABLE II

RETRIEVED LOADS DYNAMIC ANALYSIS

	Axial Load [kN]	Shear X [kN]	Shear Y [kN]
Load configuration 1	350	151	80
Load configuration 2	224	57	76
Load configuration 3	503	54	141

C. FEA results

The loads of table II are applied on the beam model of figure 5 that is modelled as FEA model. As the maximum deformation should stay below 760 mm in X-, Y- and Z-direction ($delta_x$, $delta_y$ and $delta_z$ respectively). Furthermore the equivalent stress σ should not exceed 240 MPa as this is the allowable yield limit of S355 steel including a safety factor [DNV, 2018]. The dimensions of the geometry are considered optimized if the FEA results are as close to the allowable limits as possible (See Tab. III). Since the first load case yields a stress that is equal to the allowable limit, no further optimization is possible.

TABLE III

FEA RESULTS

	δ_x [mm]	δ_y [mm]	δ_z [mm]	σ [MPa]
Load configuration 1	141	10	161	240
Load configuration 2	53	8	158	192
Load configuration 3	51	9	199	226

The stress in the first load case is limiting further optimization and it is cause by the large shear load in X-direction. The conceptual model is designed to absorb loads in axial direction and in shear Y-direction. In order to improve the model further, constant tension winches could be attached to the end of the arm to reduce the loads in the first load configuration. After that, the dimensions can be reduced more as lower stress will be present at the load configurations because the winches absorb part of these loads.

D. Motion reduced

For determining how much payload motion can be reduced by the conceptual model, a comparison between a model with and without the gripper is required. This comparison is made for the three selected sea states and the dynamic response of the payload is compared to each other (See Tab. IV). The dynamic response is largely reduced in X-direction, as this is in line with the gripper so all loads are absorbed axially.

TABLE IV

REDUCED PAYLOAD MOTION IN PERCENTAGES

	Dynamic X [%]	Dynamic Y [%]	Dynamic Z [%]
H_s = 2 m & T_p = 8 s	87.16	26.42	32.88
H_s = 2.5 m & T_p = 10 s	83.68	4.15	16.41
H_s = 3 m & T_p = 8 s	82.94	28.38	37.04

Although, the conceptual model reduces the payload motion overall, more motion reduction is possible if two adjustments are added to the model. First of all, motion reduction in Z-direction can be cancelled out of the equation by adding a passive heave compensator to the lifting arrangement. This is already commonly done in offshore operations and its effect would be significant. Secondly, the movement of the payload in Y-direction can occur due to a modelling inaccuracy. As the model has a slew bearing similar to the crane (See Fig. 1), it also has a stiffness in slew direction. However, this motion is not reduced in the current dynamic model. By accurately modelling the slew bearing of the gripper, the motion is Y-direction will be reduced. This will also increase the forces that need to be absorbed in that direction and thus further structural analysis would also be required.

VI. Conclusion and Future Work

In this paper, the development of a conceptual model for motion reduction during offshore lifting operations of a crane vessel is presented. The geometry of the model is based on an automated side loader of the waste management industry. The under-actuated system receives additional control from the gripper and can make the lifting operation more safe and efficient. To validate the models effectiveness, a dynamic model is designed. Simulation results of the designed model showed the influence of the gripper on the occurring motion and the loads that are applied on the side loader. To verify the structural integrity, an FEA is conducted with the retrieved loads. Thus, the developed conceptual model enables for a reduced payload motion and an improved operating time within the limits of the offshore standards during offshore lifting operations.

Future work should include:

1) Detailed FEA including buckling, fatigue and modal analysis
2) Extended dynamic analysis including accurate modelling slew constraint and simulating entire lifting cycle
3) Focus on gripper/payload attachment, including development of tool and simulation of attachment through splash zone.

References

[Altare et al., 2016] Altare, G., Franzoni, G., Harsia, J., and Hickey, T. (2016). Latest Technology Advancements in Hydraulic Systems for Refuse Vehicle Applications: The Case of an Automated Side Loader. In *10th International Fluid Power Conference*.

[Buijs, 2017] Buijs, J. (2017). *3D Motion Compensation for an Offshore crane*. PhD thesis, Delft University of Technology, Delft.

[Det Norske Veritas, 2011] Det Norske Veritas (2011). Modelling and Analysis of Marine Operations. *Practice*, DNV-RP-H103(April).

[DNV, 2018] DNV (2018). DNVGL-ST-0377 Shipboard lifting appliances. Technical report, DNV.

[Huisman, 2022] Huisman (2022). Personal communication (mail).

[Journee and Massie, 2001] Journee, J. and Massie, W. (2001). *Offshore Hydrodynamics, First Edition*. Delft University of Technology, Delft.

[Jumbo Maritime, 2021] Jumbo Maritime (2021). Internal data.

[Jumbo Maritime, 2022] Jumbo Maritime (2022). JM-MEMO-701 J-Type Validation in Orcaflex.

[Lageveen, 2014] Lageveen, H. (2014). Modelling and Steering of Tuggerwinch. Technical report, University of Technology Delft, Delft.

[Li et al., 2020] Li, Z., Ma, X., and Li, Y. (2020). Anti-swing control for a double-pendulum offshore boom crane with ship roll and heave movements. In *IEEE International Conference on Control and Automation, ICCA*, volume 2020-October.

[Raymax Equipment, 2020] Raymax Equipment (2020). HEIL Automated Side Loader.

[van Wel, 2021] van Wel, D. (2021). The next step for load control with tugger winches. Technical report, Rotterdam Mainport Institute, Rotterdam.

[Wang et al., 2020] Wang, S. H., Ren, Z. P., Du, J. L., Chen, H. Q., and Sun, Y. Q. (2020). Payload swing suppression for offshore cranes using a novel triple-tagline system: Theory and experiment. *Proceedings of the Institution of Mechanical Engineers Part M: Journal of Engineering for the Maritime Environment*, 234(2).

Appendix I
RAOs vessel

In this appendix the RAOs of the fairplayer are shown. These RAOs are used by a maritime company in previous projects and since they are validated they are assumed to be accurate [Jumbo Maritime, 2022]. The RAOs are shown for a wave direction of 165 degrees as indicated in III.

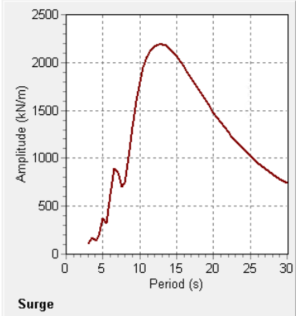

Fig. 6. RAO Surge

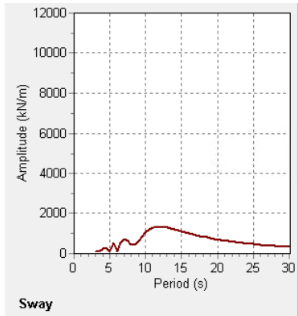

Fig. 7. RAO Sway

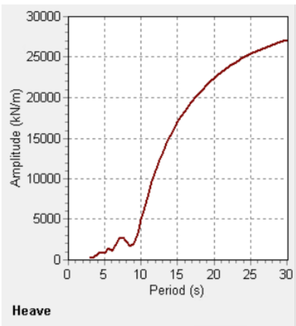

Fig. 8. RAO Heave

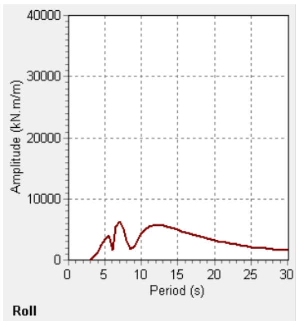

Fig. 9. RAO Roll

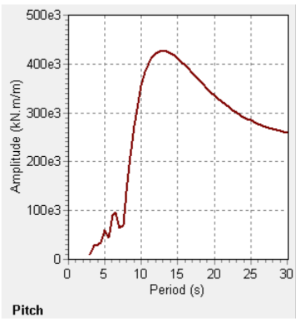

Fig. 10. RAO Pitch

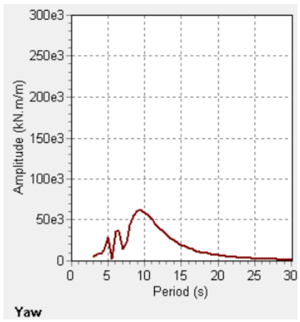

Fig. 11. RAO Yaw

Appendix B

Pairwise comparison matrices

Table B-1: Pairwise comparison time reduced

	Control system	Gyro stabilizer	Rails with support basket	Automated side loader	**Eigenvector**
Control system	1	1	1	3	**0,300**
Gyro stabilizer	1	1	1	3	**0,300**
Rails with support basket	1	1	1	3	**0,300**
Automated side loader	1/3	1/3	1/3	1	**0,100**

CR = 0,00

Table B-2: Pairwise comparison motion reduced

	Control system	Gyro stabilizer	Rails with support basket	Automated side loader	**Eigenvector**
Control system	1	4	1	1	**0,308**
Gyro stabilizer	1/4	1	1/4	1/4	**0,077**
Rails with support basket	1	4	1	1	**0,308**
Automated side loader	1	4	1	1	**0,308**

CR = 0,00

Table B-3: Pairwise comparison initial investment

	Control system	Gyro stabilizer	Rails with support basket	Automated side loader	**Eigenvector**
Control system	1	1/4	1	1/9	**0,064**
Gyro stabilizer	4	1	4	1/4	**0,221**
Rails with support basket	1	1/4	1	1/9	**0,064**
Automated side loader	9	4	9	1	**0,652**

CR = 0,01547

Table B-4: Pairwise comparison power required

	Control system	Gyro stabilizer	Rails with support basket	Automated side loader	**Eigenvector**
Control system	1	1/7	2	1/4	**0,083**
Gyro stabilizer	7	1	9	3	**0,587**
Rails with support basket	1/2	1/9	1	1/7	**0,049**
Automated side loader	4	1/3	7	1	**0,282**

CR = 0,02869

Appendix C

RAOs of Fairplayer

In this appendix the RAOs of the fairplayer are shown. These RAOs are used by Jumbo Maritime in previous projects and therefore these are assumed to be accurate. The RAOs are shown for a wave direction of 165 degrees as indicated in Section 2-2.

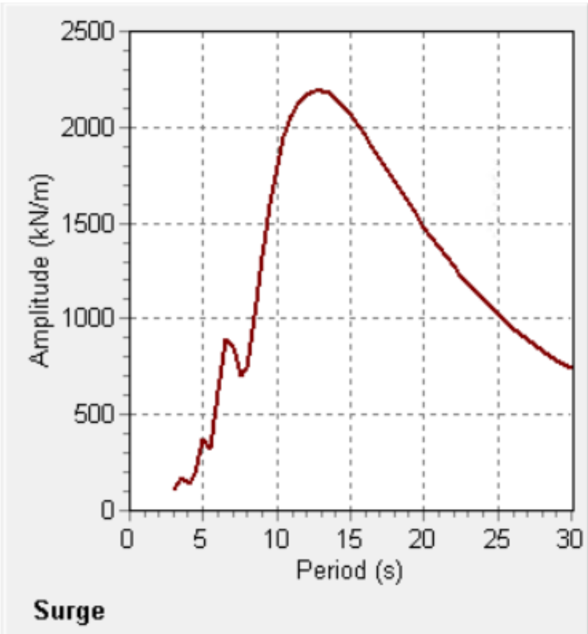

Figure C-1: RAO Surge

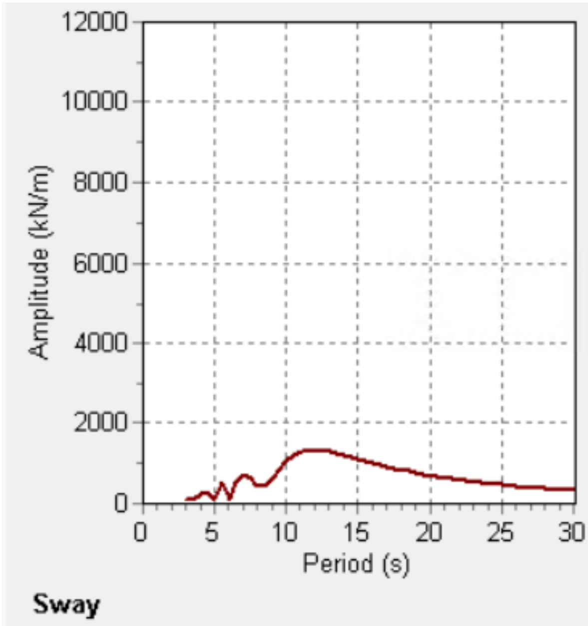

Figure C-2: RAO Sway

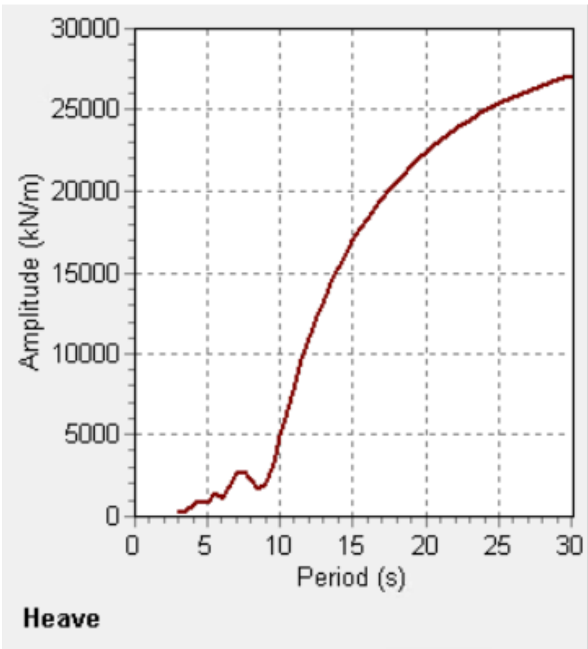

Figure C-3: RAO Heave

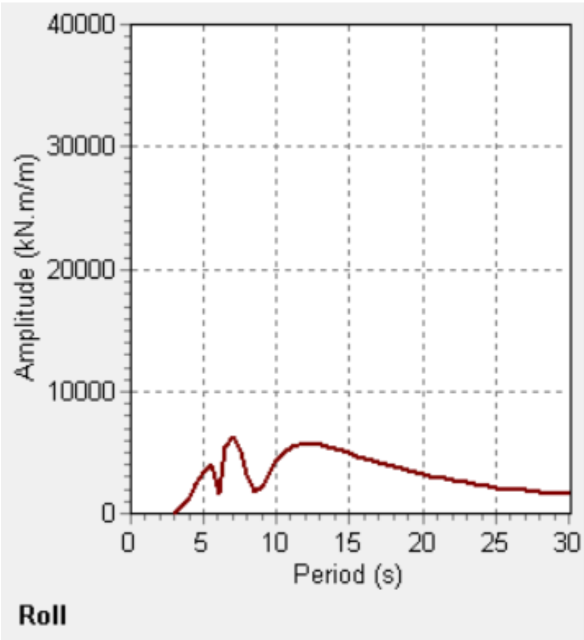

Figure C-4: RAO Roll

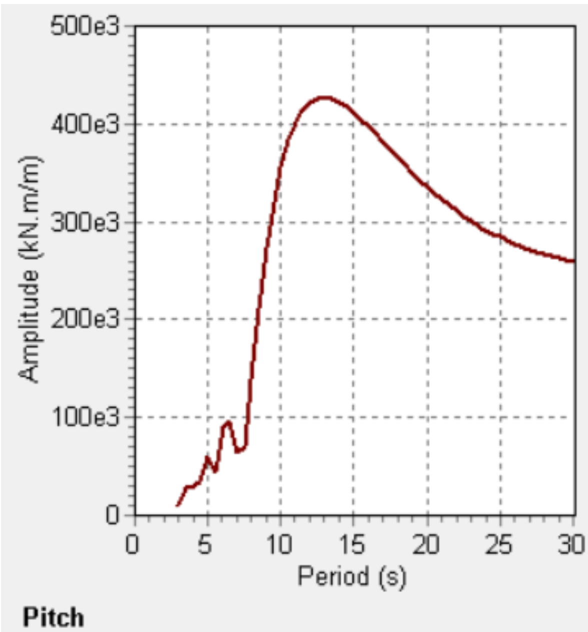

Figure C-5: RAO Pitch

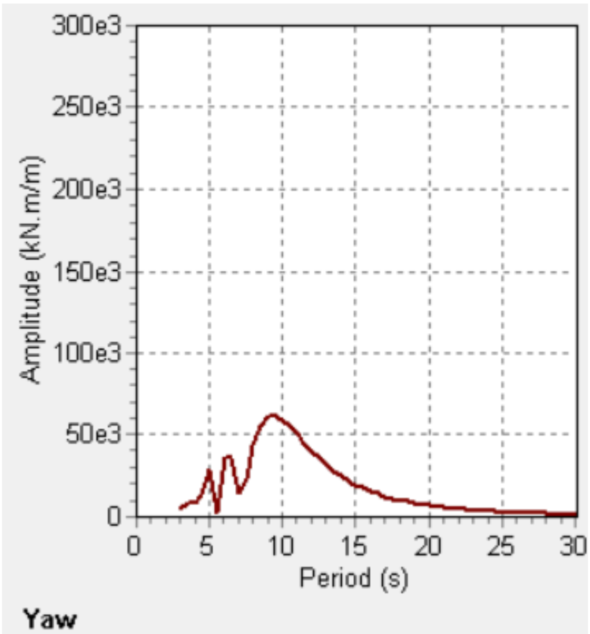

Figure C-6: RAO Yaw

Appendix D

Structural Report Ansys

Project*

First Saved	Tuesday, July 5, 2022
Last Saved	Friday, July 8, 2022
Product Version	2021 R2
Save Project Before Solution	No
Save Project After Solution	No

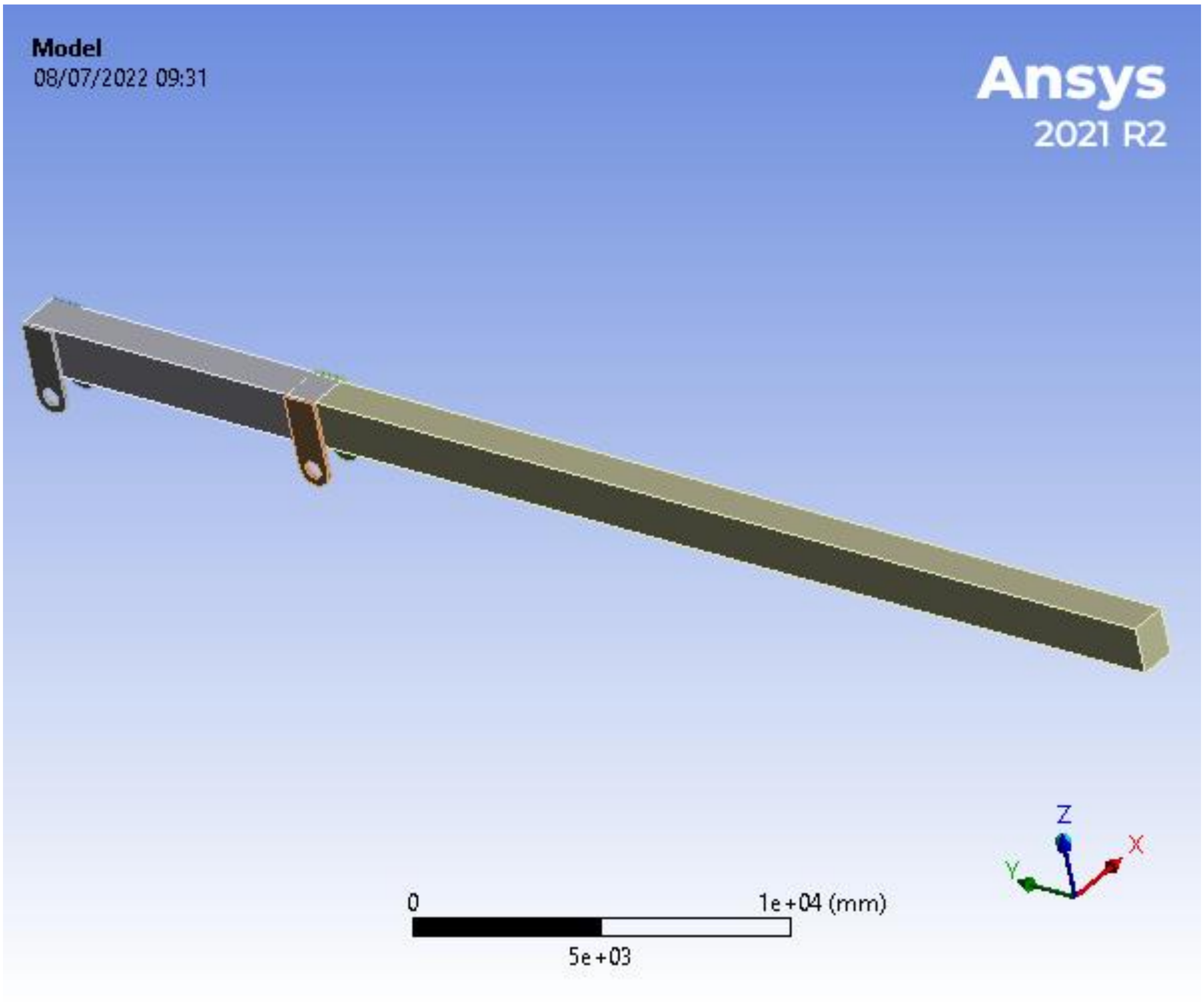

Contents

Report Not Finalized

Not all objects described below are in a finalized state. As a result, data may be incomplete, obsolete or in error. View first state problem. To finalize this report, edit objects as needed and solve the analyses.

Units

TABLE 1

Unit System	Metric (mm, t, N, s, mV, mA) Degrees rad/s Celsius
Angle	Degrees
Rotational Velocity	rad/s
Temperature	Celsius

Model (A4, B4, C4)

Geometry

TABLE 2
Model (A4, B4, C4) > Geometry

Object Name	*Geometry*
State	Fully Defined
Definition	
Source	C:\Users\timde\Ansys\final versions\structural analysis_files\dp0\SYS\DM\SYS.scdoc
Type	SpaceClaim
Length Unit	Meters
Element Control	Program Controlled
Display Style	Body Color
Bounding Box	
Length X	1380. mm
Length Y	38092 mm
Length Z	2700. mm
Properties	
Volume	9.0379e+009 mm³
Mass	70.948 t
Scale Factor Value	1.
2D Tolerance	Default (1.e-005)
Statistics	
Bodies	6
Active Bodies	6
Nodes	28310
Elements	21300
Mesh Metric	None
Update Options	
Assign Default Material	No
Basic Geometry Options	
Solid Bodies	Yes
Surface Bodies	Yes
Line Bodies	Yes
Parameters	Independent
Parameter Key	
Attributes	Yes
Attribute Key	
Named Selections	Yes
Named Selection Key	
Material Properties	Yes
Advanced Geometry Options	
Use Associativity	Yes
Coordinate Systems	Yes
Coordinate System Key	
Reader Mode Saves Updated File	No
Use Instances	Yes
Smart CAD Update	Yes
Compare Parts On Update	No
Analysis Type	3-D
Mixed Import Resolution	None

Import Facet Quality	Source
Clean Bodies On Import	No
Stitch Surfaces On Import	None
Decompose Disjoint Geometry	Yes
Enclosure and Symmetry Processing	Yes

TABLE 3
Model (A4, B4, C4) > Geometry > Parts

Object Name	*1 large outrigger\Surface1*	*2 outrigger\Surface1*	*padeye telescopic arm\Solid1*	*padeye telescopic arm\Solid1*	*padeye telescopic arm\Solid1*	*padeye telescopic arm\Solid1*
State	Meshed					
Graphics Properties						
Visible	Yes					
Transparency	1					
Definition						
Suppressed	No					
Dimension	3D					
Model Type	Shell					
Stiffness Behavior	Flexible					
Stiffness Option	Membrane and Bending					
Coordinate System	Default Coordinate System					
Reference Temperature	By Environment					
Thickness	40. mm					
Thickness Mode	Manual					
Offset Type	Bottom					
Treatment	None					
Material						
Assignment	S355					
Nonlinear Effects	Yes					
Thermal Strain Effects	Yes					
Bounding Box						
Length X	1180. mm	1100. mm	100. mm			
Length Y	10000 mm	29100 mm	1000. mm			
Length Z	1480. mm	1400. mm	2700. mm			
Properties						
Volume	2.1979e+009 mm³	5.8816e+009 mm³	2.3962e+008 mm³			
Mass	17.253 t	46.171 t	1.881 t			
Centroid X	2009.1 mm		1369.1 mm	2649.1 mm		1369.1 mm
Centroid Y	797.59 mm	-18056 mm	5138.7 mm		-3861.3 mm	
Centroid Z	4449.9 mm		3965.3 mm			
Moment of Inertia Ip1	1.5833e+008 t·mm²	3.3394e+009 t·mm²	1.0153e+006 t·mm²			
Moment of Inertia Ip2	1.5664e+008 t·mm²	3.3351e+009 t·mm²	1.6228e+005 t·mm²			
Moment of Inertia Ip3	1.0013e+007 t·mm²	2.3923e+007 t·mm²	1.1745e+006 t·mm²			

Surface Area(approx.)	5.4946e+007 mm²	1.4704e+008 mm²	
Statistics			
Nodes	5608	14730	1993
Elements	5580	14704	254
Mesh Metric	None		
CAD Attributes			
PartTolerance:	0.00000001		
Color:143.149.175			

FIGURE 1
Model (A4, B4, C4) > Geometry > 1 large outrigger > Surface1 > Telescopic arm non-extendable part

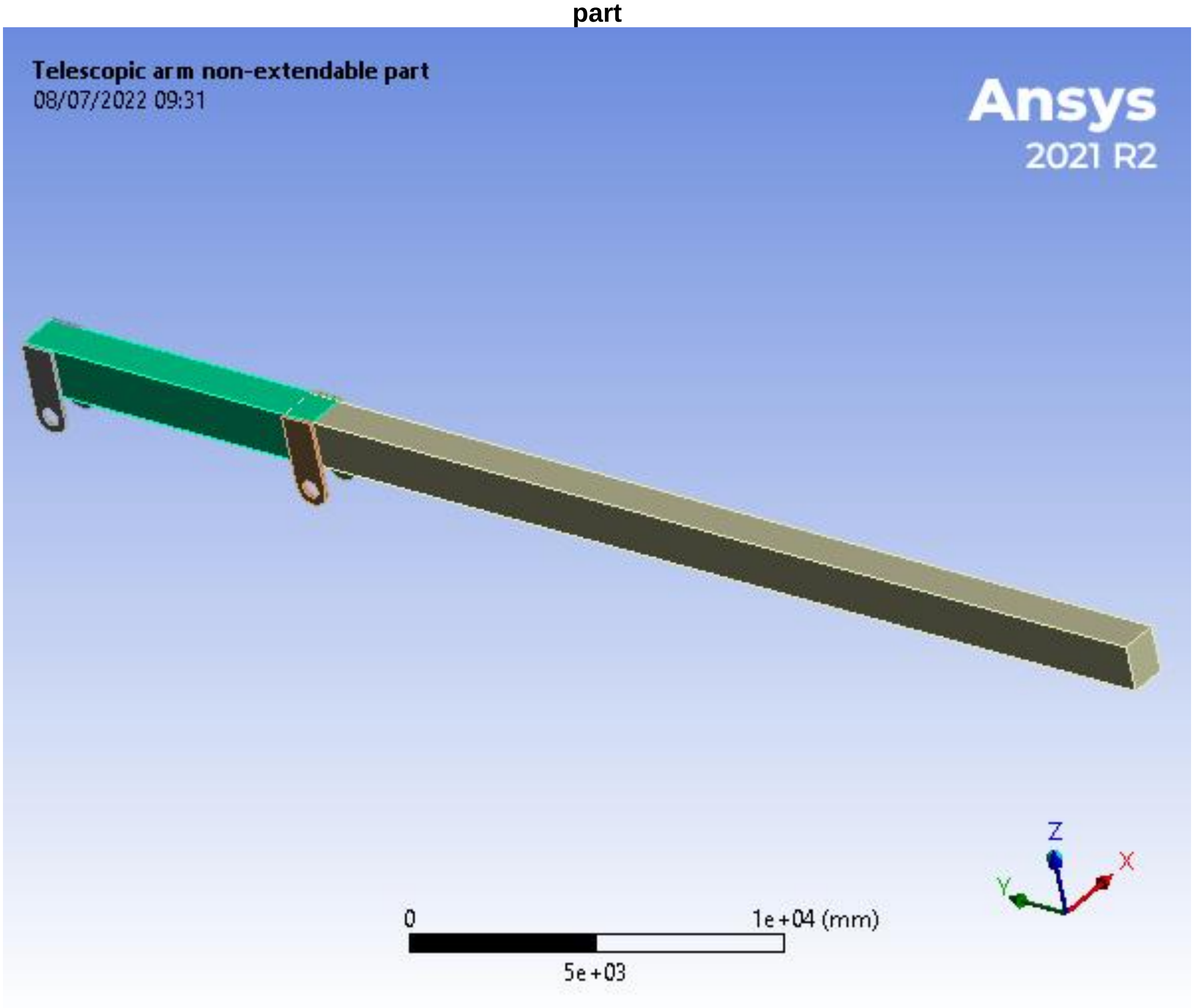

FIGURE 2
Model (A4, B4, C4) > Geometry > 2 outrigger > Surface1 > Telescopic arm extendable part

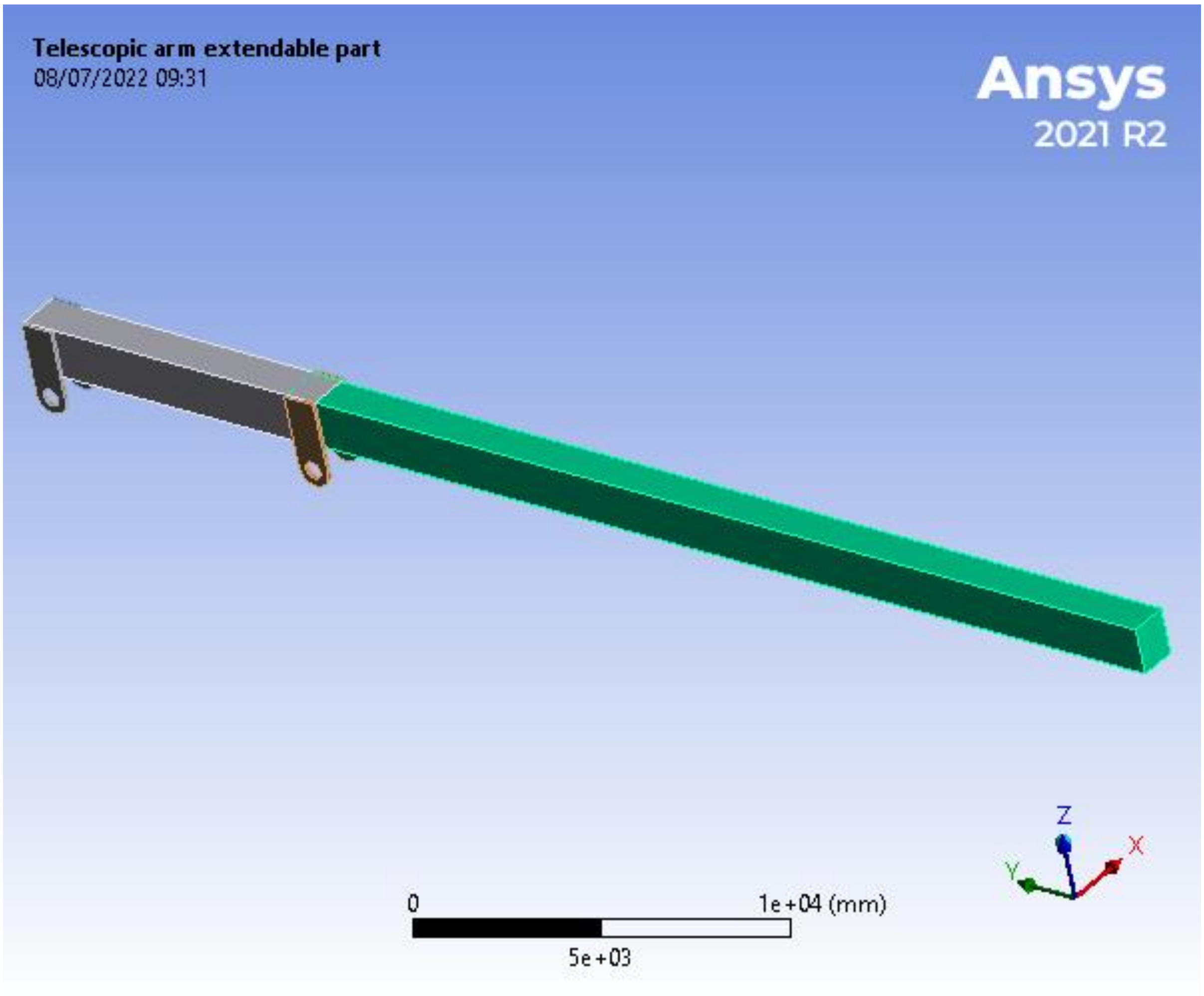

FIGURE 3
Model (A4, B4, C4) > Geometry > padeye telescopic arm > Solid1 > Padeye telescopic arm

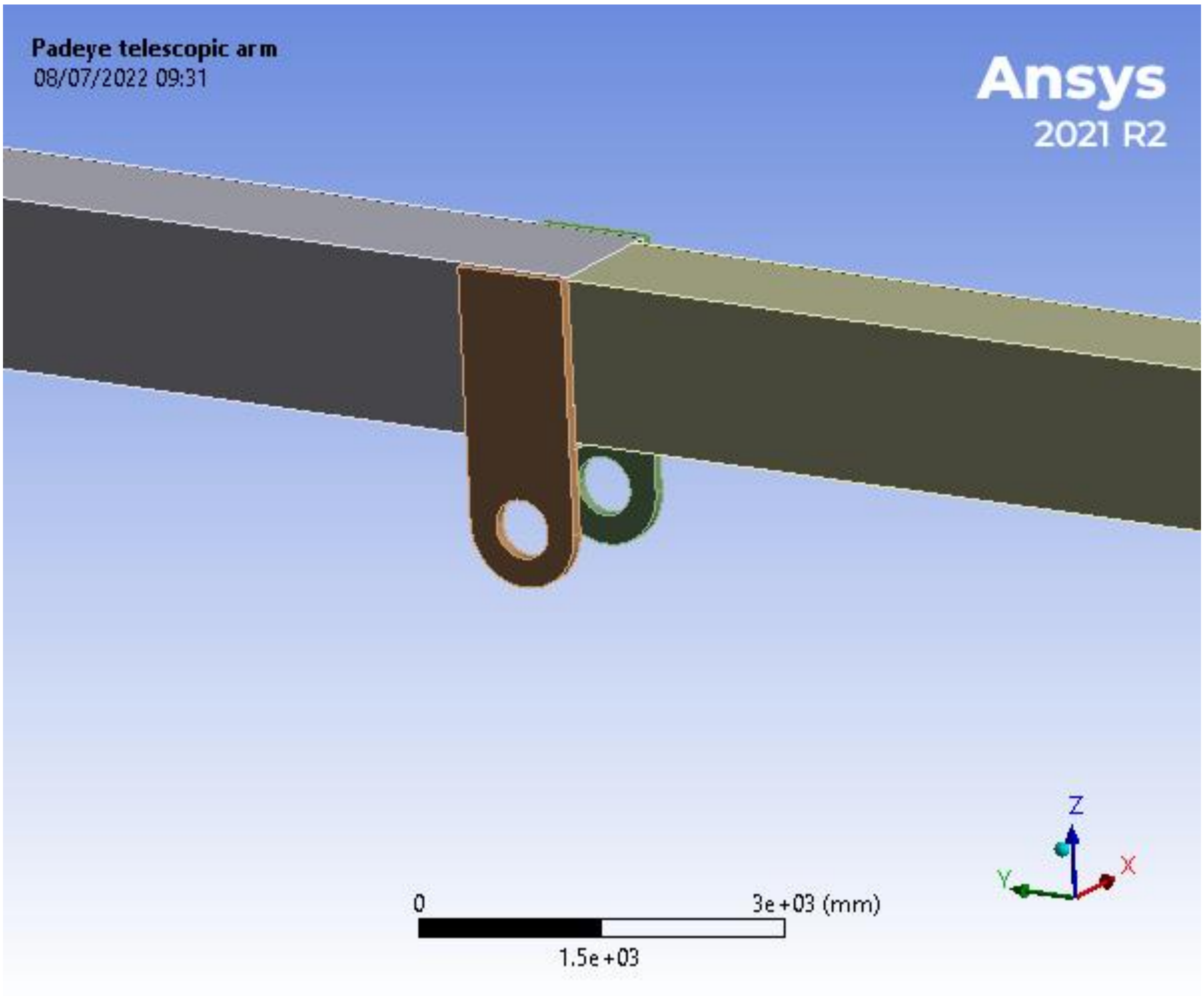

TABLE 4
Model (A4, B4, C4) > Materials

Object Name	*Materials*
State	Fully Defined
Statistics	
Materials	3
Material Assignments	1

TABLE 5
Model (A4, B4, C4) > Materials > S355 Assignment

Object Name	*S355 Assignment*
State	Fully Defined
General	
Scoping Method	Geometry Selection
Geometry	6 Bodies
Definition	
Material Name	S355
Nonlinear Effects	Yes
Thermal Strain Effects	Yes
Reference Temperature	By Environment
Suppressed	No

Coordinate Systems

TABLE 6
Model (A4, B4, C4) > Coordinate Systems > Coordinate System

Object Name	*Global Coordinate System*
State	Fully Defined
Definition	
Type	Cartesian
Coordinate System ID	0.
Origin	
Origin X	0. mm
Origin Y	0. mm
Origin Z	0. mm
Directional Vectors	
X Axis Data	[1. 0. 0.]
Y Axis Data	[0. 1. 0.]
Z Axis Data	[0. 0. 1.]

Connections

TABLE 7
Model (A4, B4, C4) > Connections

Object Name	*Connections*
State	Fully Defined
Auto Detection	
Generate Automatic Connection On Refresh	Yes
Transparency	
Enabled	Yes

TABLE 8
Model (A4, B4, C4) > Connections > Contacts

Object Name	*Contacts*
State	Fully Defined
Definition	
Connection Type	Contact
Scope	
Scoping Method	Geometry Selection
Geometry	All Bodies
Auto Detection	
Tolerance Type	Value
Tolerance Value	115. mm
Use Range	No
Face/Face	Yes
Face-Face Angle Tolerance	75. °
Face Overlap Tolerance	Off
Cylindrical Faces	Include
Face/Edge	No
Edge/Edge	No
Priority	Include All
Group By	Bodies
Search Across	Bodies
Statistics	
Connections	5
Active Connections	5

TABLE 9
Model (A4, B4, C4) > Connections > Contacts > Contact Regions

Object Name	*Bonded - 1 large outrigger\Surface1 To 2 outrigger\Surface1*	*Bonded - 1 large outrigger\Surface1 To padeye telescopic arm\Solid1*	*Bonded - 1 large outrigger\Surface1 To padeye telescopic arm\Solid1*	*Bonded - 1 large outrigger\Surface1 To padeye telescopic arm\Solid1*	*Bonded - 1 large outrigger\Surface1 To padeye telescopic arm\Solid1*
State	Fully Defined				
Scope					
Scoping Method	Geometry Selection				
Contact	4 Faces	1 Face			
Target	4 Faces	2 Faces			
Contact Bodies	1 large outrigger\Surface1				
Target Bodies	2 outrigger\Surface1	padeye telescopic arm\Solid1			
Contact Shell Face	Program Controlled				
Target Shell Face	Program Controlled				
Shell Thickness Effect	No				
Protected	No				
Definition					
Type	Bonded				
Scope Mode	Automatic				
Behavior	Program Controlled				
Trim Contact	Program Controlled				
Trim Tolerance	115. mm				
Suppressed	No				
Advanced					
Formulation	Program Controlled				
Small Sliding	Program Controlled				
Detection Method	Program Controlled				
Penetration Tolerance	Program Controlled				
Elastic Slip Tolerance	Program Controlled				
Normal Stiffness	Program Controlled				
Update Stiffness	Program Controlled				
Pinball Region	Program Controlled				
Geometric Modification					
Contact Geometry Correction	None				

Target Geometry Correction	None

FIGURE 4
Model (A4, B4, C4) > Connections > Contacts > Bonded - 1 large outrigger > Surface1 To 2 outrigger > Surface1 > Telescopic arm connection

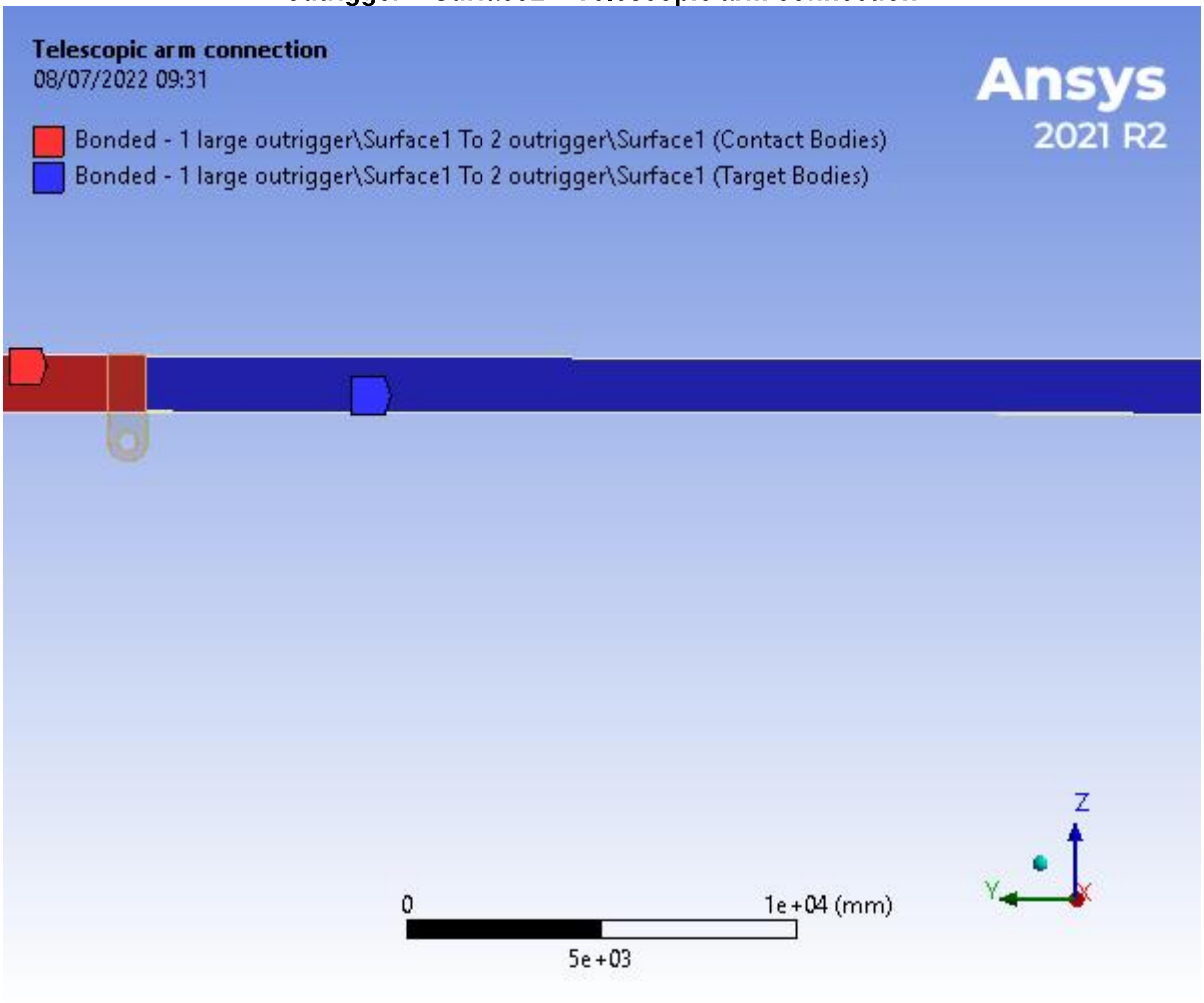

FIGURE 5
Model (A4, B4, C4) > Connections > Contacts > Bonded - 1 large outrigger > Surface1 To padeye telescopic arm > Solid1 > Telescopic arm to padeye 1

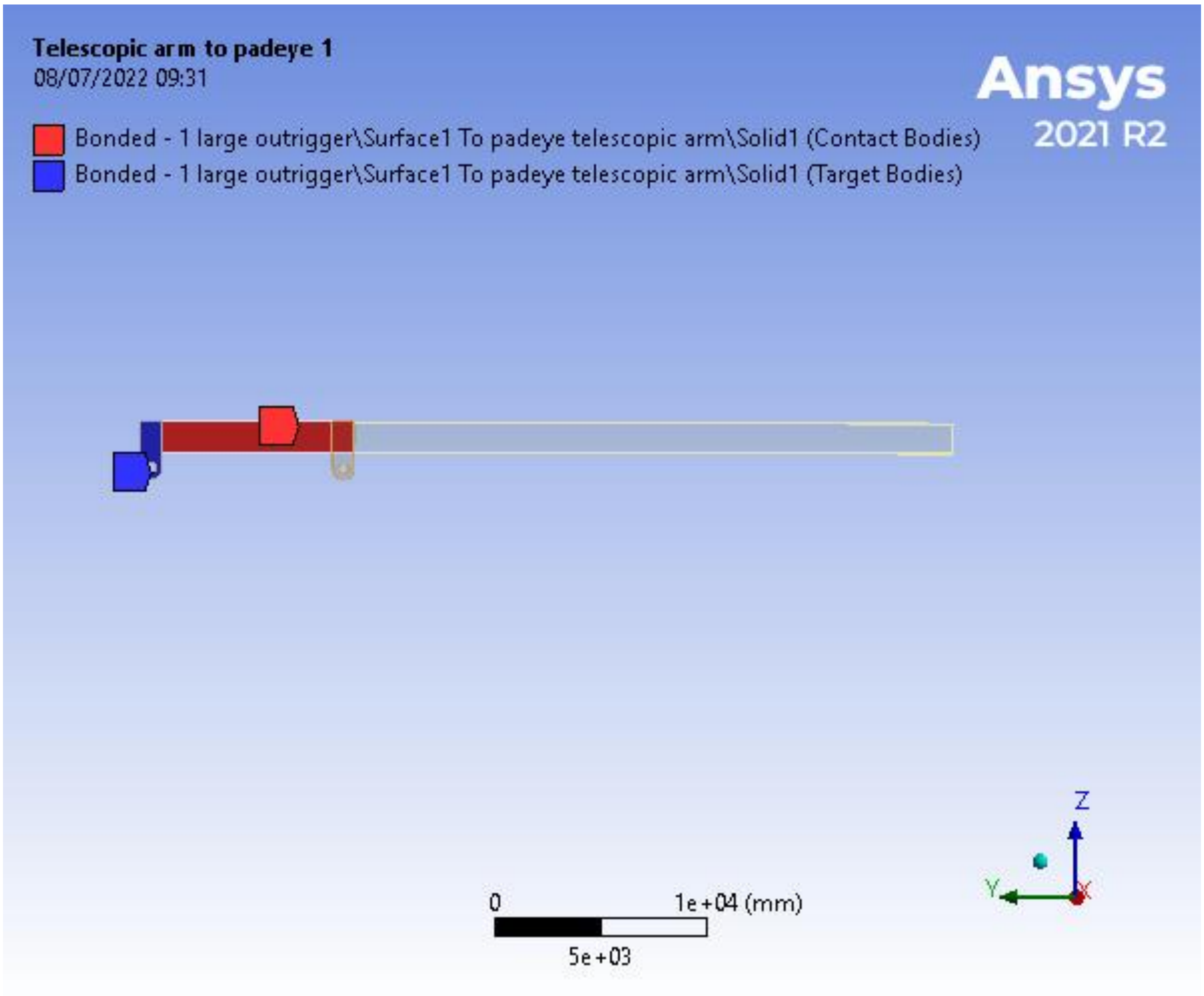

FIGURE 6
Model (A4, B4, C4) > Connections > Contacts > Bonded - 1 large outrigger > Surface1 To padeye telescopic arm > Solid1 > Telescopic arm to padeye 2

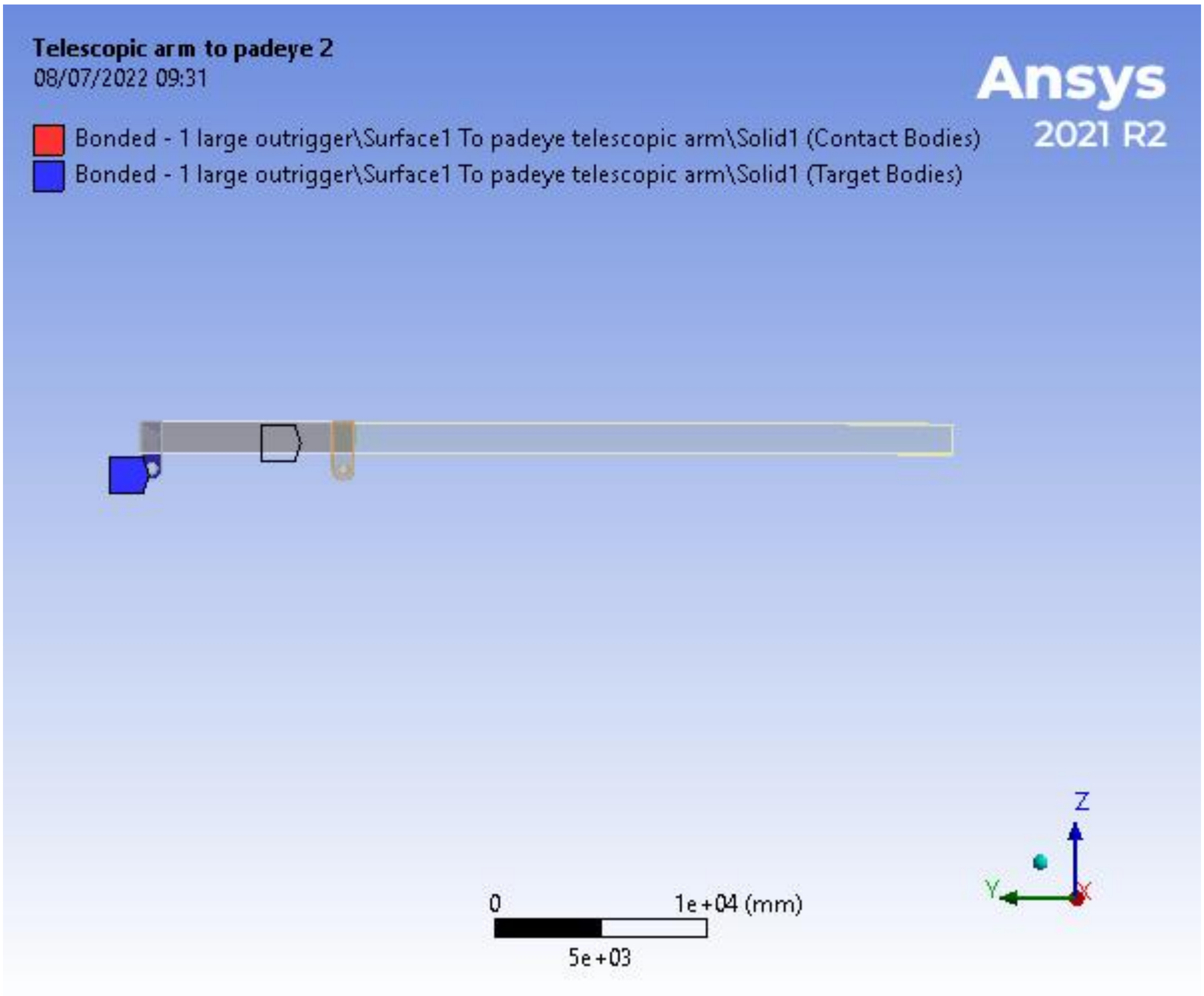

FIGURE 7
Model (A4, B4, C4) > Connections > Contacts > Bonded - 1 large outrigger > Surface1 To padeye telescopic arm > Solid1 > Telescopic arm to padeye 3

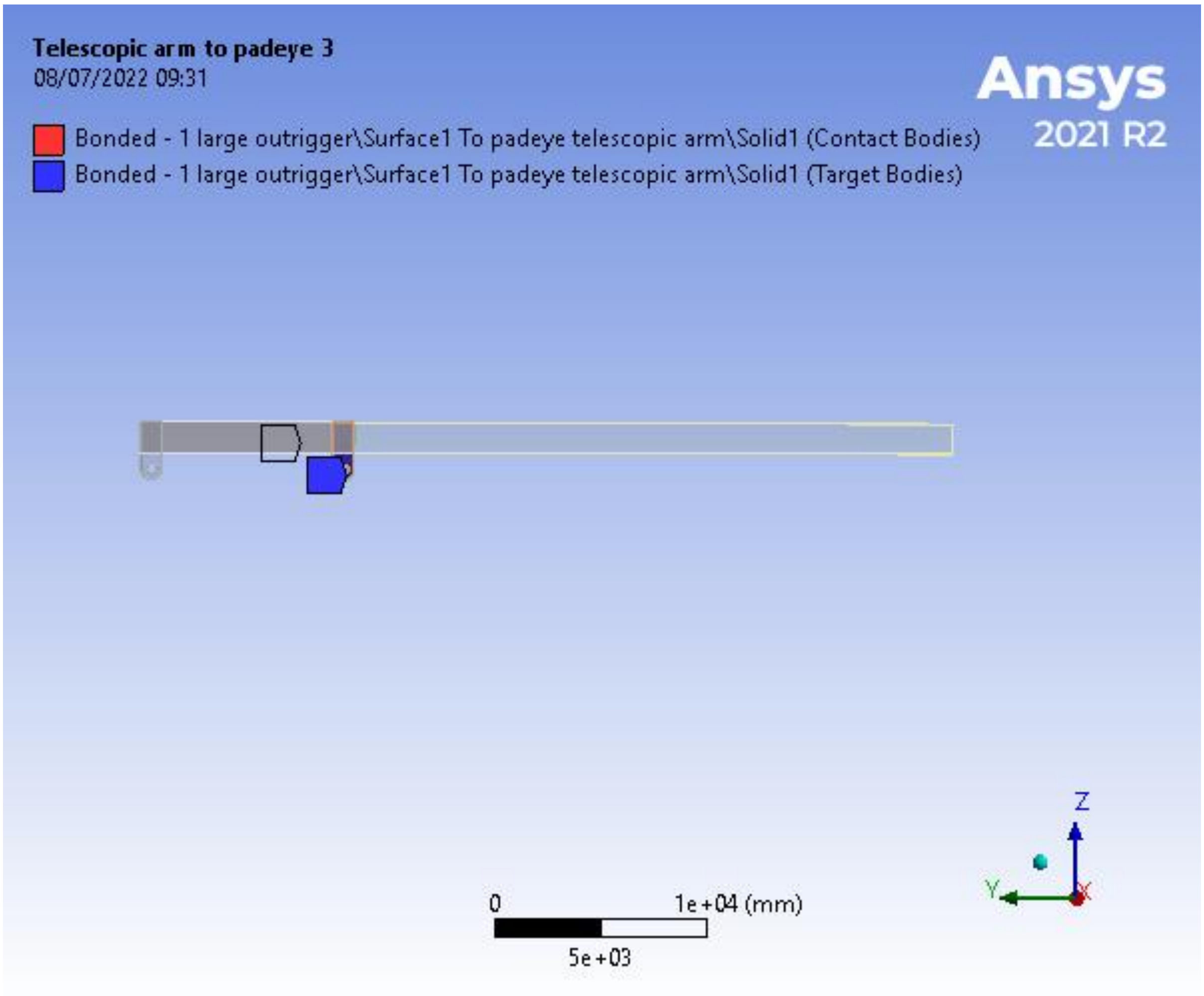

FIGURE 8
Model (A4, B4, C4) > Connections > Contacts > Bonded - 1 large outrigger > Surface1 To padeye telescopic arm > Solid1 > Telescopic arm to padeye 4

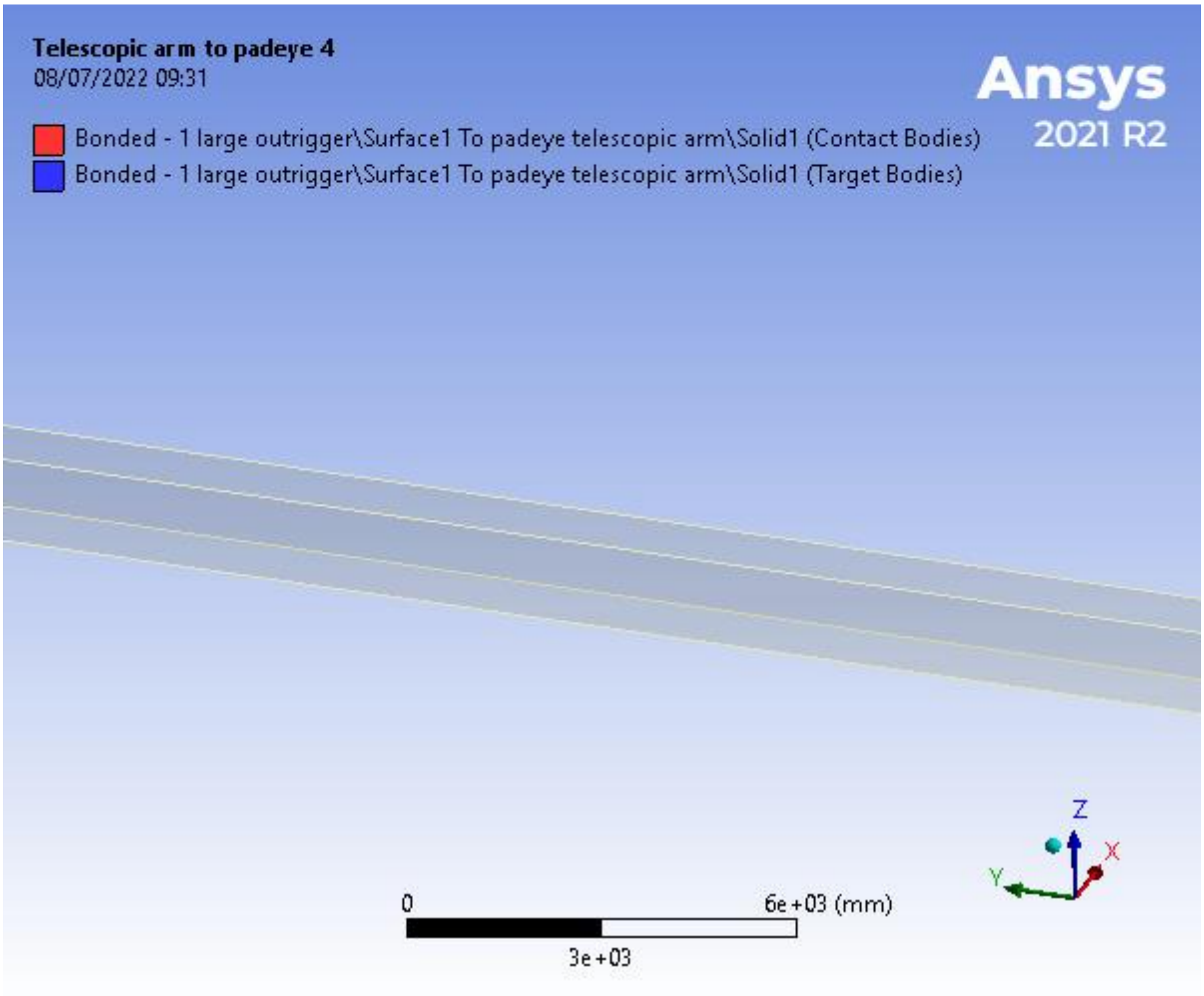

Mesh

TABLE 10
Model (A4, B4, C4) > Mesh

Object Name	*Mesh*
State	Solved
Display	
Display Style	Use Geometry Setting
Defaults	
Physics Preference	Mechanical
Element Order	Program Controlled
Element Size	100.0 mm
Sizing	
Use Adaptive Sizing	No
Use Uniform Size Function For Sheets	No
Growth Rate	Default (1.2)
Max Size	Default (100.0 mm)
Mesh Defeaturing	Yes
Defeature Size	Default (0.5 mm)
Capture Curvature	Yes
Curvature Min Size	Default (1.0 mm)
Curvature Normal Angle	Default (30.0°)
Capture Proximity	No

Bounding Box Diagonal	38212 mm
Average Surface Area	5.3469e+006 mm²
Minimum Edge Length	24.544 mm
Quality	
Check Mesh Quality	Yes, Errors
Error Limits	Aggressive Mechanical
Target Quality	Default (0.050000)
Smoothing	Medium
Mesh Metric	None
Inflation	
Use Automatic Inflation	None
Inflation Option	Smooth Transition
Transition Ratio	0.272
Maximum Layers	2
Growth Rate	1.2
Inflation Algorithm	Pre
View Advanced Options	No
Batch Connections	
Mesh Based Connection	No
Advanced	
Number of CPUs for Parallel Part Meshing	Program Controlled
Straight Sided Elements	No
Rigid Body Behavior	Dimensionally Reduced
Triangle Surface Mesher	Program Controlled
Topology Checking	Yes
Pinch Tolerance	Default (0.9 mm)
Generate Pinch on Refresh	No
Sheet Loop Removal	No
Statistics	
Nodes	28310
Elements	21300

Static Structural State 1 (A5)

TABLE 11
Model (A4, B4, C4) > Analysis

Object Name	*Static Structural State 1 (A5)*
State	Not Solved
Definition	
Physics Type	Structural
Analysis Type	Static Structural
Solver Target	Mechanical APDL
Options	
Environment Temperature	22. °C
Generate Input Only	No

TABLE 12
Model (A4, B4, C4) > Static Structural State 1 (A5) > Analysis Settings

Object Name	*Analysis Settings*
State	Fully Defined
Step Controls	
Number Of Steps	1.

Current Step Number	1.
Step End Time	1. s
Auto Time Stepping	Program Controlled
Solver Controls	
Solver Type	Program Controlled
Weak Springs	Off
Solver Pivot Checking	Program Controlled
Large Deflection	Off
Inertia Relief	Off
Quasi-Static Solution	Off
Rotordynamics Controls	
Coriolis Effect	Off
Restart Controls	
Generate Restart Points	Program Controlled
Retain Files After Full Solve	No
Combine Restart Files	Program Controlled
Nonlinear Controls	
Newton-Raphson Option	Program Controlled
Force Convergence	Program Controlled
Moment Convergence	Program Controlled
Displacement Convergence	Program Controlled
Rotation Convergence	Program Controlled
Line Search	Program Controlled
Stabilization	Program Controlled
Advanced	
Inverse Option	No
Contact Split (DMP)	Off
Output Controls	
Stress	Yes
Surface Stress	No
Back Stress	No
Strain	Yes
Contact Data	Yes
Nonlinear Data	No
Nodal Forces	No
Volume and Energy	Yes
Euler Angles	Yes
General Miscellaneous	No
Contact Miscellaneous	No
Store Results At	All Time Points
Result File Compression	Program Controlled
Analysis Data Management	
Solver Files Directory	C:\Users\timde\Ansys\final versions\structural analysis_files\dp0\SYS\MECH\
Future Analysis	None
Scratch Solver Files Directory	
Save MAPDL db	No
Contact Summary	Program Controlled
Delete Unneeded Files	Yes
Nonlinear Solution	No
Solver Units	Active System

Solver Unit System	nmm

FIGURE 9
Model (A4, B4, C4) > Static Structural State 1 (A5) > Load configuration 1

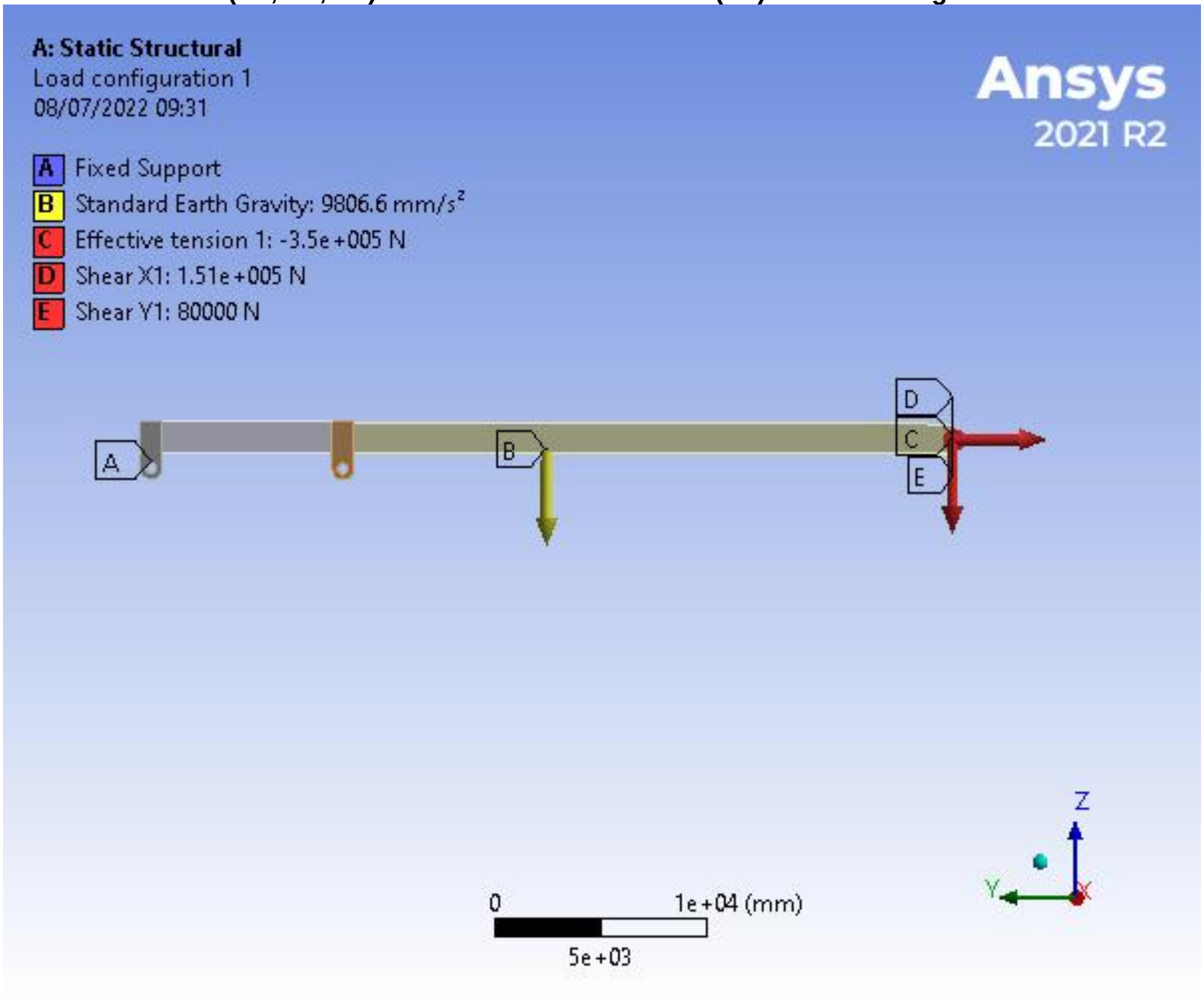

TABLE 13
Model (A4, B4, C4) > Static Structural State 1 (A5) > Accelerations

Object Name	*Standard Earth Gravity*
State	Fully Defined
Scope	
Geometry	All Bodies
Definition	
Coordinate System	Global Coordinate System
X Component	0. mm/s² (ramped)
Y Component	0. mm/s² (ramped)
Z Component	-9806.6 mm/s² (ramped)
Suppressed	No
Direction	-Z Direction

FIGURE 10
Model (A4, B4, C4) > Static Structural State 1 (A5) > Standard Earth Gravity

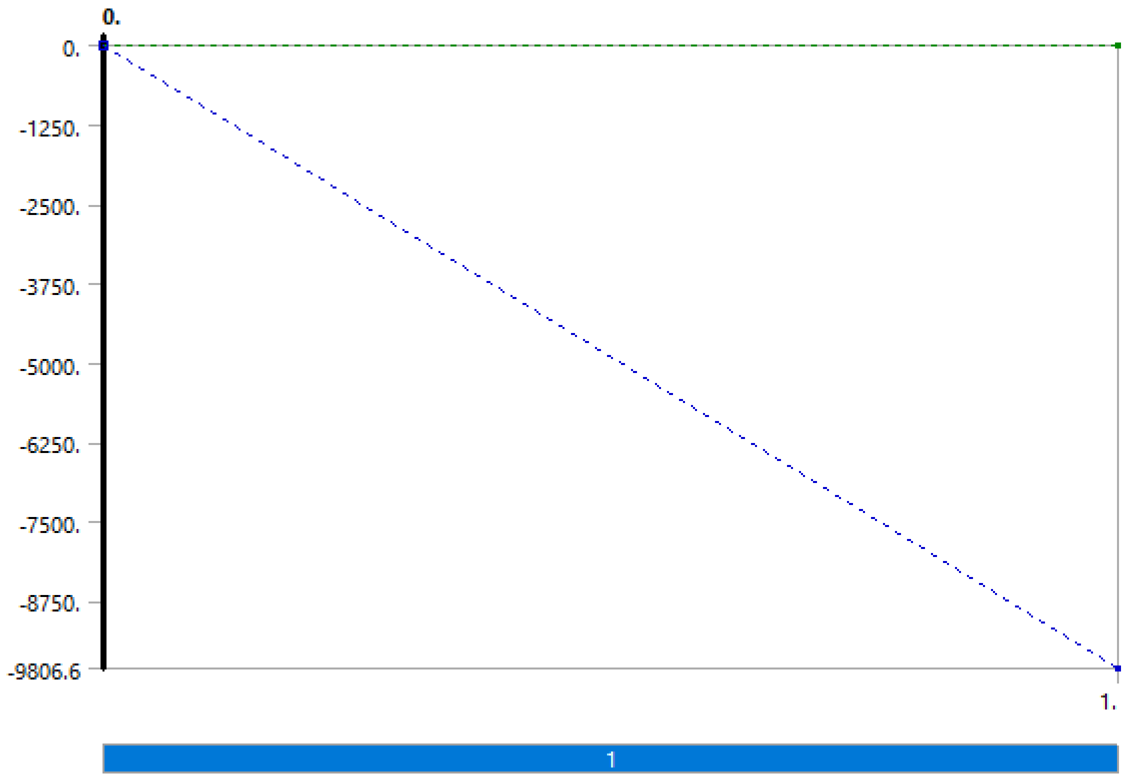

TABLE 14
Model (A4, B4, C4) > Static Structural State 1 (A5) > Loads

Object Name	*Fixed Support*	*Effective tension 1*	*Shear X1*	*Shear Y1*
State	Fully Defined			
Scope				
Scoping Method	Geometry Selection			
Geometry	8 Faces	1 Face		
Definition				
Type	Fixed Support	Force		
Suppressed	No			
Define By		Vector		
Applied By		Surface Effect		
Magnitude		-3.5e+005 N (ramped)	1.51e+005 N (ramped)	80000 N (ramped)
Direction		Defined		

FIGURE 11
Model (A4, B4, C4) > Static Structural State 1 (A5) > Effective tension 1

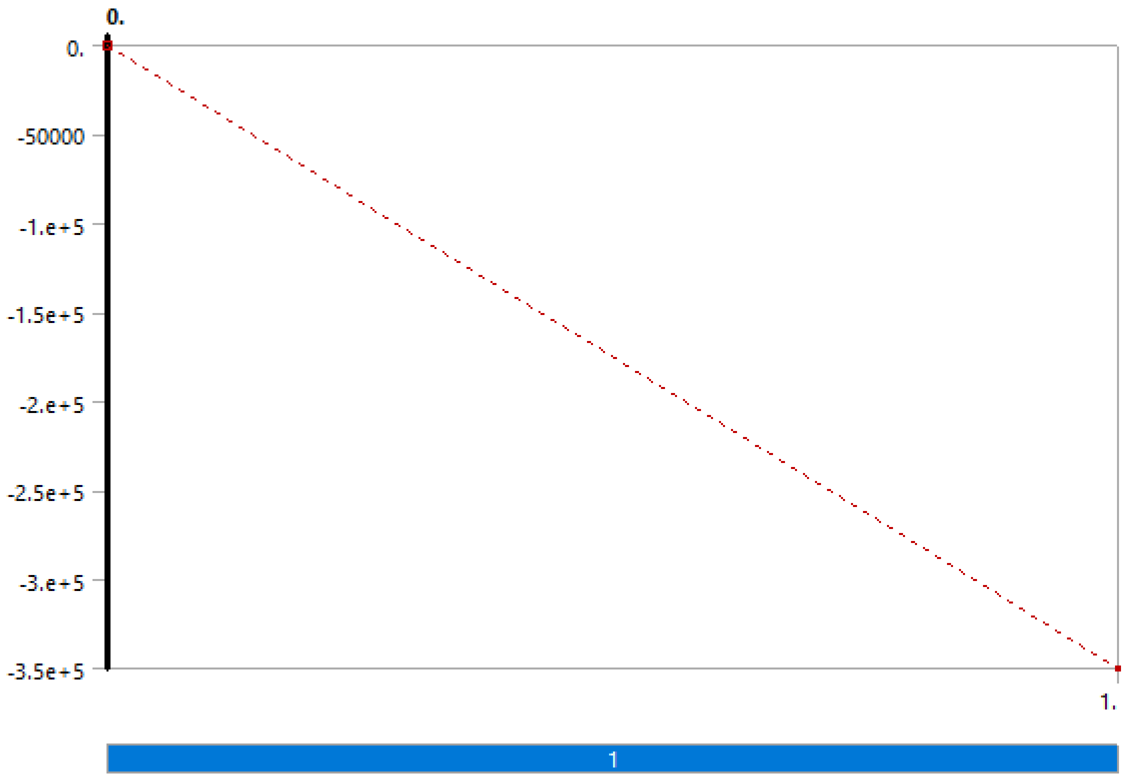

FIGURE 12
Model (A4, B4, C4) > Static Structural State 1 (A5) > Shear X1

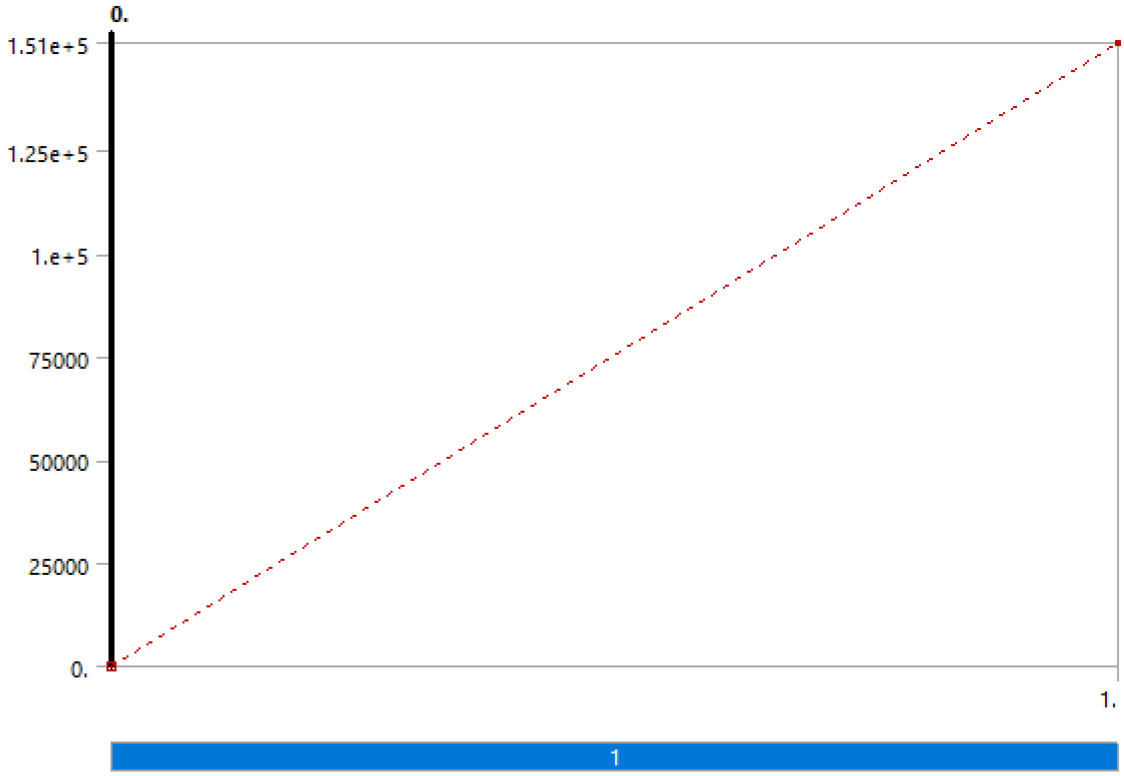

FIGURE 13
Model (A4, B4, C4) > Static Structural State 1 (A5) > Shear Y1

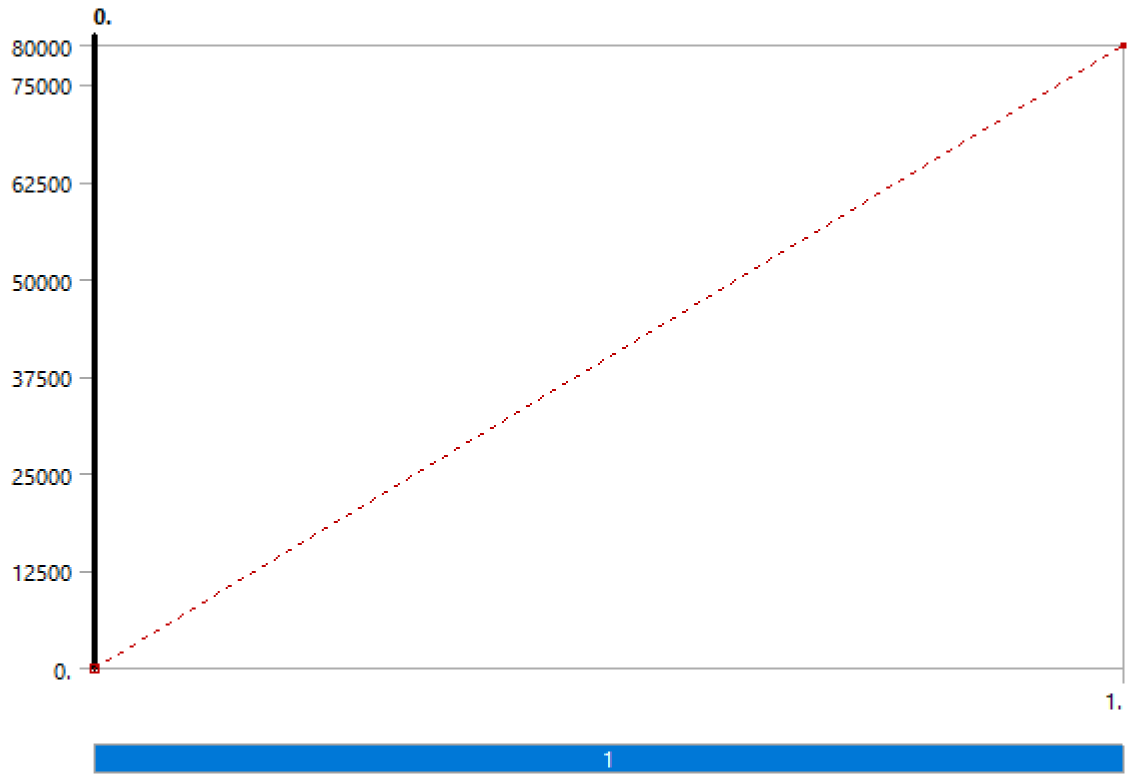

Solution (A6)

TABLE 15
Model (A4, B4, C4) > Static Structural State 1 (A5) > Solution

Object Name	*Solution (A6)*
State	Obsolete
Adaptive Mesh Refinement	
Max Refinement Loops	1.
Refinement Depth	2.
Information	
Status	Solve Required
MAPDL Elapsed Time	6. s
MAPDL Memory Used	748. MB
MAPDL Result File Size	23.5 MB
Post Processing	
Beam Section Results	No
On Demand Stress/Strain	No

TABLE 16
Model (A4, B4, C4) > Static Structural State 1 (A5) > Solution (A6) > Solution Information

Object Name	*Solution Information*
State	Obsolete
Solution Information	
Solution Output	Solver Output
Newton-Raphson Residuals	0
Identify Element Violations	0
Update Interval	2.5 s
Display Points	All
FE Connection Visibility	

Activate Visibility	Yes
Display	All FE Connectors
Draw Connections Attached To	All Nodes
Line Color	Connection Type
Visible on Results	No
Line Thickness	Single
Display Type	Lines

TABLE 17
Model (A4, B4, C4) > Static Structural State 1 (A5) > Solution (A6) > Results

Object Name	*X Axis - Directional Deformation - End Time*	*Y Axis - Directional Deformation - End Time*	*Z Axis - Directional Deformation - End Time*	*Equivalent Stress*
State	Obsolete			
Scope				
Scoping Method	Geometry Selection			
Geometry	All Bodies			
Position				Top/Bottom
Definition				
Type	Directional Deformation			Equivalent (von-Mises) Stress
Orientation	X Axis	Y Axis	Z Axis	
By	Time			
Display Time	Last		First	Last
Coordinate System	Global Coordinate System			
Calculate Time History	Yes			
Identifier				
Suppressed	No			
Results				
Minimum	-1.0646 mm	-9.9655 mm	-160.67 mm	4.2315e-002 MPa
Maximum	140.85 mm	8.3666 mm	1.2103 mm	240.04 MPa
Average	28.609 mm	-0.48942 mm	-33.455 mm	27.72 MPa
Minimum Occurs On	1 large outrigger\Surface1	2 outrigger\Surface1		padeye telescopic arm\Solid1
Maximum Occurs On	2 outrigger\Surface1		1 large outrigger\Surface1	2 outrigger\Surface1
Information				
Time	1. s			
Load Step	1			
Substep	1			
Iteration Number	1			
Integration Point Results				
Display Option				Averaged
Average Across Bodies				No

FIGURE 14
Model (A4, B4, C4) > Static Structural State 1 (A5) > Solution (A6) > X Axis - Directional Deformation - End Time

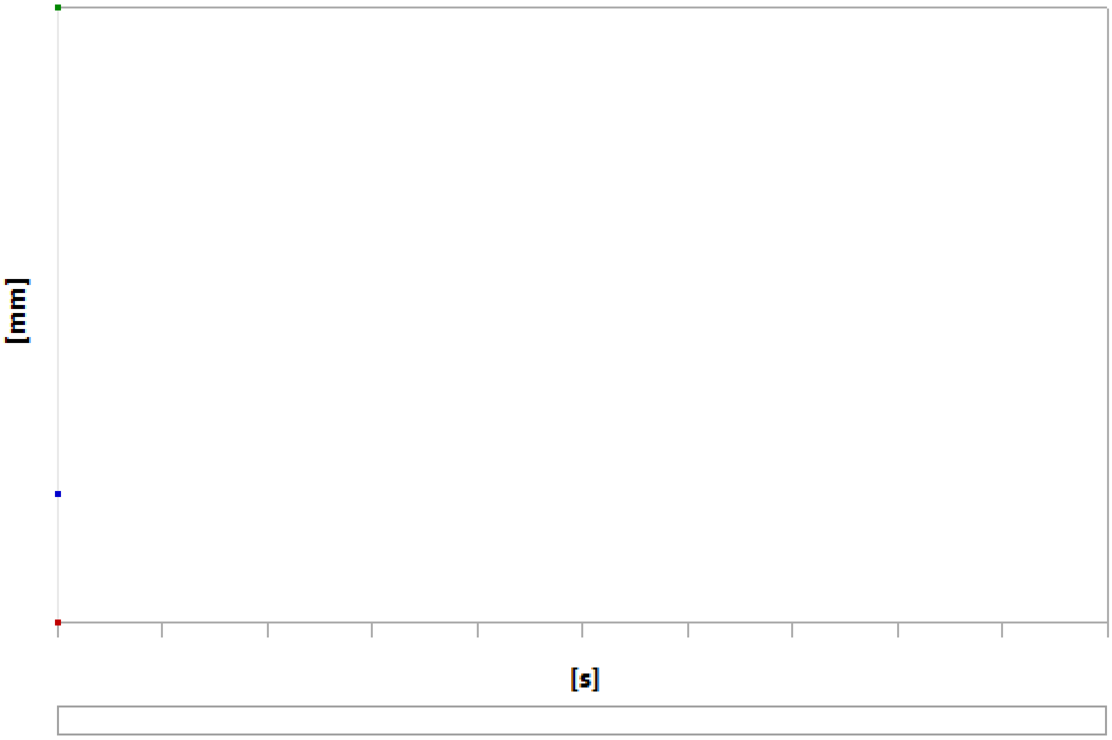

TABLE 18
Model (A4, B4, C4) > Static Structural State 1 (A5) > Solution (A6) > X Axis - Directional Deformation - End Time

Time [s]	Minimum [mm]	Maximum [mm]	Average [mm]
1.	-1.0646	140.85	28.609

FIGURE 15
Model (A4, B4, C4) > Static Structural State 1 (A5) > Solution (A6) > X Axis - Directional Deformation - End Time > State 1 Deformation X

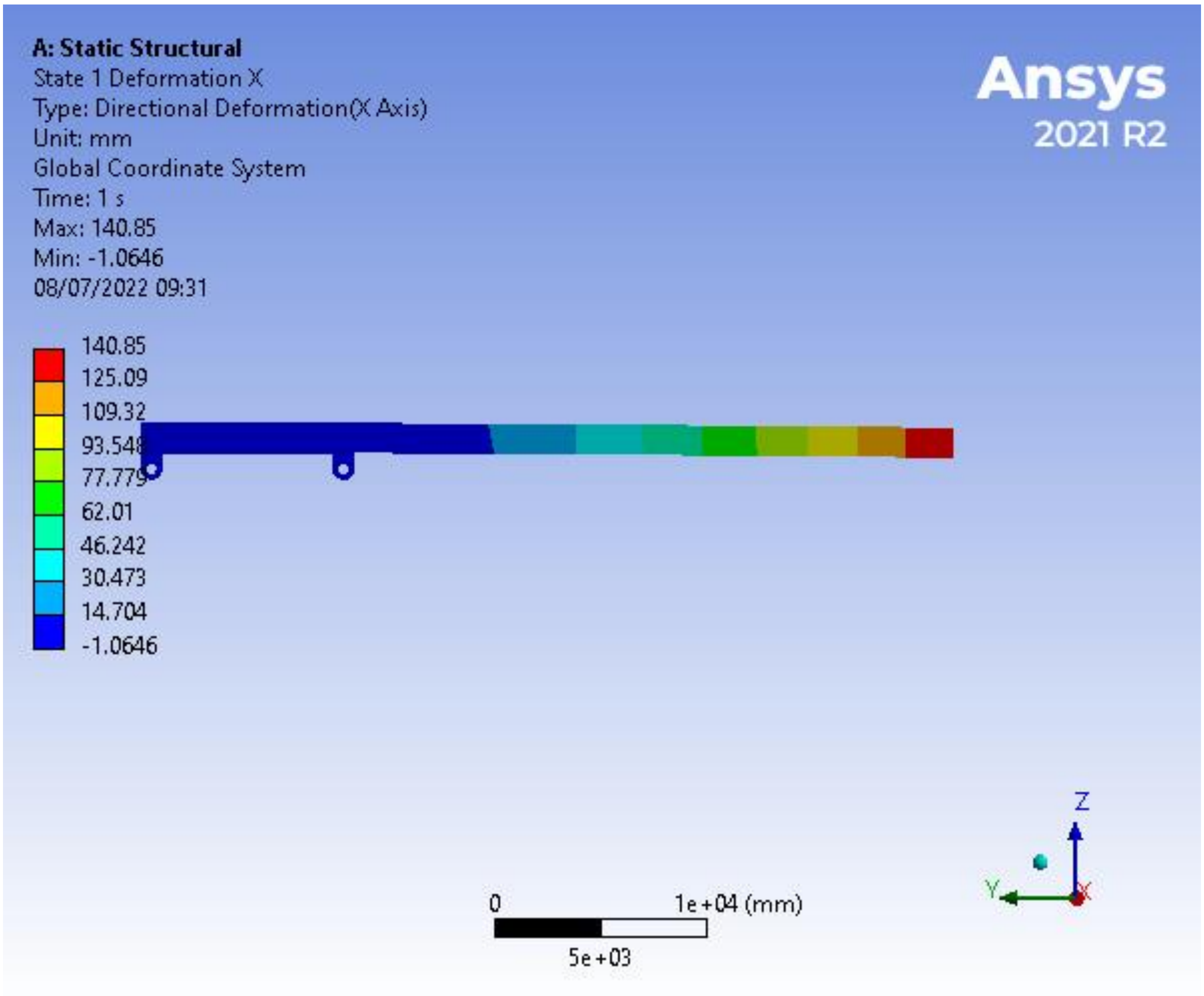

FIGURE 16
Model (A4, B4, C4) > Static Structural State 1 (A5) > Solution (A6) > Y Axis - Directional Deformation - End Time

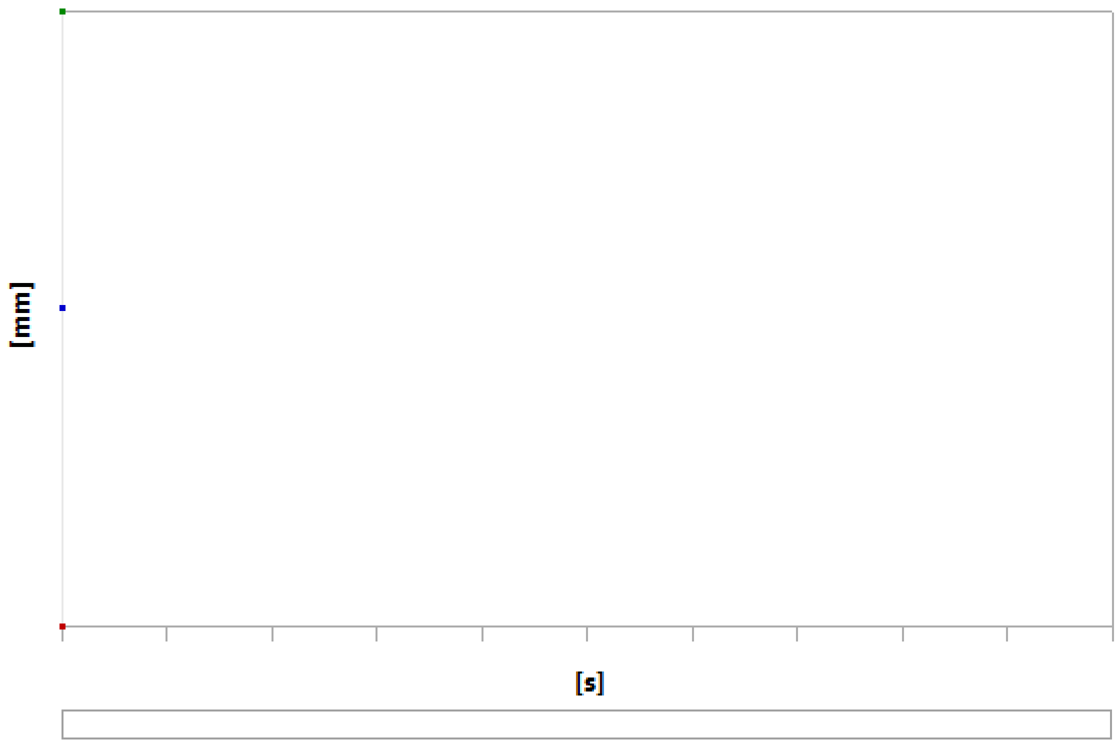

TABLE 19
Model (A4, B4, C4) > Static Structural State 1 (A5) > Solution (A6) > Y Axis - Directional Deformation - End Time

Time [s]	Minimum [mm]	Maximum [mm]	Average [mm]
1.	-9.9655	8.3666	-0.48942

FIGURE 17
Model (A4, B4, C4) > Static Structural State 1 (A5) > Solution (A6) > Y Axis - Directional Deformation - End Time > State 1 Deformation Y

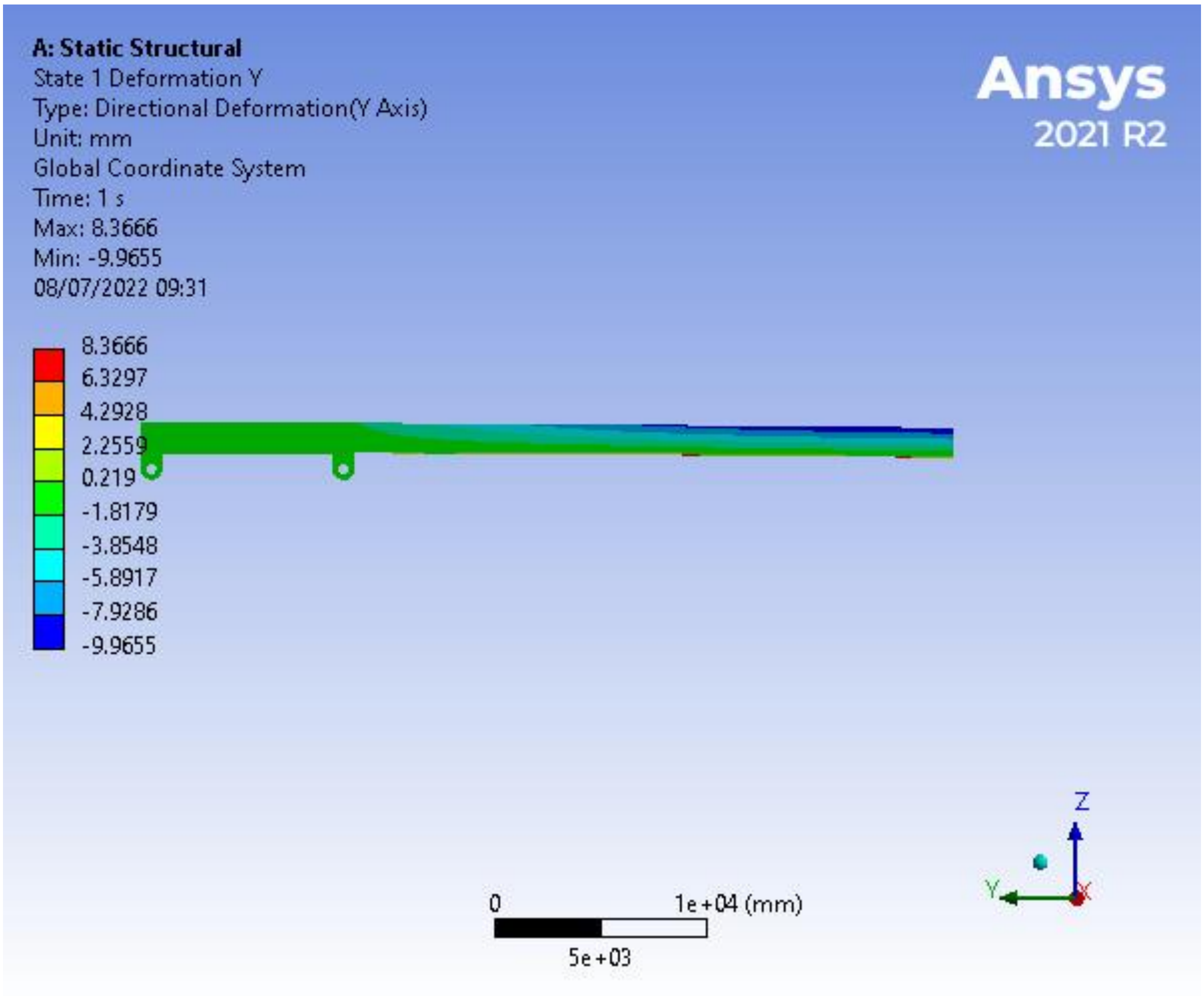

FIGURE 18
Model (A4, B4, C4) > Static Structural State 1 (A5) > Solution (A6) > Z Axis - Directional Deformation - End Time

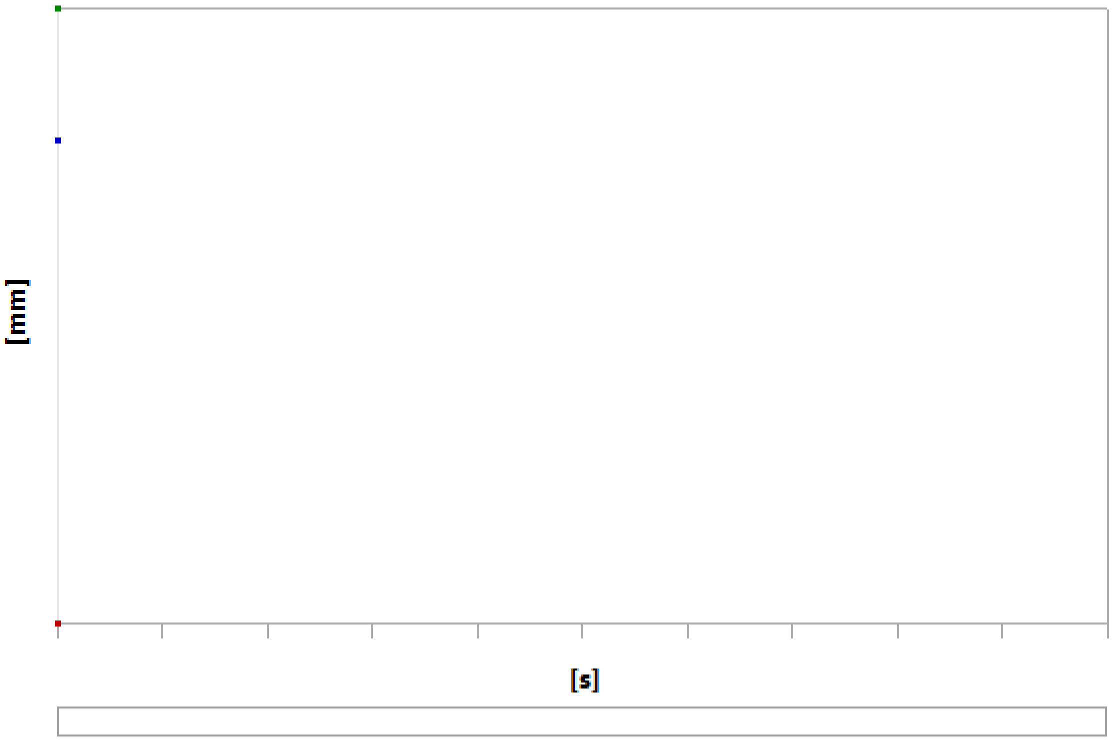

TABLE 20
Model (A4, B4, C4) > Static Structural State 1 (A5) > Solution (A6) > Z Axis - Directional Deformation - End Time

Time [s]	Minimum [mm]	Maximum [mm]	Average [mm]
1.	-160.67	1.2103	-33.455

FIGURE 19
Model (A4, B4, C4) > Static Structural State 1 (A5) > Solution (A6) > Z Axis - Directional Deformation - End Time > State 1 Deformation Z

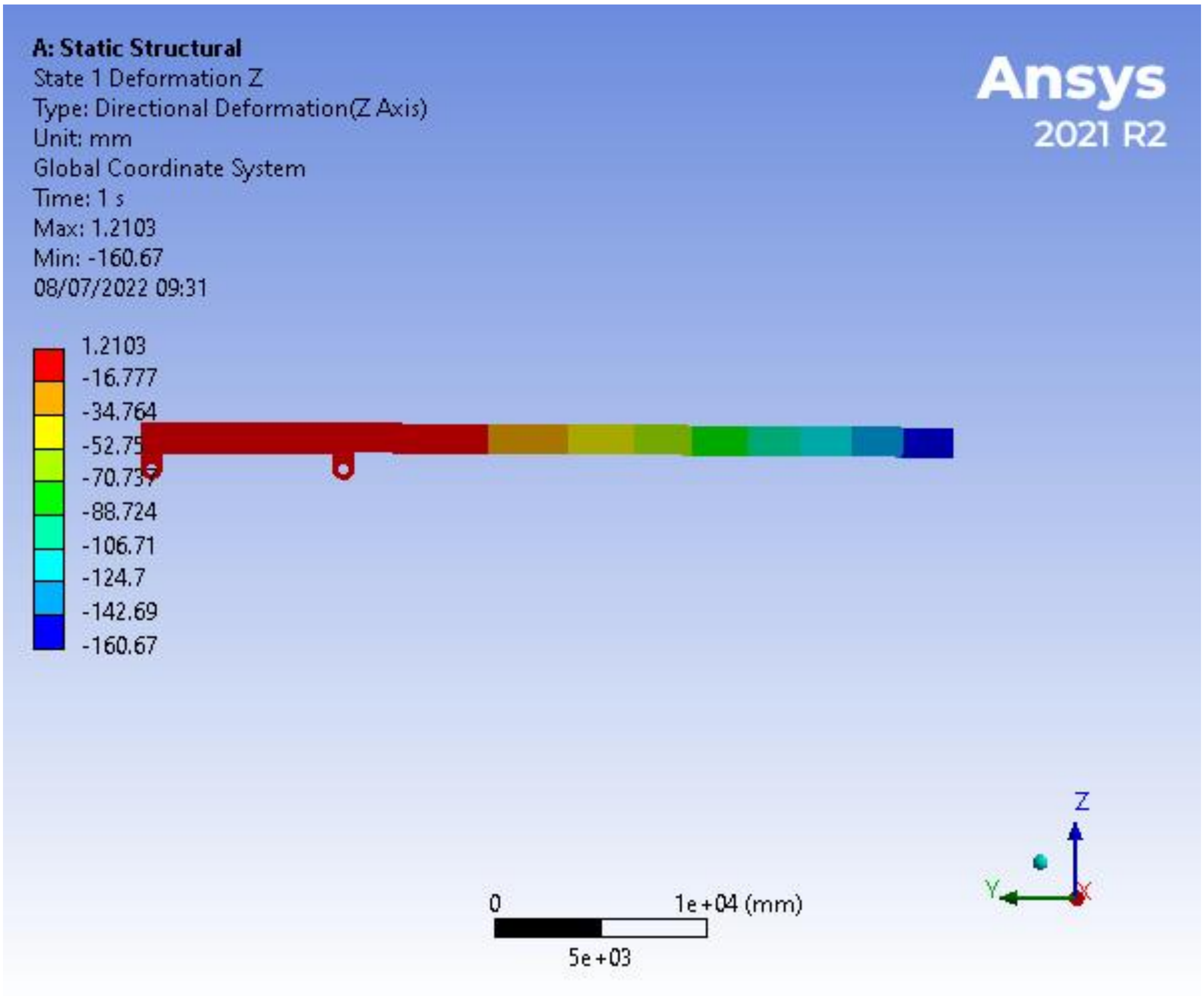

FIGURE 20
Model (A4, B4, C4) > Static Structural State 1 (A5) > Solution (A6) > Equivalent Stress

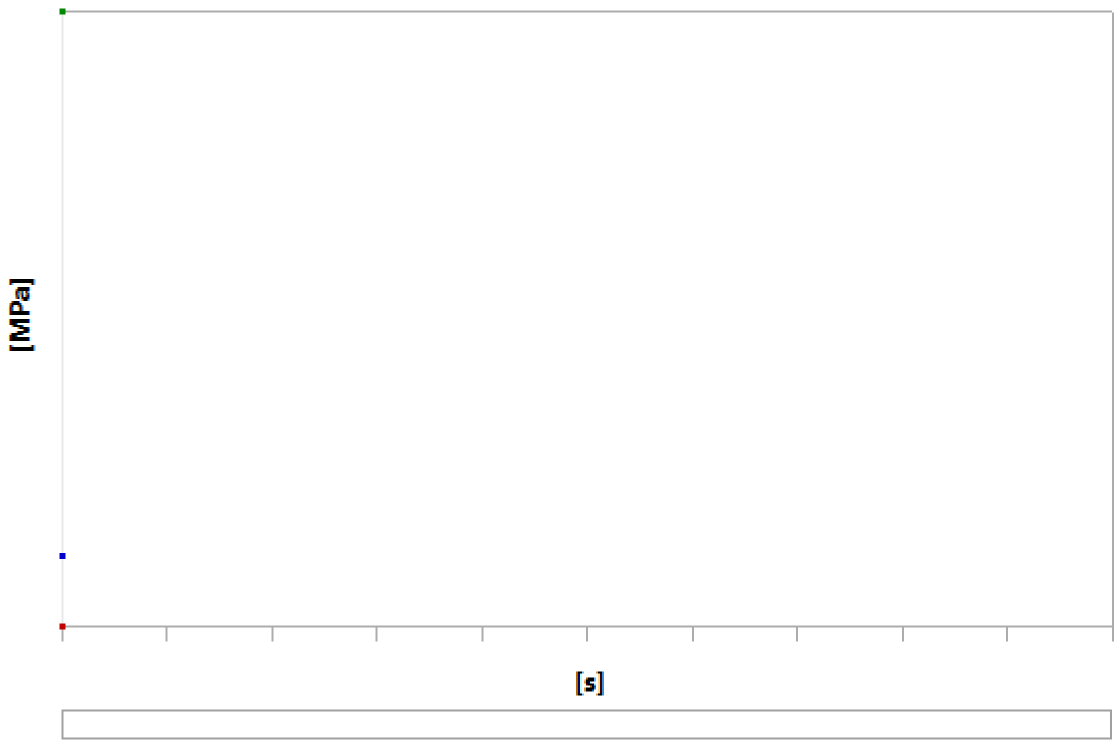

TABLE 21
Model (A4, B4, C4) > Static Structural State 1 (A5) > Solution (A6) > Equivalent Stress

Time [s]	Minimum [MPa]	Maximum [MPa]	Average [MPa]
1.	4.2315e-002	240.04	27.72

FIGURE 21
Model (A4, B4, C4) > Static Structural State 1 (A5) > Solution (A6) > Equivalent Stress > State 1 Equivalent Stress

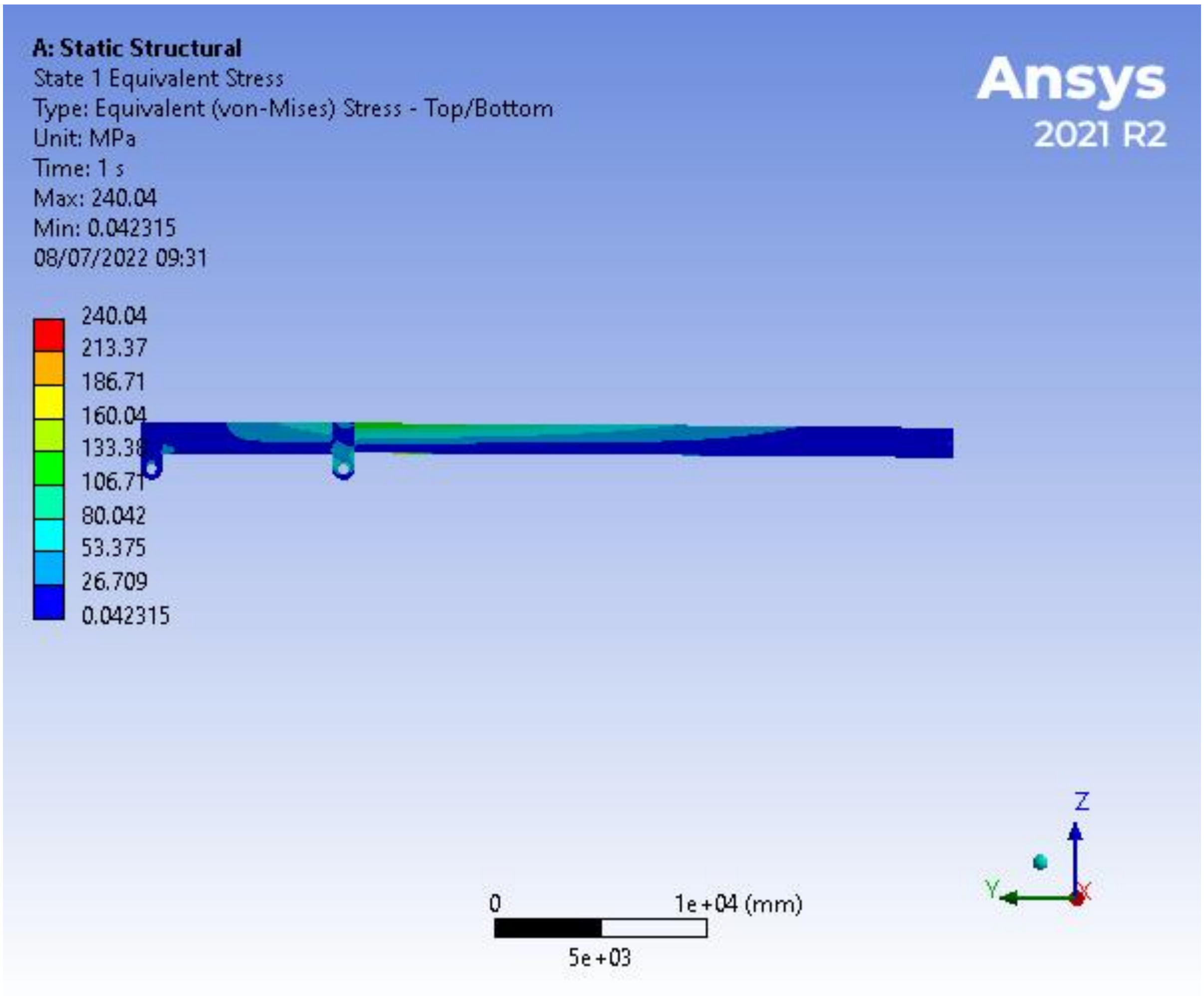

Static Structural State 2 (C5)

TABLE 22
Model (A4, B4, C4) > Analysis

Object Name	*Static Structural State 2 (C5)*
State	Not Solved
Definition	
Physics Type	Structural
Analysis Type	Static Structural
Solver Target	Mechanical APDL
Options	
Environment Temperature	22. °C
Generate Input Only	No

TABLE 23
Model (A4, B4, C4) > Static Structural State 2 (C5) > Analysis Settings

Object Name	*Analysis Settings*
State	Fully Defined
Step Controls	
Number Of Steps	1.
Current Step Number	1.
Step End Time	1. s
Auto Time Stepping	Program Controlled

Solver Controls	
Solver Type	Program Controlled
Weak Springs	Off
Solver Pivot Checking	Program Controlled
Large Deflection	Off
Inertia Relief	Off
Quasi-Static Solution	Off
Rotordynamics Controls	
Coriolis Effect	Off
Restart Controls	
Generate Restart Points	Program Controlled
Retain Files After Full Solve	No
Combine Restart Files	Program Controlled
Nonlinear Controls	
Newton-Raphson Option	Program Controlled
Force Convergence	Program Controlled
Moment Convergence	Program Controlled
Displacement Convergence	Program Controlled
Rotation Convergence	Program Controlled
Line Search	Program Controlled
Stabilization	Program Controlled
Advanced	
Inverse Option	No
Contact Split (DMP)	Off
Output Controls	
Stress	Yes
Surface Stress	No
Back Stress	No
Strain	Yes
Contact Data	Yes
Nonlinear Data	No
Nodal Forces	No
Volume and Energy	Yes
Euler Angles	Yes
General Miscellaneous	No
Contact Miscellaneous	No
Store Results At	All Time Points
Result File Compression	Program Controlled
Analysis Data Management	
Solver Files Directory	C:\Users\timde\Ansys\final versions\structural analysis_files\dp0\SYS-1\MECH\
Future Analysis	None
Scratch Solver Files Directory	
Save MAPDL db	No
Contact Summary	Program Controlled
Delete Unneeded Files	Yes
Nonlinear Solution	No
Solver Units	Active System
Solver Unit System	nmm

FIGURE 22
Model (A4, B4, C4) > Static Structural State 2 (C5) > Load configuration 2

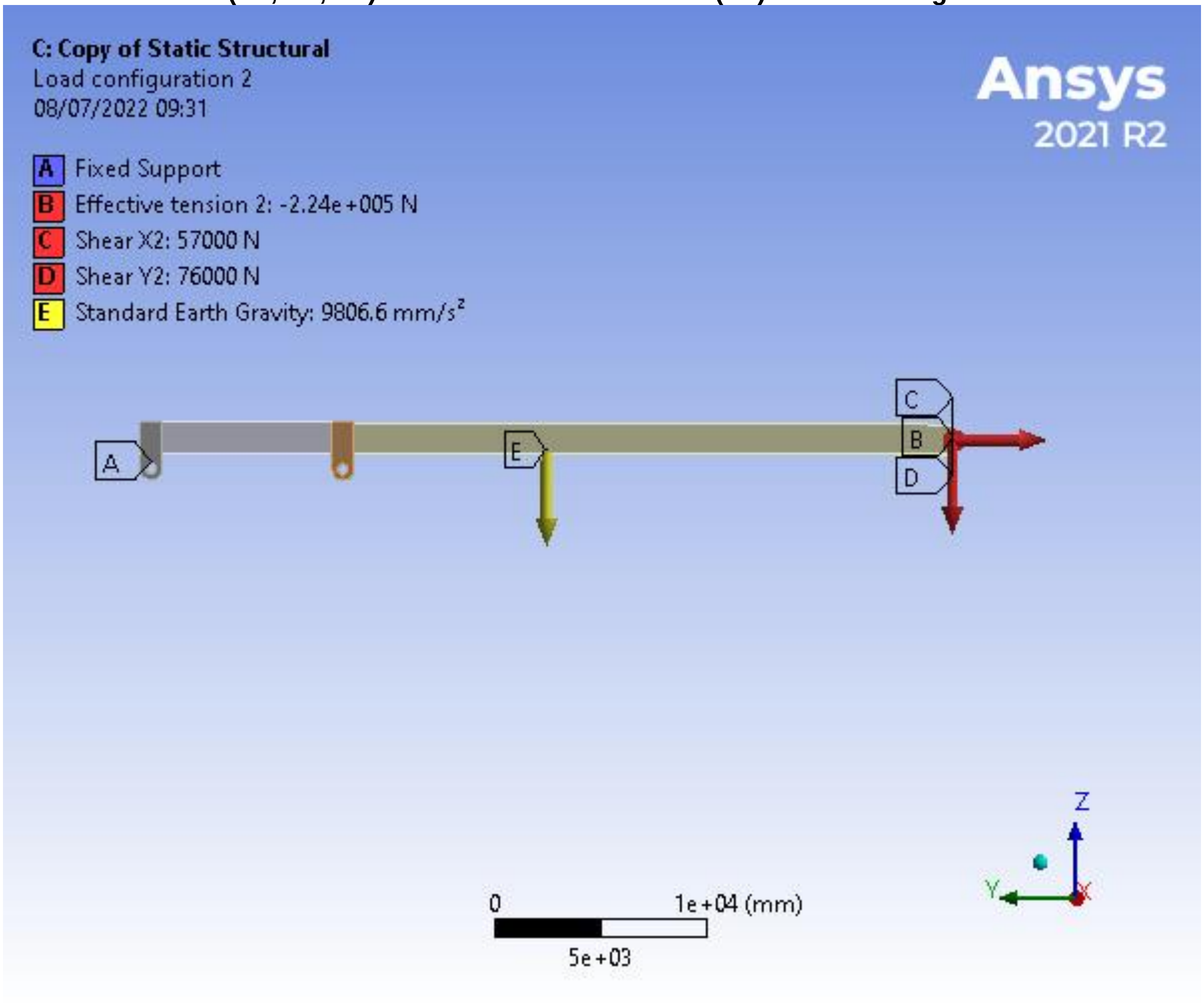

TABLE 24
Model (A4, B4, C4) > Static Structural State 2 (C5) > Accelerations

Object Name	*Standard Earth Gravity*
State	Fully Defined
Scope	
Geometry	All Bodies
Definition	
Coordinate System	Global Coordinate System
X Component	0. mm/s² (ramped)
Y Component	0. mm/s² (ramped)
Z Component	-9806.6 mm/s² (ramped)
Suppressed	No
Direction	-Z Direction

FIGURE 23
Model (A4, B4, C4) > Static Structural State 2 (C5) > Standard Earth Gravity

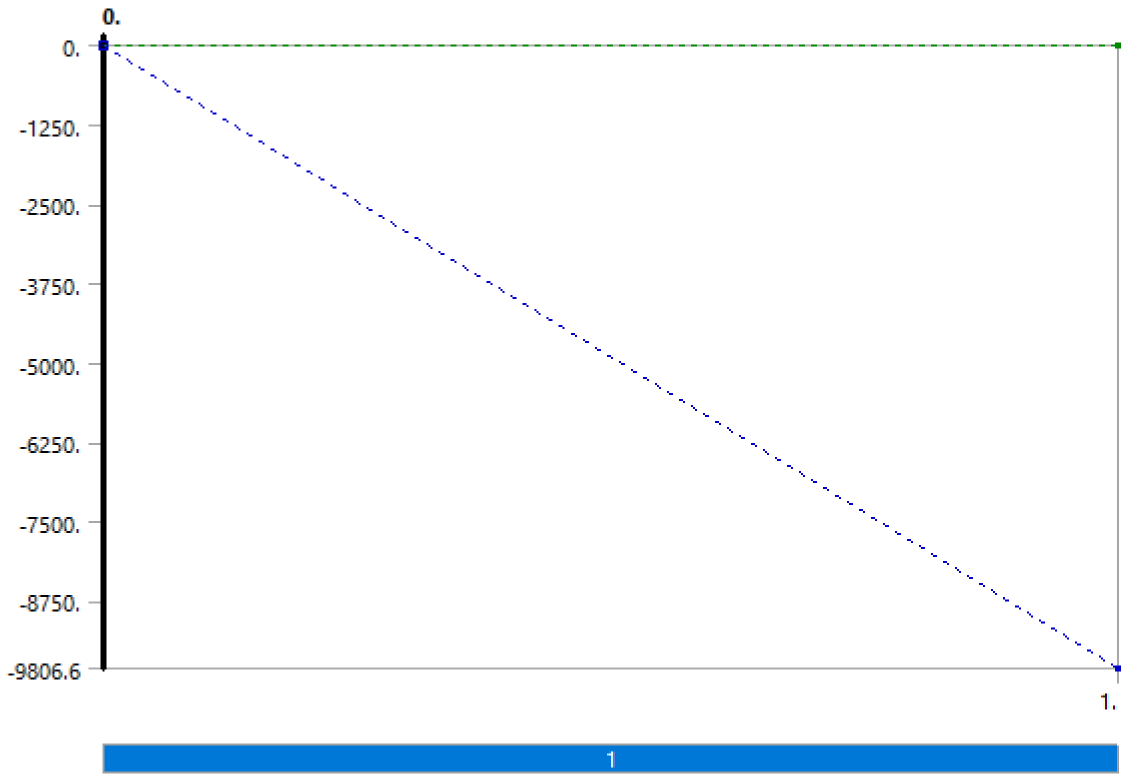

TABLE 25
Model (A4, B4, C4) > Static Structural State 2 (C5) > Loads

Object Name	*Fixed Support*	*Effective tension 2*	*Shear X2*	*Shear Y2*
State	Fully Defined			
Scope				
Scoping Method	Geometry Selection			
Geometry	8 Faces	1 Face		
Definition				
Type	Fixed Support	Force		
Suppressed	No			
Define By		Vector		
Applied By		Surface Effect		
Magnitude		-2.24e+005 N (ramped)	57000 N (ramped)	76000 N (ramped)
Direction		Defined		

FIGURE 24
Model (A4, B4, C4) > Static Structural State 2 (C5) > Effective tension 2

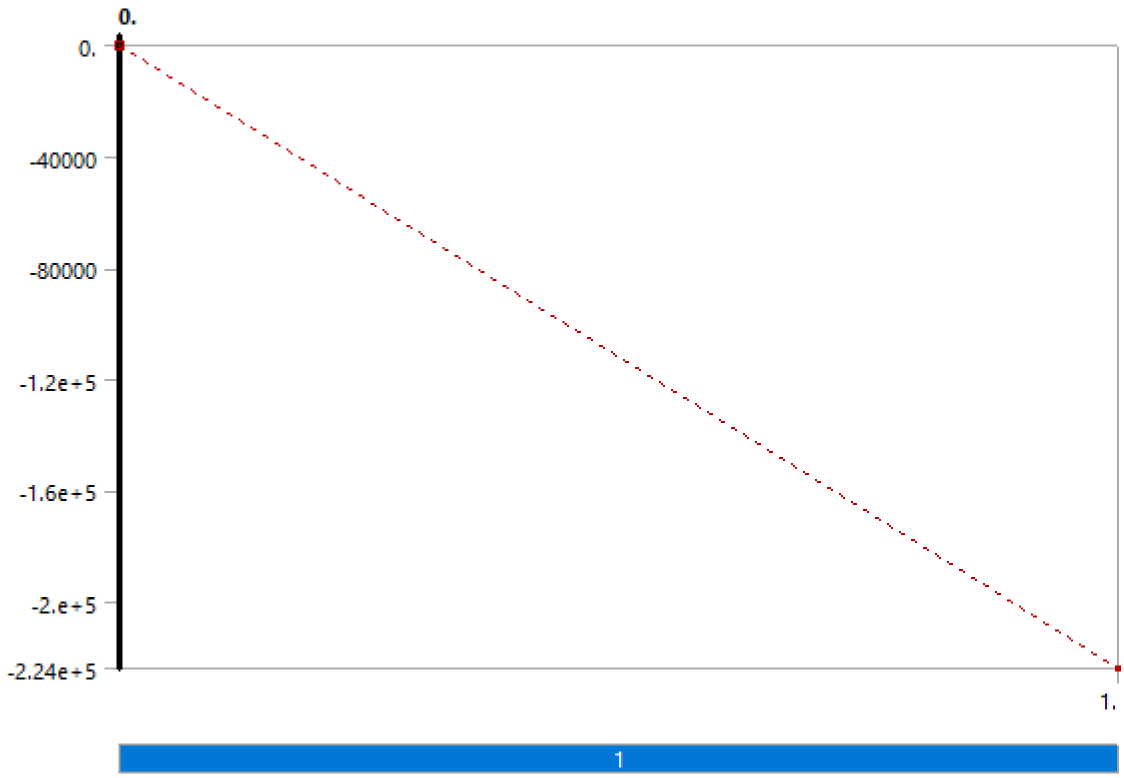

FIGURE 25
Model (A4, B4, C4) > Static Structural State 2 (C5) > Shear X2

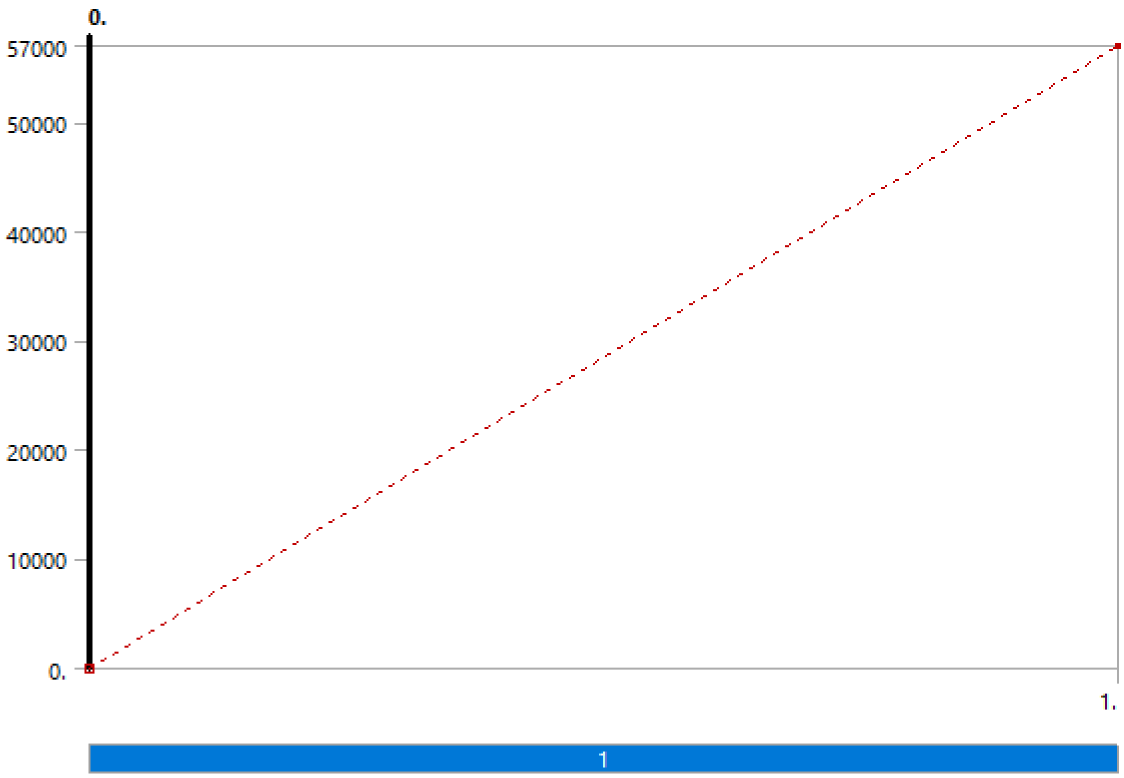

FIGURE 26
Model (A4, B4, C4) > Static Structural State 2 (C5) > Shear Y2

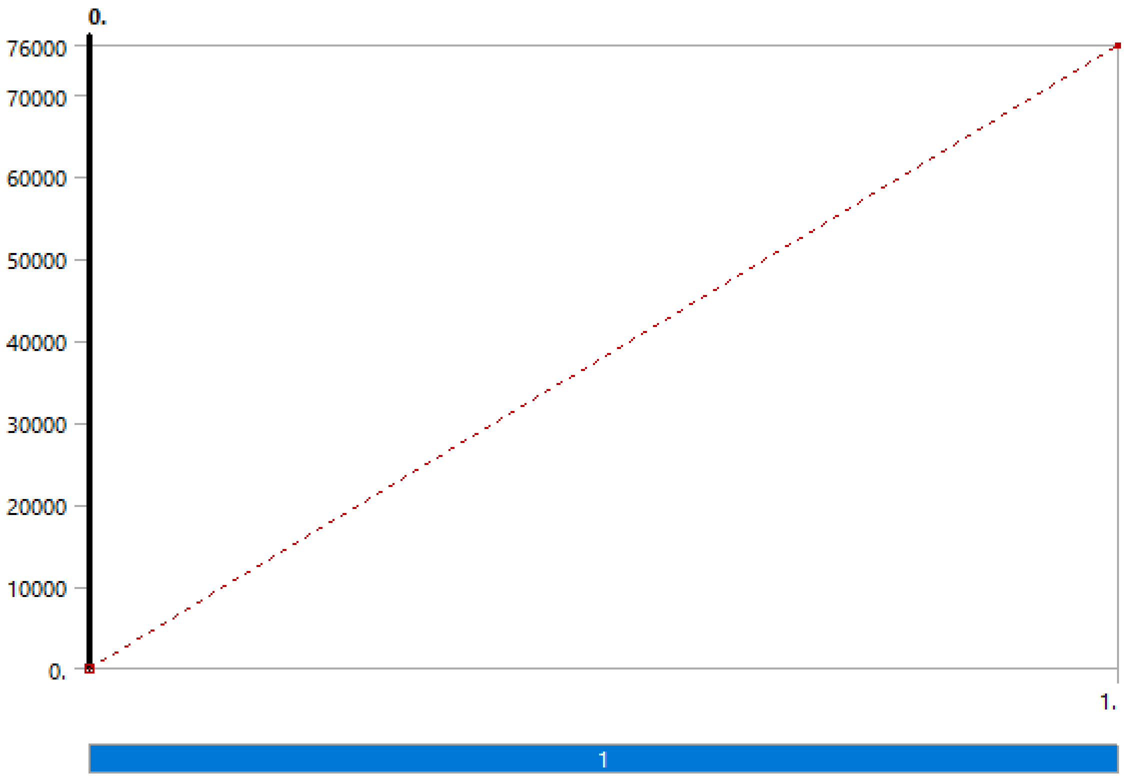

Solution (C6)

TABLE 26
Model (A4, B4, C4) > Static Structural State 2 (C5) > Solution

Object Name	*Solution (C6)*
State	Obsolete
Adaptive Mesh Refinement	
Max Refinement Loops	1.
Refinement Depth	2.
Information	
Status	Solve Required
MAPDL Elapsed Time	6. s
MAPDL Memory Used	748. MB
MAPDL Result File Size	23.5 MB
Post Processing	
Beam Section Results	No
On Demand Stress/Strain	No

TABLE 27
Model (A4, B4, C4) > Static Structural State 2 (C5) > Solution (C6) > Solution Information

Object Name	*Solution Information*
State	Obsolete
Solution Information	
Solution Output	Solver Output
Newton-Raphson Residuals	0
Identify Element Violations	0
Update Interval	2.5 s
Display Points	All
FE Connection Visibility	

Activate Visibility	Yes
Display	All FE Connectors
Draw Connections Attached To	All Nodes
Line Color	Connection Type
Visible on Results	No
Line Thickness	Single
Display Type	Lines

TABLE 28
Model (A4, B4, C4) > Static Structural State 2 (C5) > Solution (C6) > Results

Object Name	*X Axis - Directional Deformation - End Time*	*Y Axis - Directional Deformation - End Time*	*Z Axis - Directional Deformation - End Time*	*Equivalent Stress*
State	Obsolete			
Scope				
Scoping Method	Geometry Selection			
Geometry	All Bodies			
Position				Top/Bottom
Definition				
Type	Directional Deformation			Equivalent (von-Mises) Stress
Orientation	X Axis	Y Axis	Z Axis	
By	Time			
Display Time	Last		First	Last
Coordinate System	Global Coordinate System			
Calculate Time History	Yes			
Identifier				
Suppressed	No			
Results				
Minimum	-0.40963 mm	-7.3542 mm	-157.84 mm	5.1992e-002 MPa
Maximum	53.174 mm	5.9627 mm	0.97569 mm	191.7 MPa
Average	10.8 mm	-0.45171 mm	-32.896 mm	23.072 MPa
Minimum Occurs On	1 large outrigger\Surface1	2 outrigger\Surface1		padeye telescopic arm\Solid1
Maximum Occurs On	2 outrigger\Surface1		1 large outrigger\Surface1	padeye telescopic arm\Solid1
Information				
Time	1. s			
Load Step	1			
Substep	1			
Iteration Number	1			
Integration Point Results				
Display Option				Averaged

Average Across Bodies		No

FIGURE 27
Model (A4, B4, C4) > Static Structural State 2 (C5) > Solution (C6) > X Axis - Directional Deformation - End Time

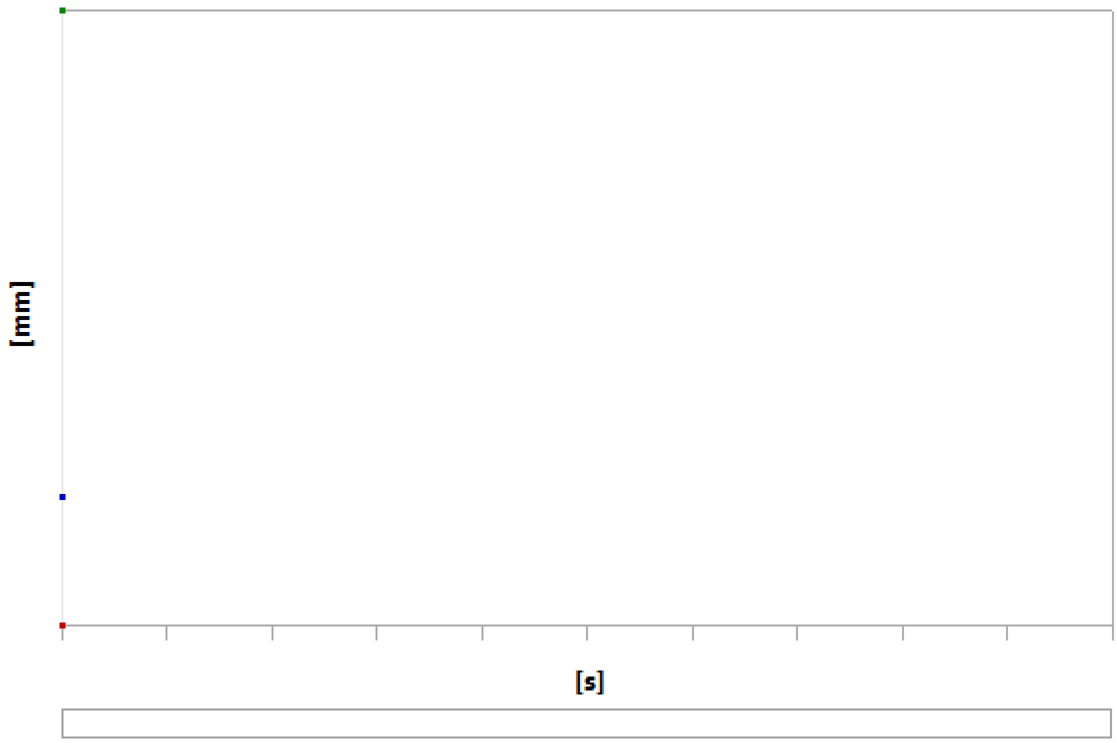

TABLE 29
Model (A4, B4, C4) > Static Structural State 2 (C5) > Solution (C6) > X Axis - Directional Deformation - End Time

Time [s]	Minimum [mm]	Maximum [mm]	Average [mm]
1.	-0.40963	53.174	10.8

FIGURE 28
Model (A4, B4, C4) > Static Structural State 2 (C5) > Solution (C6) > X Axis - Directional Deformation - End Time > State 2 Deformation X

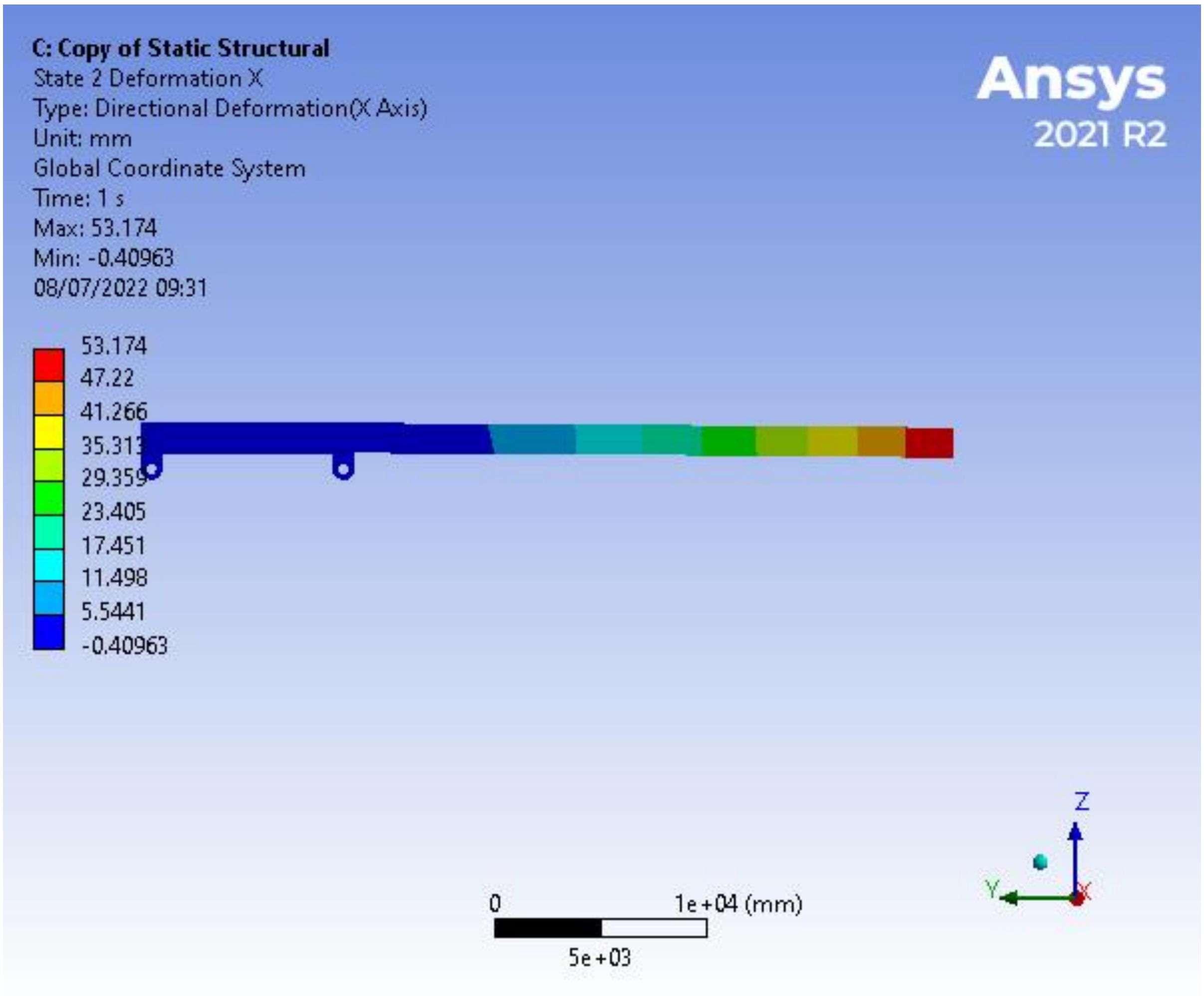

FIGURE 29
Model (A4, B4, C4) > Static Structural State 2 (C5) > Solution (C6) > Y Axis - Directional Deformation - End Time

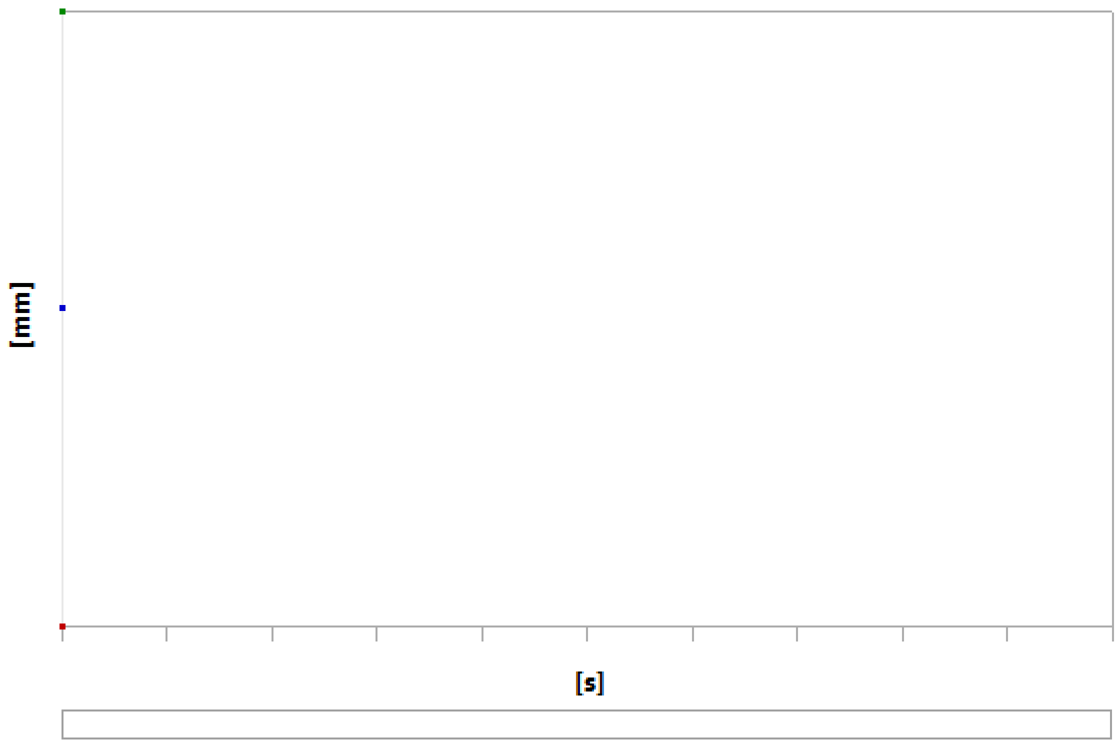

TABLE 30
Model (A4, B4, C4) > Static Structural State 2 (C5) > Solution (C6) > Y Axis - Directional Deformation - End Time

Time [s]	Minimum [mm]	Maximum [mm]	Average [mm]
1.	-7.3542	5.9627	-0.45171

FIGURE 30
Model (A4, B4, C4) > Static Structural State 2 (C5) > Solution (C6) > Y Axis - Directional Deformation - End Time > State 2 Deformation Y

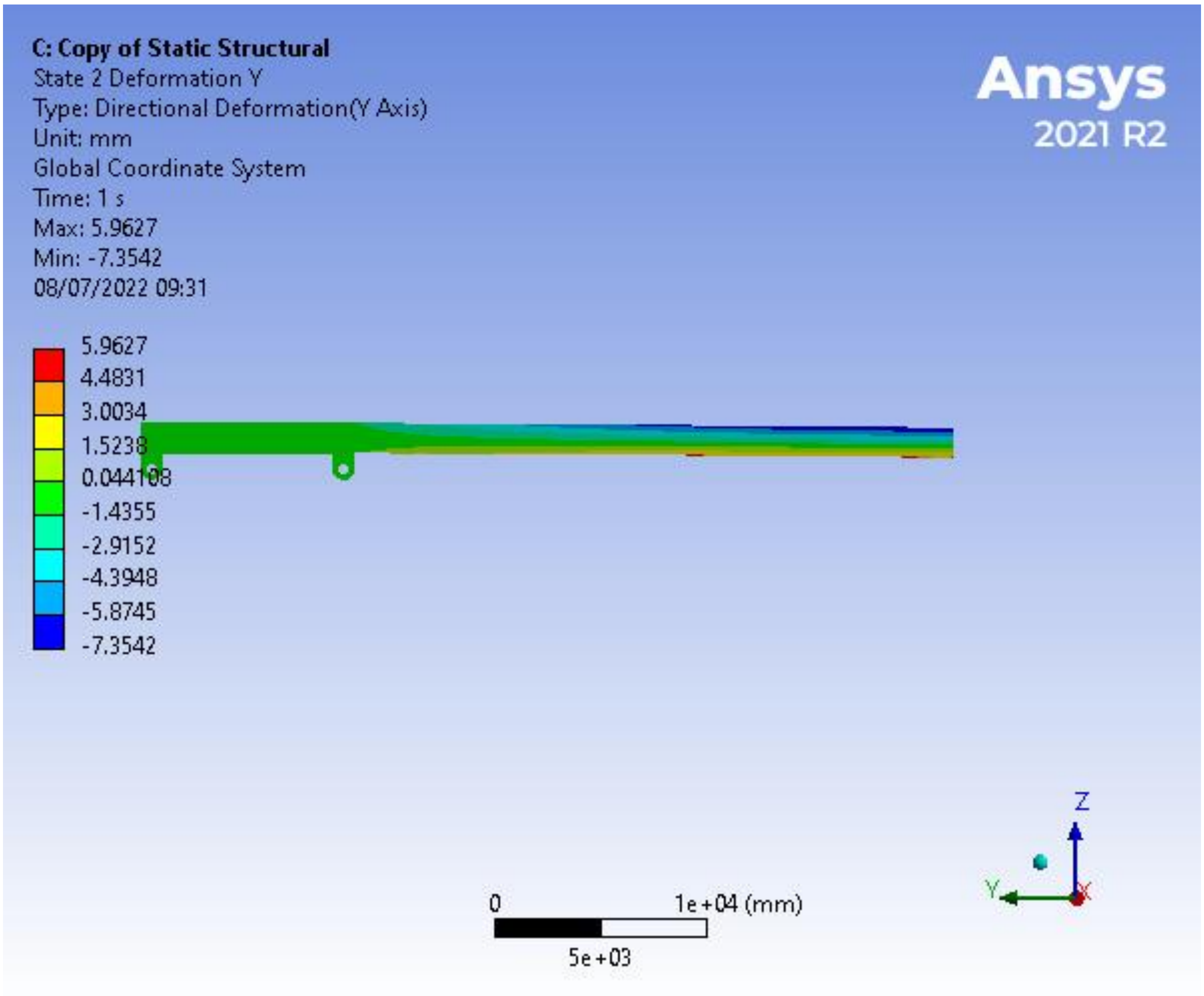

FIGURE 31
Model (A4, B4, C4) > Static Structural State 2 (C5) > Solution (C6) > Z Axis - Directional Deformation - End Time

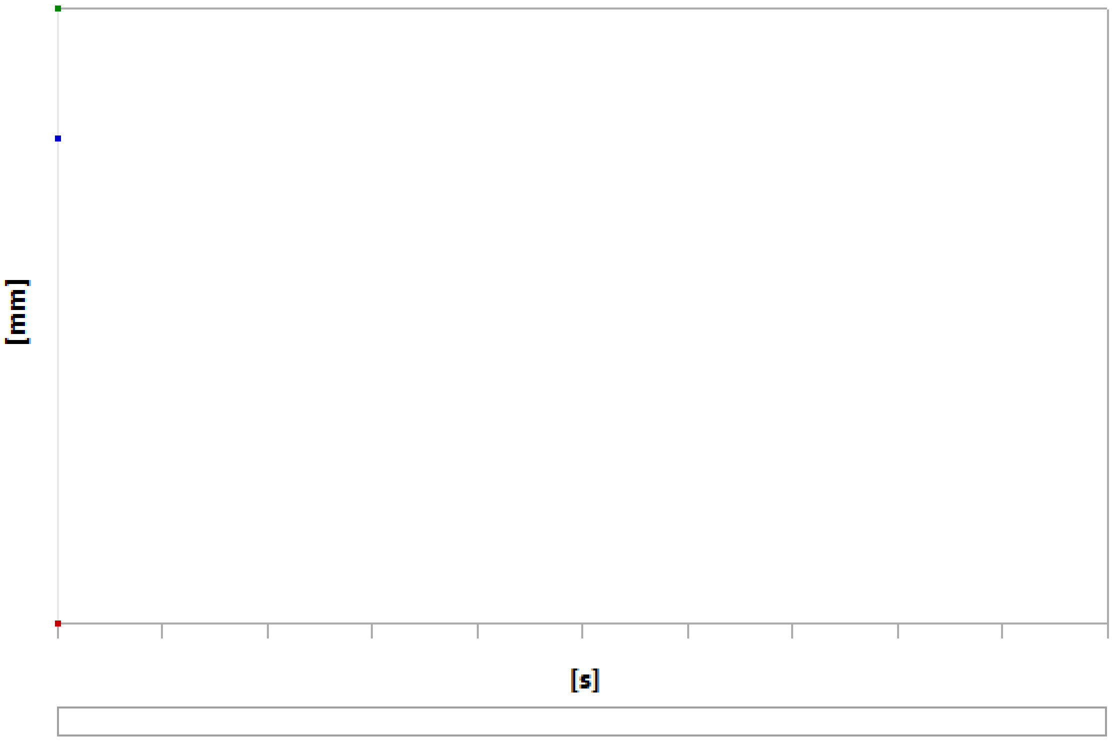

TABLE 31
Model (A4, B4, C4) > Static Structural State 2 (C5) > Solution (C6) > Z Axis - Directional Deformation - End Time

Time [s]	Minimum [mm]	Maximum [mm]	Average [mm]
1.	-157.84	0.97569	-32.896

FIGURE 32
Model (A4, B4, C4) > Static Structural State 2 (C5) > Solution (C6) > Z Axis - Directional Deformation - End Time > State 2 Deformation Z

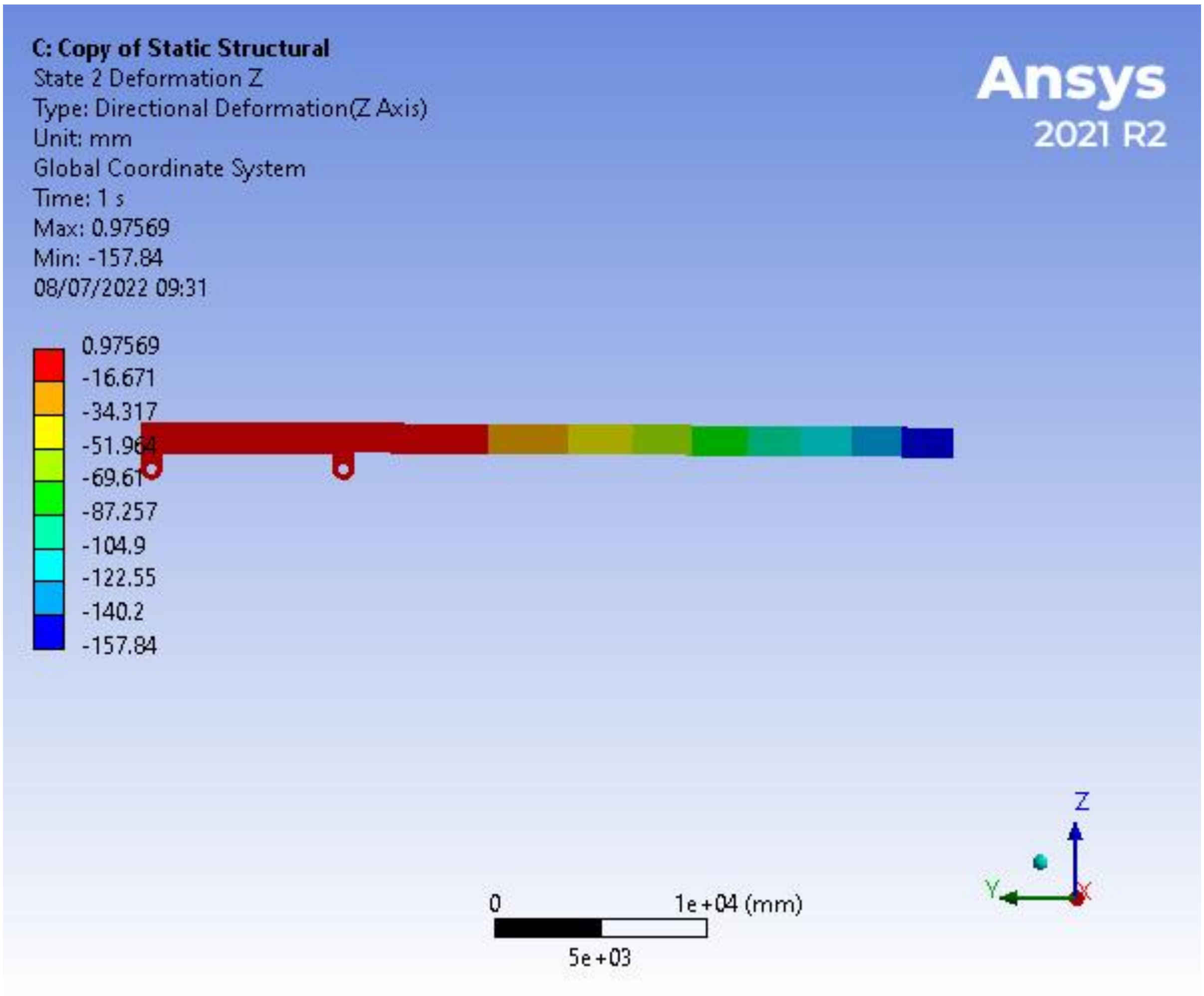

FIGURE 33
Model (A4, B4, C4) > Static Structural State 2 (C5) > Solution (C6) > Equivalent Stress

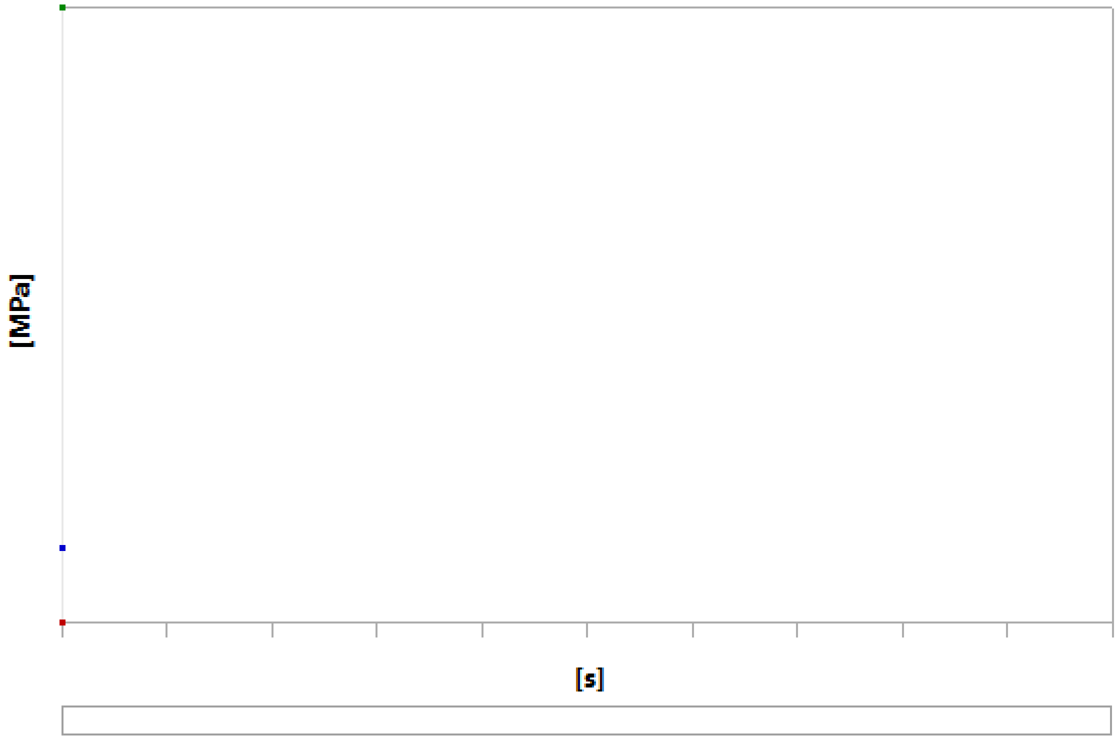

TABLE 32
Model (A4, B4, C4) > Static Structural State 2 (C5) > Solution (C6) > Equivalent Stress

Time [s]	Minimum [MPa]	Maximum [MPa]	Average [MPa]
1.	5.1992e-002	191.7	23.072

FIGURE 34
Model (A4, B4, C4) > Static Structural State 2 (C5) > Solution (C6) > Equivalent Stress > State 2 Equivalent Stress

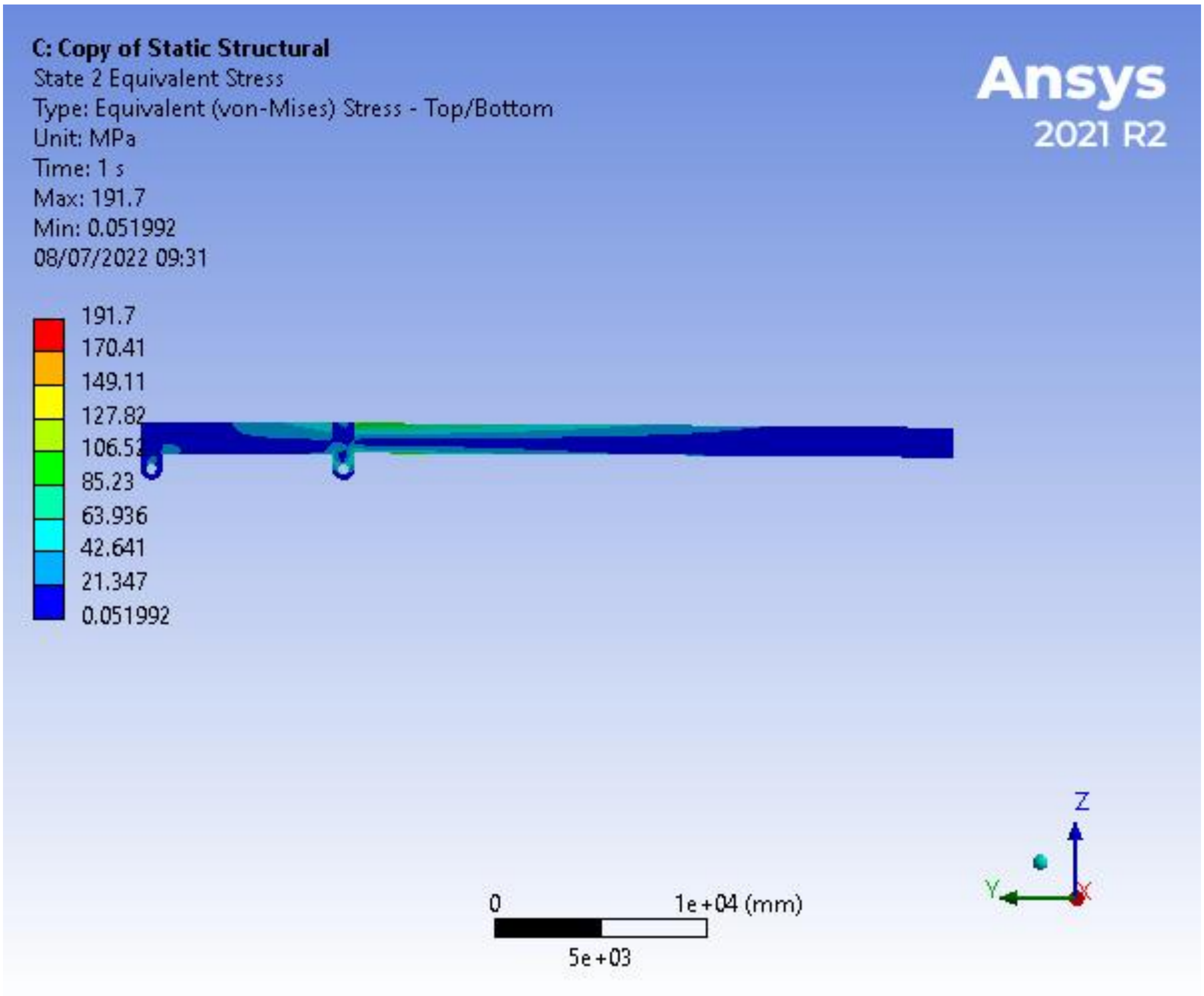

Static Structural State 3 (B5)

TABLE 33
Model (A4, B4, C4) > Analysis

Object Name	*Static Structural State 3 (B5)*
State	Not Solved
Definition	
Physics Type	Structural
Analysis Type	Static Structural
Solver Target	Mechanical APDL
Options	
Environment Temperature	22. °C
Generate Input Only	No

TABLE 34
Model (A4, B4, C4) > Static Structural State 3 (B5) > Analysis Settings

Object Name	*Analysis Settings*
State	Fully Defined
Step Controls	
Number Of Steps	1.
Current Step Number	1.
Step End Time	1. s
Auto Time Stepping	Program Controlled

Solver Controls	
Solver Type	Program Controlled
Weak Springs	Off
Solver Pivot Checking	Program Controlled
Large Deflection	Off
Inertia Relief	Off
Quasi-Static Solution	Off
Rotordynamics Controls	
Coriolis Effect	Off
Restart Controls	
Generate Restart Points	Program Controlled
Retain Files After Full Solve	No
Combine Restart Files	Program Controlled
Nonlinear Controls	
Newton-Raphson Option	Program Controlled
Force Convergence	Program Controlled
Moment Convergence	Program Controlled
Displacement Convergence	Program Controlled
Rotation Convergence	Program Controlled
Line Search	Program Controlled
Stabilization	Program Controlled
Advanced	
Inverse Option	No
Contact Split (DMP)	Off
Output Controls	
Stress	Yes
Surface Stress	No
Back Stress	No
Strain	Yes
Contact Data	Yes
Nonlinear Data	No
Nodal Forces	No
Volume and Energy	Yes
Euler Angles	Yes
General Miscellaneous	No
Contact Miscellaneous	No
Store Results At	All Time Points
Result File Compression	Program Controlled
Analysis Data Management	
Solver Files Directory	C:\Users\timde\Ansys\final versions\structural analysis_files\dp0\SYS-2\MECH\
Future Analysis	None
Scratch Solver Files Directory	
Save MAPDL db	No
Contact Summary	Program Controlled
Delete Unneeded Files	Yes
Nonlinear Solution	No
Solver Units	Active System
Solver Unit System	nmm

FIGURE 35
Model (A4, B4, C4) > Static Structural State 3 (B5) > Load configuration 3

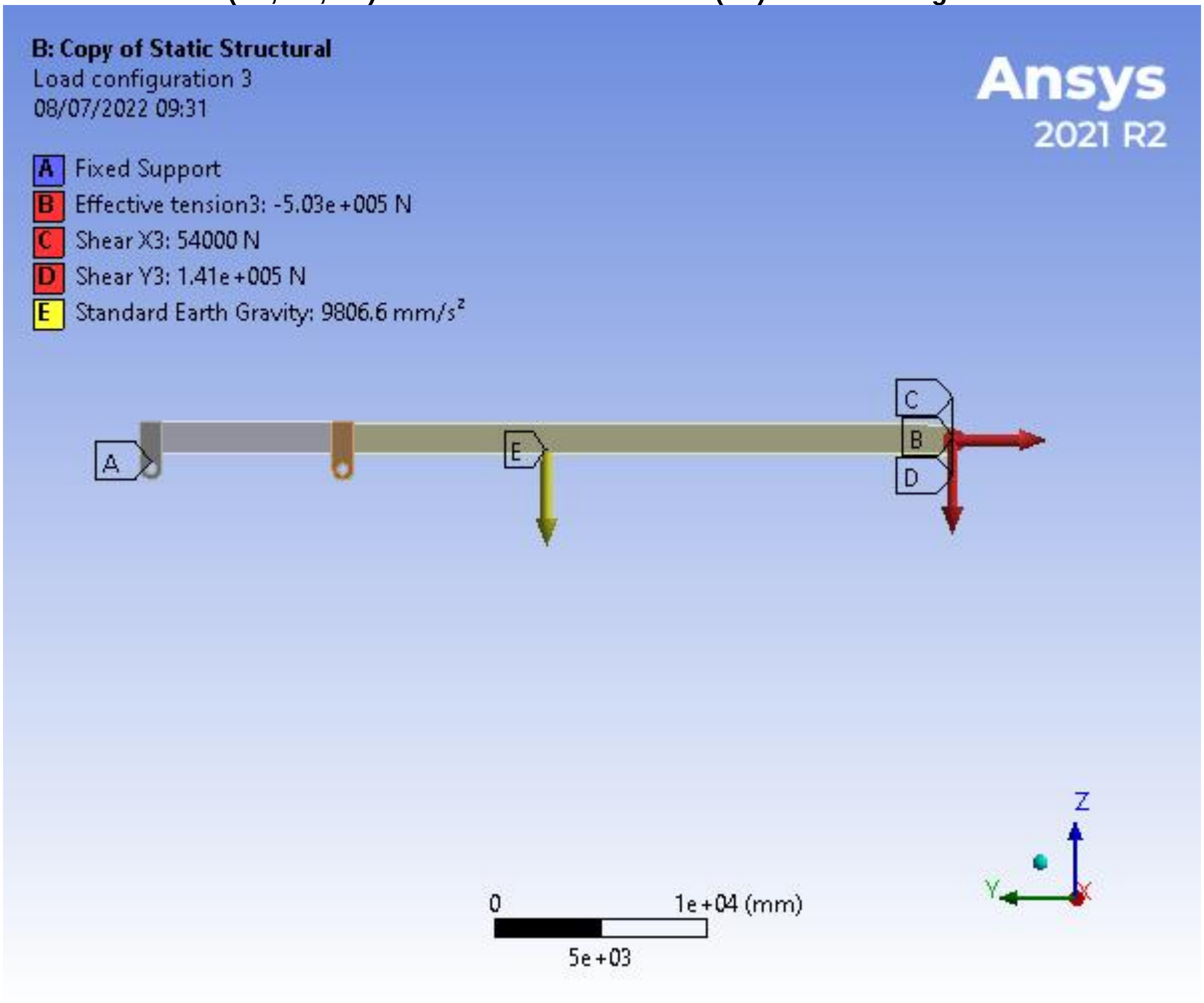

TABLE 35
Model (A4, B4, C4) > Static Structural State 3 (B5) > Accelerations

Object Name	*Standard Earth Gravity*
State	Fully Defined
Scope	
Geometry	All Bodies
Definition	
Coordinate System	Global Coordinate System
X Component	0. mm/s² (ramped)
Y Component	0. mm/s² (ramped)
Z Component	-9806.6 mm/s² (ramped)
Suppressed	No
Direction	-Z Direction

FIGURE 36
Model (A4, B4, C4) > Static Structural State 3 (B5) > Standard Earth Gravity

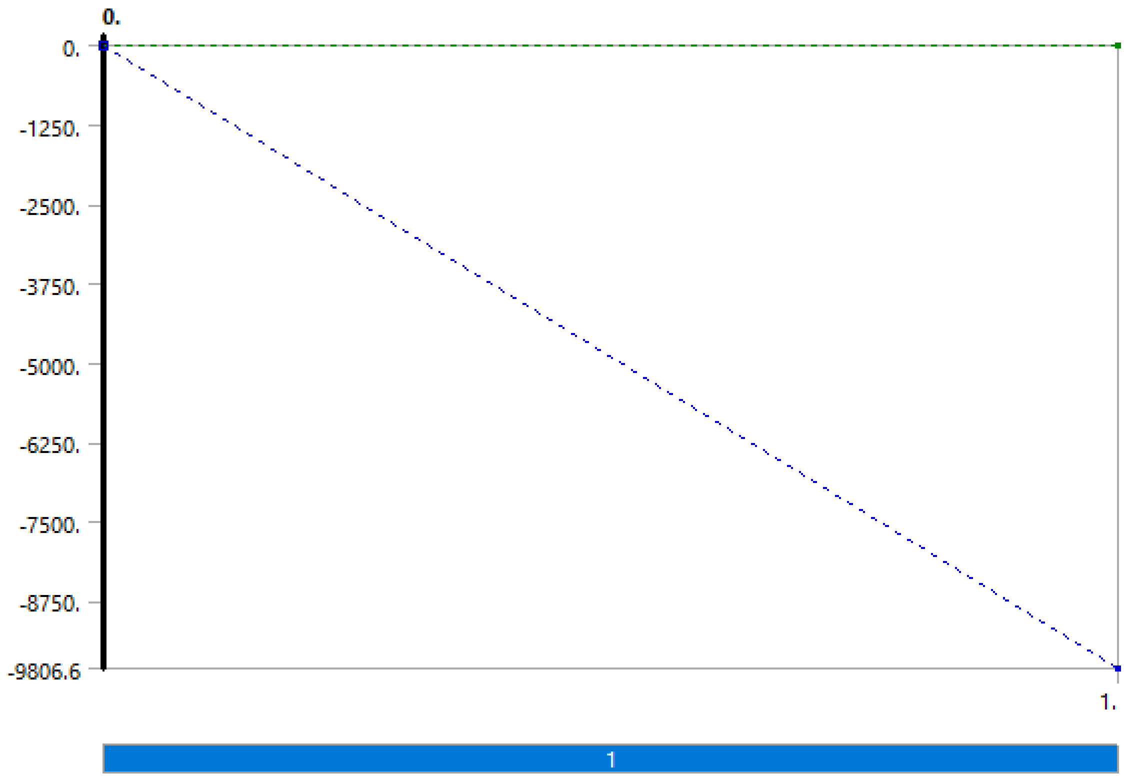

TABLE 36
Model (A4, B4, C4) > Static Structural State 3 (B5) > Loads

Object Name	*Fixed Support*	*Effective tension3*	*Shear X3*	*Shear Y3*
State	Fully Defined			
Scope				
Scoping Method	Geometry Selection			
Geometry	8 Faces	1 Face		
Definition				
Type	Fixed Support	Force		
Suppressed	No			
Define By		Vector		
Applied By		Surface Effect		
Magnitude		-5.03e+005 N (ramped)	54000 N (ramped)	1.41e+005 N (ramped)
Direction		Defined		

FIGURE 37
Model (A4, B4, C4) > Static Structural State 3 (B5) > Effective tension3

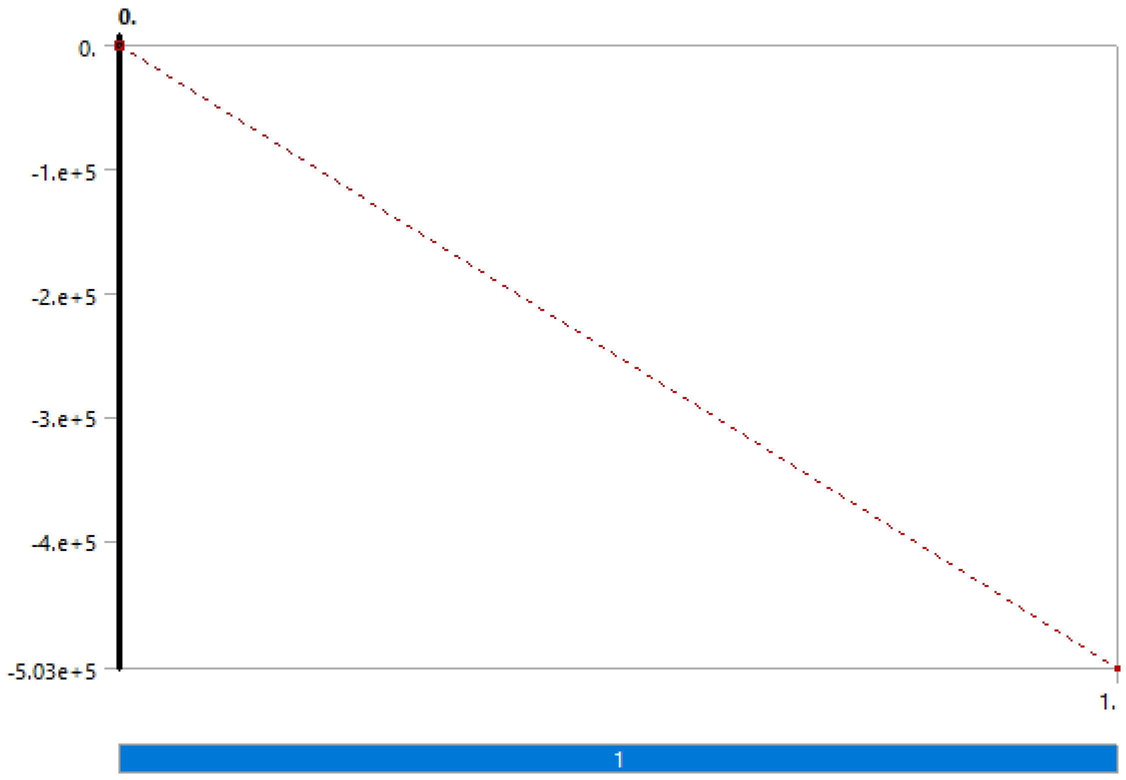

FIGURE 38
Model (A4, B4, C4) > Static Structural State 3 (B5) > Shear X3

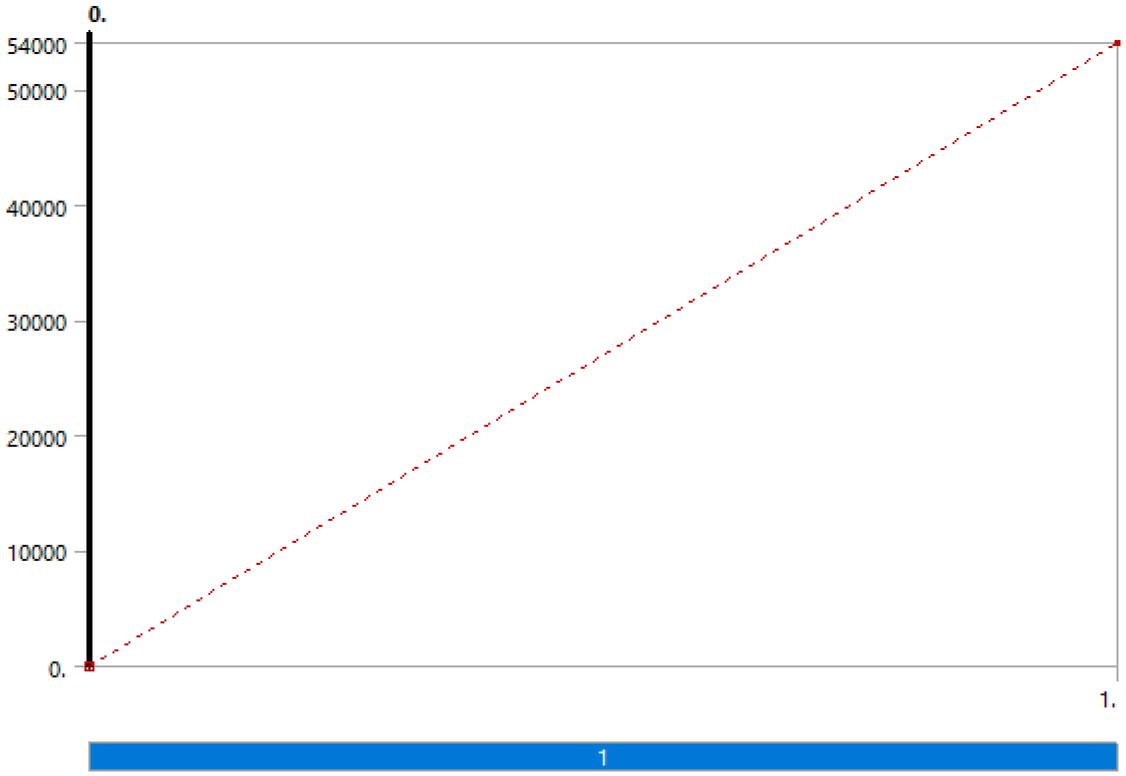

FIGURE 39
Model (A4, B4, C4) > Static Structural State 3 (B5) > Shear Y3

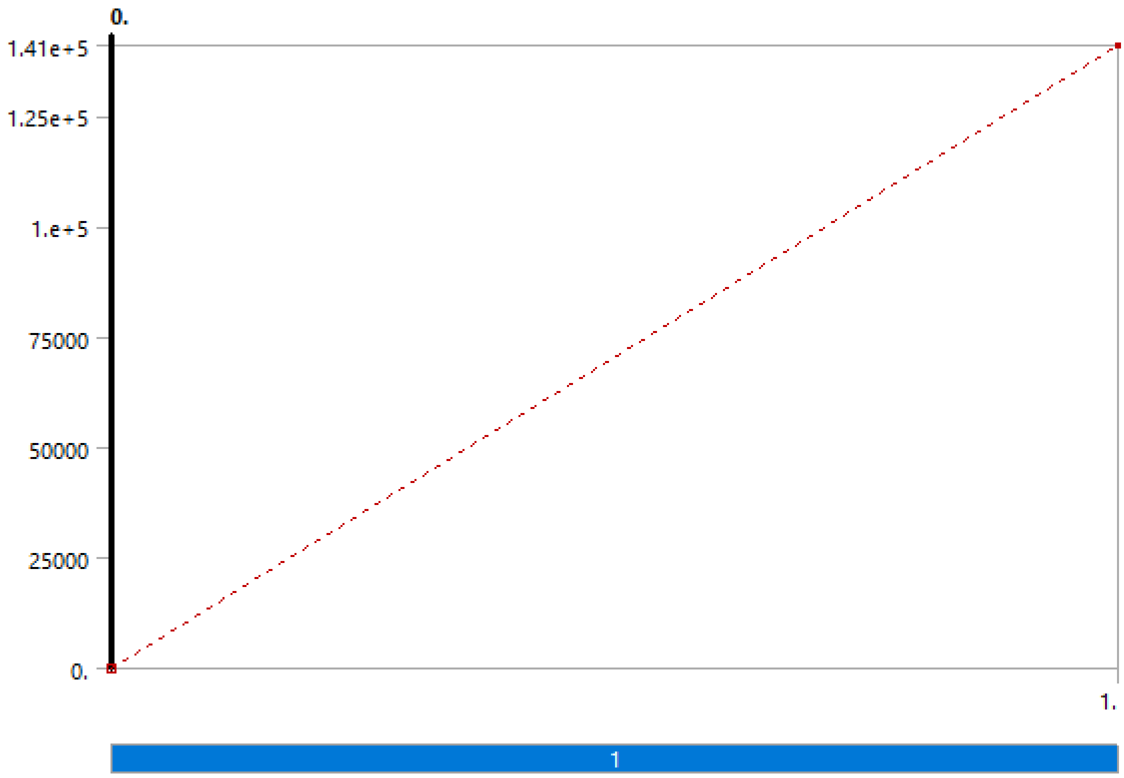

Solution (B6)

TABLE 37
Model (A4, B4, C4) > Static Structural State 3 (B5) > Solution

Object Name	*Solution (B6)*
State	Obsolete
Adaptive Mesh Refinement	
Max Refinement Loops	1.
Refinement Depth	2.
Information	
Status	Solve Required
MAPDL Elapsed Time	5. s
MAPDL Memory Used	748. MB
MAPDL Result File Size	23.5 MB
Post Processing	
Beam Section Results	No
On Demand Stress/Strain	No

TABLE 38
Model (A4, B4, C4) > Static Structural State 3 (B5) > Solution (B6) > Solution Information

Object Name	*Solution Information*
State	Obsolete
Solution Information	
Solution Output	Solver Output
Newton-Raphson Residuals	0
Identify Element Violations	0
Update Interval	2.5 s
Display Points	All
FE Connection Visibility	

Activate Visibility	Yes
Display	All FE Connectors
Draw Connections Attached To	All Nodes
Line Color	Connection Type
Visible on Results	No
Line Thickness	Single
Display Type	Lines

TABLE 39
Model (A4, B4, C4) > Static Structural State 3 (B5) > Solution (B6) > Results

Object Name	*X Axis - Directional Deformation - End Time*	*Y Axis - Directional Deformation - End Time*	*Z Axis - Directional Deformation - End Time*	*Equivalent Stress*
State	Obsolete			
Scope				
Scoping Method	Geometry Selection			
Geometry	All Bodies			
Position				Top/Bottom
Definition				
Type	Directional Deformation			Equivalent (von-Mises) Stress
Orientation	X Axis	Y Axis	Z Axis	
By	Time			
Display Time	Last		First	Last
Coordinate System	Global Coordinate System			
Calculate Time History	Yes			
Identifier				
Suppressed	No			
Results				
Minimum	-0.39329 mm	-9.0777 mm	-199.3 mm	7.1717e-002 MPa
Maximum	50.395 mm	7.0297 mm	1.1783 mm	225.36 MPa
Average	10.232 mm	-0.60907 mm	-41.187 mm	29.14 MPa
Minimum Occurs On	1 large outrigger\Surface1	2 outrigger\Surface1		padeye telescopic arm\Solid1
Maximum Occurs On	2 outrigger\Surface1		1 large outrigger\Surface1	padeye telescopic arm\Solid1
Information				
Time	1. s			
Load Step	1			
Substep	1			
Iteration Number	1			
Integration Point Results				
Display Option				Averaged

Average Across Bodies		No

FIGURE 40
Model (A4, B4, C4) > Static Structural State 3 (B5) > Solution (B6) > X Axis - Directional Deformation - End Time

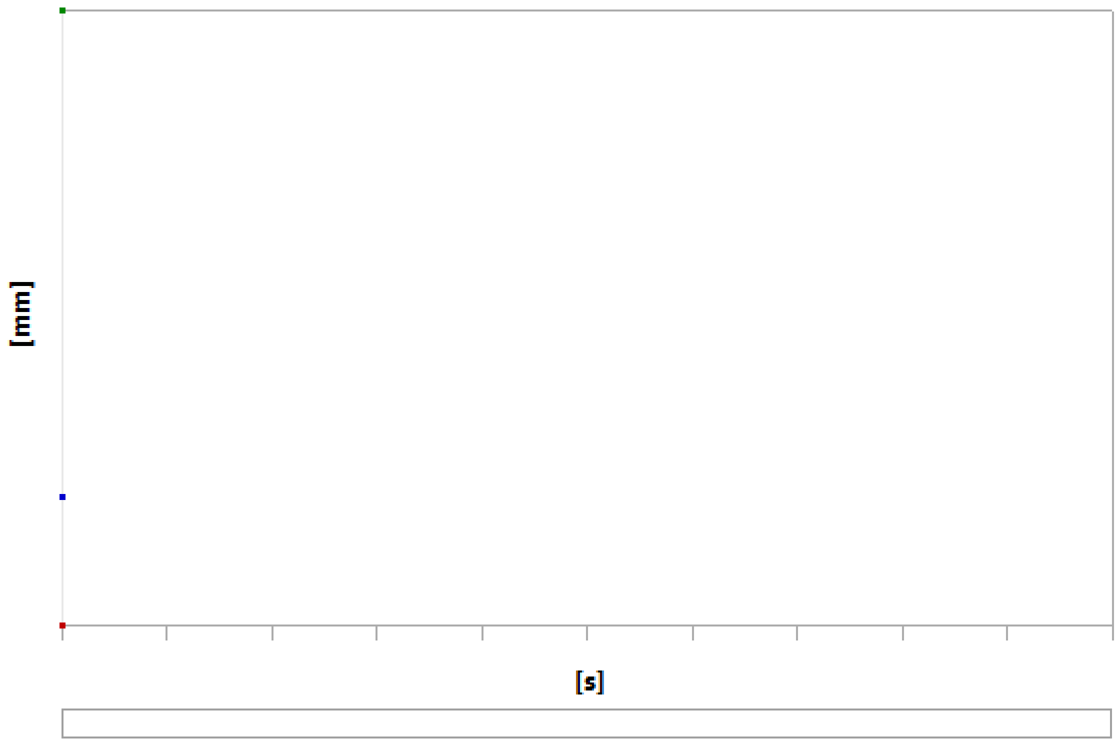

TABLE 40
Model (A4, B4, C4) > Static Structural State 3 (B5) > Solution (B6) > X Axis - Directional Deformation - End Time

Time [s]	Minimum [mm]	Maximum [mm]	Average [mm]
1.	-0.39329	50.395	10.232

FIGURE 41
Model (A4, B4, C4) > Static Structural State 3 (B5) > Solution (B6) > X Axis - Directional Deformation - End Time > State 3 Deformation X

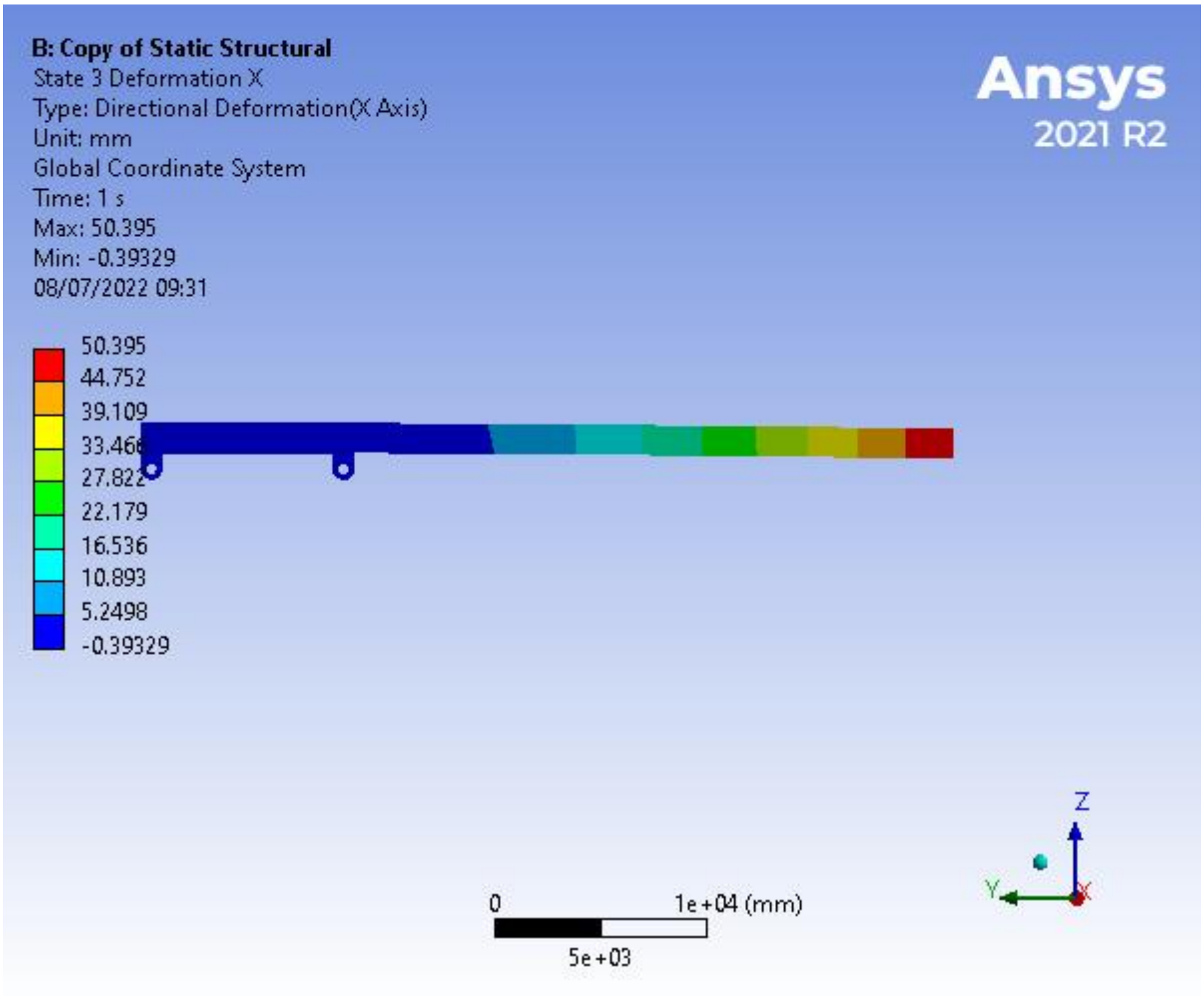

FIGURE 42
Model (A4, B4, C4) > Static Structural State 3 (B5) > Solution (B6) > Y Axis - Directional Deformation - End Time

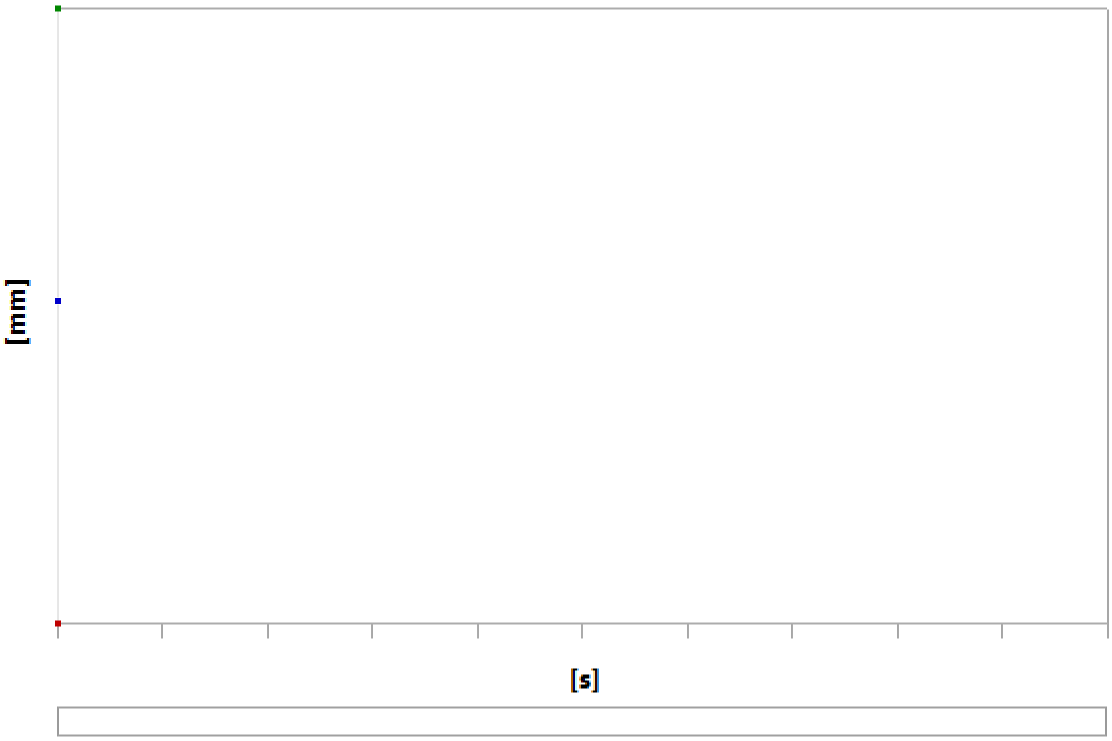

TABLE 41
Model (A4, B4, C4) > Static Structural State 3 (B5) > Solution (B6) > Y Axis - Directional Deformation - End Time

Time [s]	Minimum [mm]	Maximum [mm]	Average [mm]
1.	-9.0777	7.0297	-0.60907

FIGURE 43
Model (A4, B4, C4) > Static Structural State 3 (B5) > Solution (B6) > Y Axis - Directional Deformation - End Time > State 3 Deformation Y

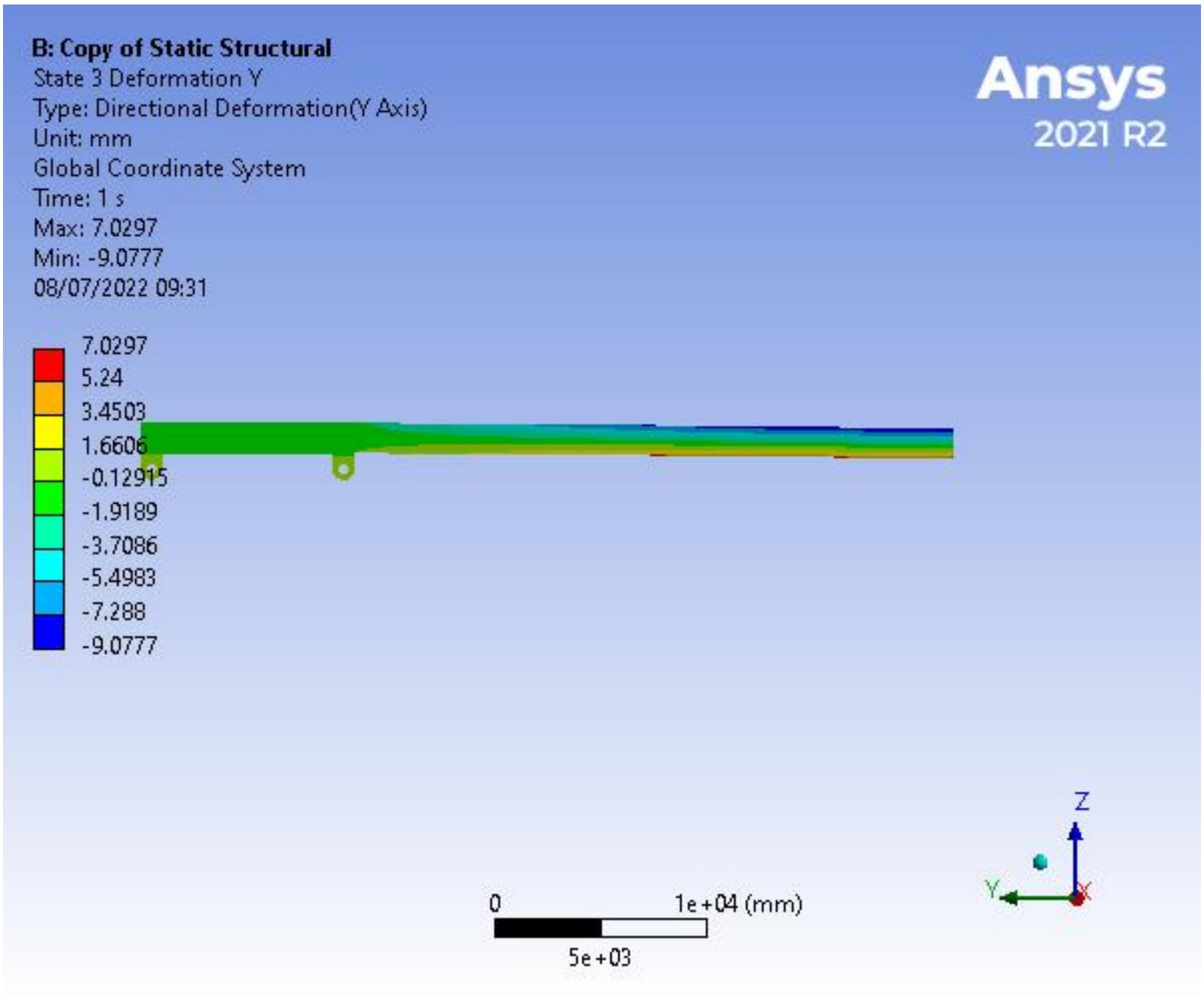

FIGURE 44
Model (A4, B4, C4) > Static Structural State 3 (B5) > Solution (B6) > Z Axis - Directional Deformation - End Time

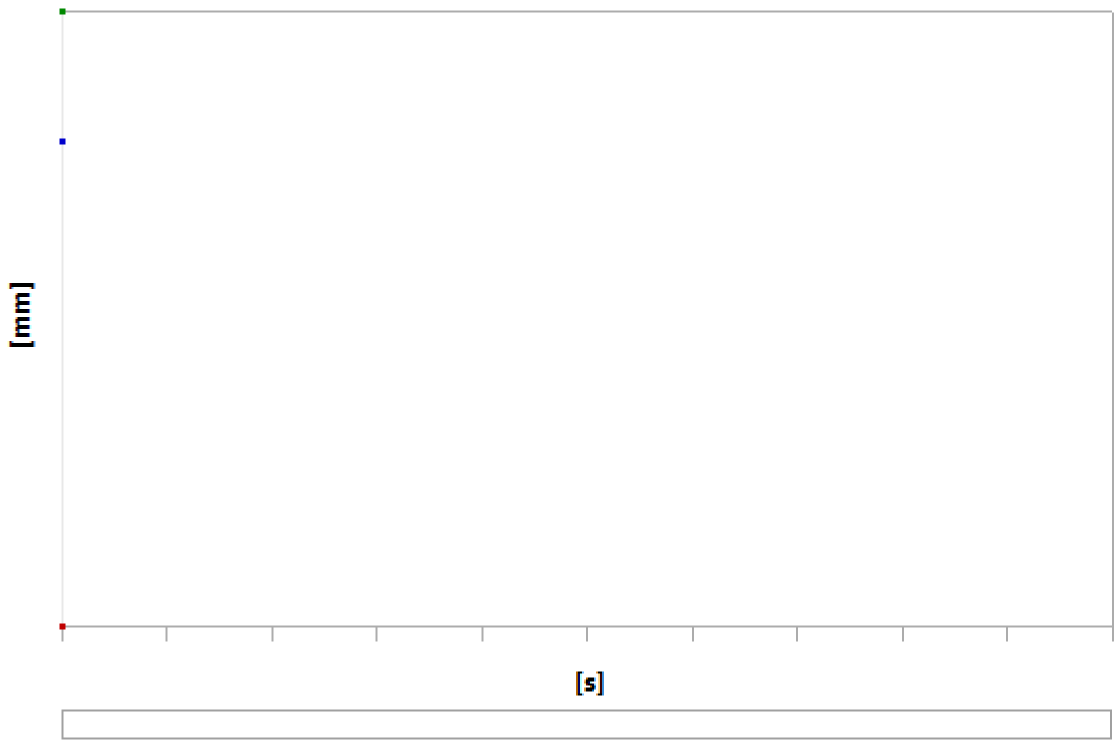

TABLE 42
Model (A4, B4, C4) > Static Structural State 3 (B5) > Solution (B6) > Z Axis - Directional Deformation - End Time

Time [s]	Minimum [mm]	Maximum [mm]	Average [mm]
1.	-199.3	1.1783	-41.187

FIGURE 45
Model (A4, B4, C4) > Static Structural State 3 (B5) > Solution (B6) > Z Axis - Directional Deformation - End Time > State 3 Deformation Z

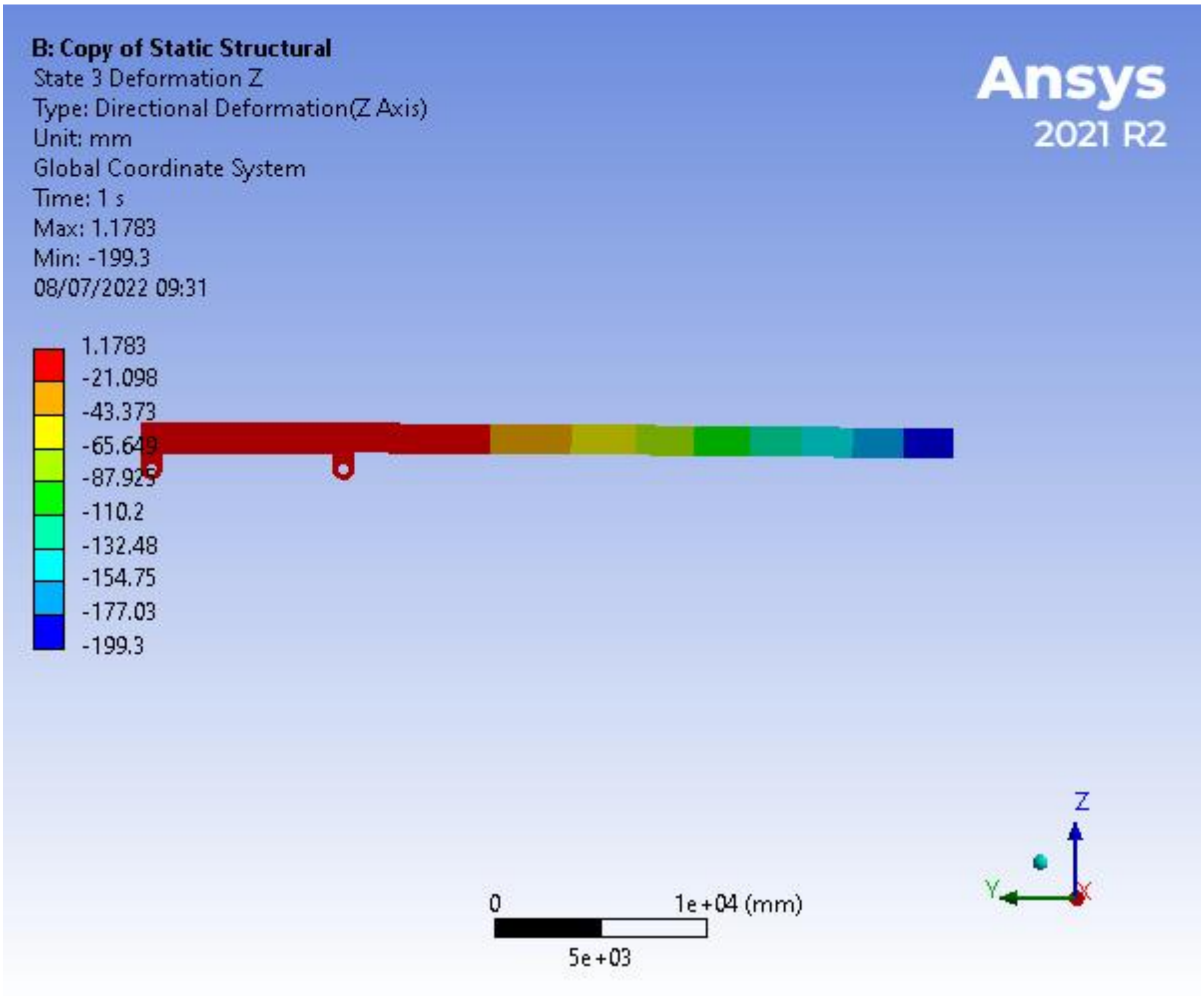

FIGURE 46
Model (A4, B4, C4) > Static Structural State 3 (B5) > Solution (B6) > Equivalent Stress

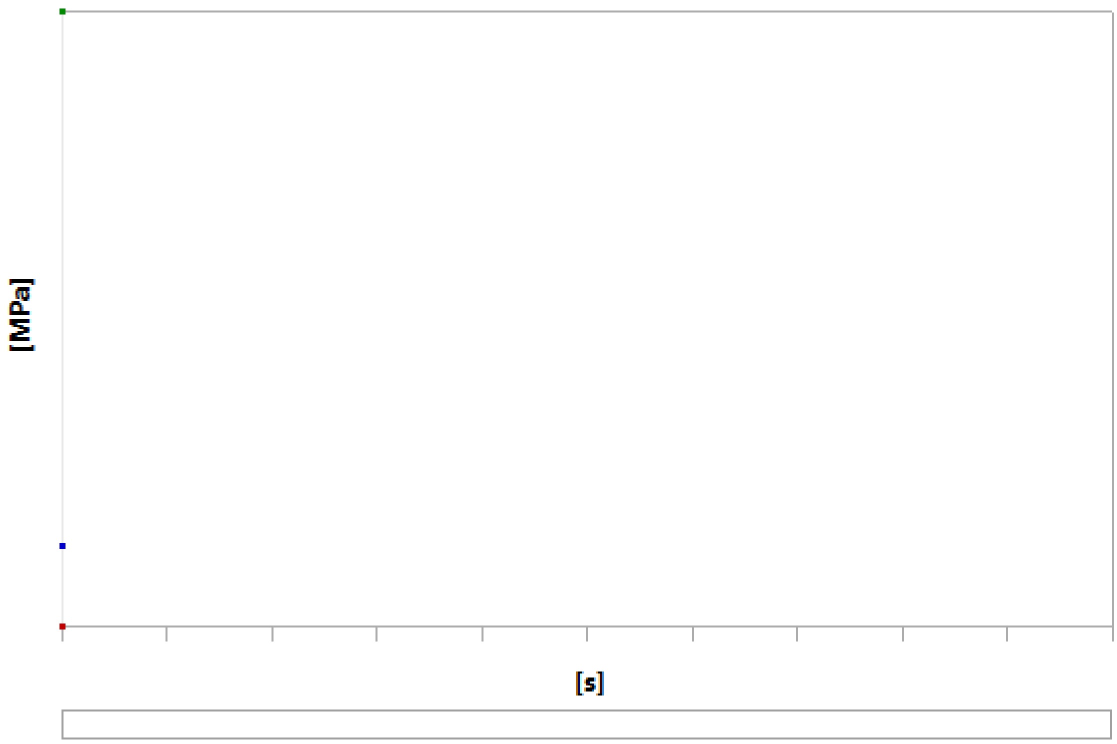

TABLE 43
Model (A4, B4, C4) > Static Structural State 3 (B5) > Solution (B6) > Equivalent Stress

Time [s]	Minimum [MPa]	Maximum [MPa]	Average [MPa]
1.	7.1717e-002	225.36	29.14

FIGURE 47
Model (A4, B4, C4) > Static Structural State 3 (B5) > Solution (B6) > Equivalent Stress > State 3 Equivalent Stress

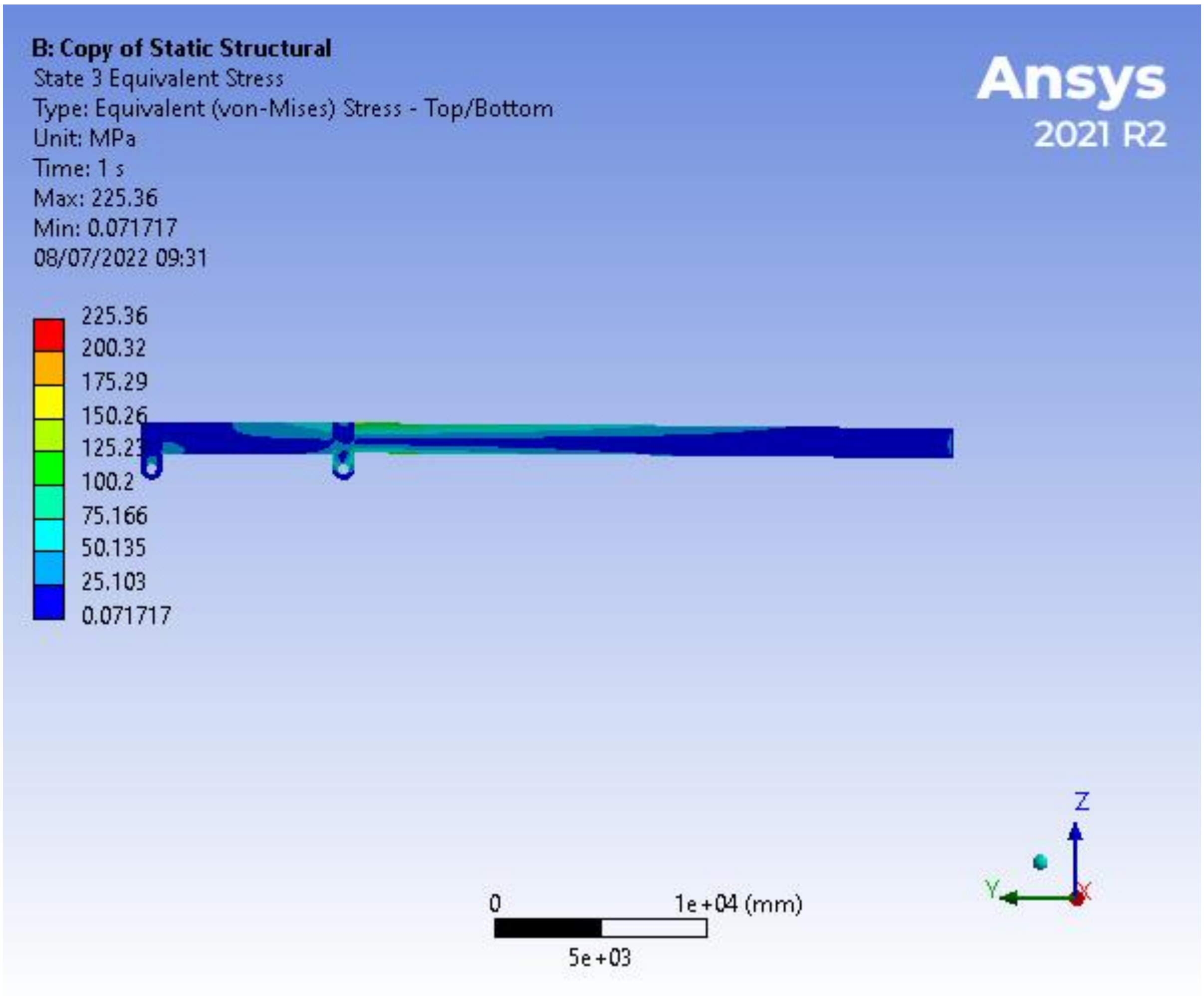

Material Data

S355

TABLE 44
S355 > Constants

Density	7.85e-009 tonne mm^-3
Coefficient of Thermal Expansion	1.2e-005 C^-1
Specific Heat	4.34e+008 mJ tonne^-1 C^-1
Thermal Conductivity	6.05e-002 W mm^-1 C^-1
Resistivity	1.7e-004 ohm mm

TABLE 45
S355 > Color

Red	Green	Blue
132	139	179

TABLE 46
S355 > Compressive Ultimate Strength

Compressive Ultimate Strength MPa
470

TABLE 47
S355 > Compressive Yield Strength

Compressive Yield Strength MPa
335

TABLE 48
S355 > Tensile Yield Strength

Tensile Yield Strength MPa
335

TABLE 49
S355 > Tensile Ultimate Strength

Tensile Ultimate Strength MPa
470

TABLE 50
S355 > Isotropic Secant Coefficient of Thermal Expansion

Zero-Thermal-Strain Reference Temperature C
22

TABLE 51
S355 > S-N Curve

Alternating Stress MPa	Cycles	Mean Stress MPa
3999	10	0
2827	20	0
1896	50	0
1413	100	0
1069	200	0
441	2000	0
262	10000	0
214	20000	0
138	1.e+005	0
114	2.e+005	0
86.2	1.e+006	0

TABLE 52
S355 > Strain-Life Parameters

Strength Coefficient MPa	Strength Exponent	Ductility Coefficient	Ductility Exponent	Cyclic Strength Coefficient MPa	Cyclic Strain Hardening Exponent
920	-0.106	0.213	-0.47	1000	0.2

TABLE 53
S355 > Isotropic Elasticity

Young's Modulus MPa	Poisson's Ratio	Bulk Modulus MPa	Shear Modulus MPa	Temperature C
2.1e+005	0.3	1.75e+005	80769	

TABLE 54
S355 > Isotropic Relative Permeability

Relative Permeability
10000

Appendix E

Dynamic response payload

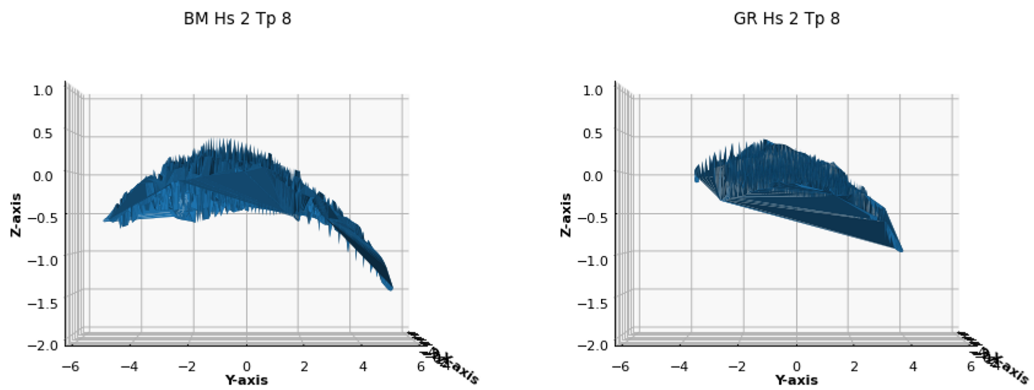

Figure E-1: Payload motion at H_s 2 m & $T_p = 8$ s

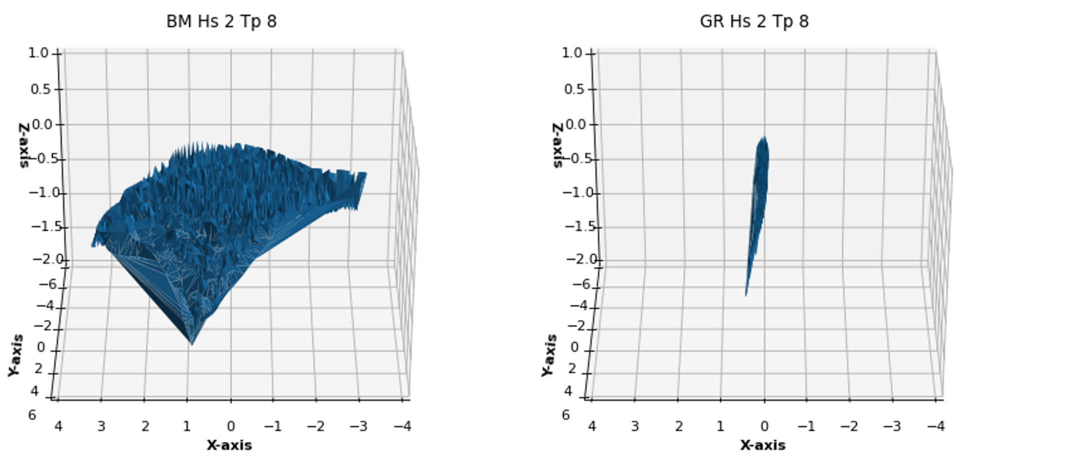

Figure E-2: Payload motion at H_s 2 m & $T_p = 8$ s

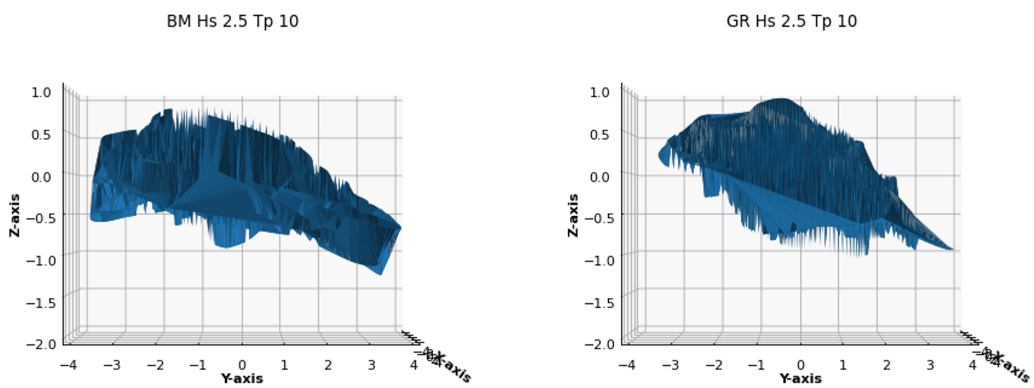

Figure E-3: Payload motion at H_s 2.5 m & $T_p = 10$ s

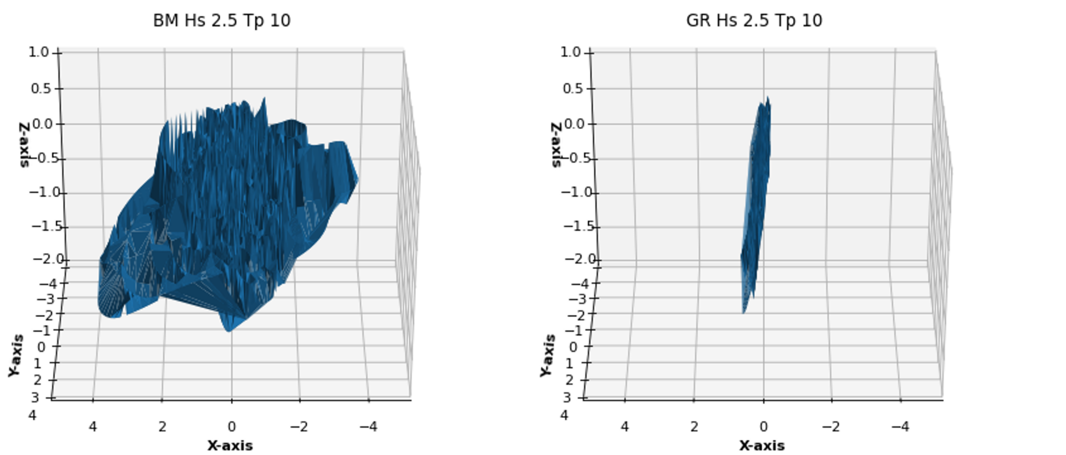

Figure E-4: Payload motion at H_s 2.5 m & $T_p = 10$ s

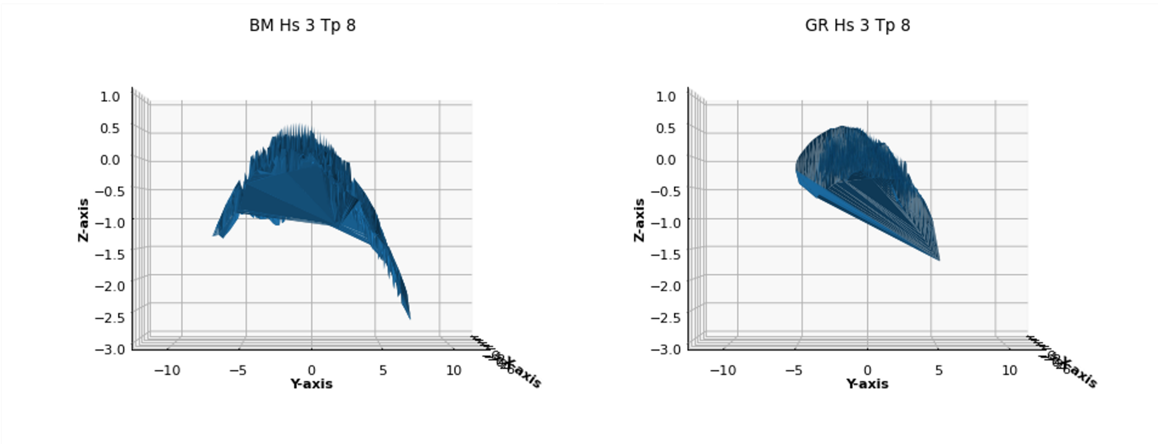

Figure E-5: Payload motion at H_s 3 m & $T_p = 8$ s

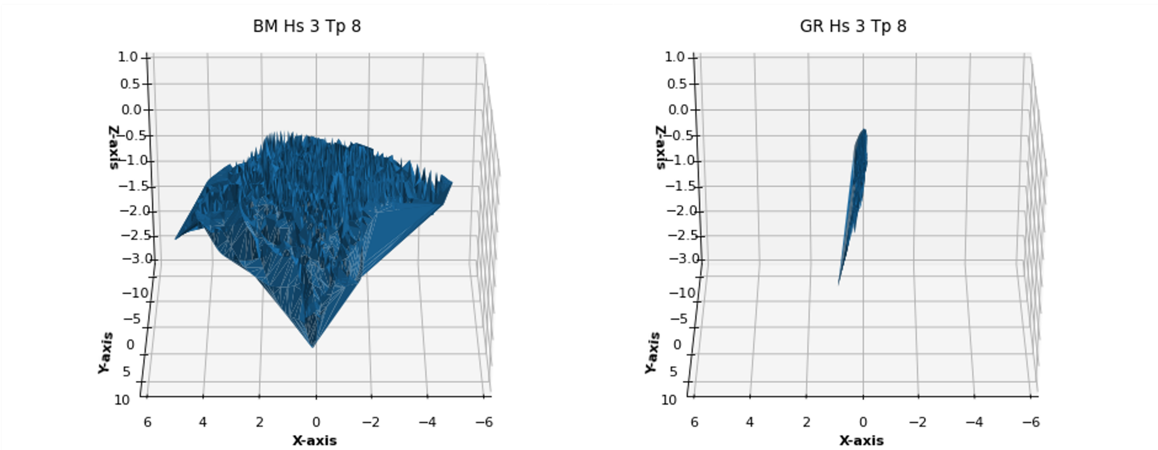

Figure E-6: Payload motion at H_s 3 m & $T_p = 8$ s